Cape Peninsula
University of Technology

ENERGY WHEELING VIABILITY OF DISTRIBUTED RENEWABLE ENERGY FOR INDUSTRY

by

WILLIAM NORMAN MURRAY

Thesis submitted in fulfilment of the requirements for the degree

Master of Engineering: Electrical Engineering

in the Faculty of Engineering

at the Cape Peninsula University of Technology

Supervisor: Dr. Marco Adonis

Bellville
Date submitted: August 2018

DECLARATION

I, William Norman Murray, declare that the contents of this dissertation/thesis represent my own unaided work, and that the dissertation/thesis has not previously been submitted for academic examination towards any qualification. Furthermore, it represents my own opinions and not necessarily those of the Cape Peninsula University of Technology.

Signed **Date**

ABSTRACT

Industry, which forms the lifeblood of South Africa's economy, is under threat as a result of increased electricity pricing and unstable supply. Wheeling of energy, which is a method to transport electricity generated from an Independent Power Producer (IPP) to an industrial consumer via the utility's network, could potentially address this problem. Unlike South Africa's electricity landscape, which is highly regulated and monopolized by Eskom, most developed countries have deregulated their electricity market, which has led to greater competition for electricity supply.

This thesis, presents an evaluation of the economic viability and technical concerns arising from third party transportation of energy between an IPP and an industrial consumer. IPP's are able to generate electricity from various renewable distributed generation (DG) sources, which are often physically removed from the load. In practice, electricity could be generated by an IPP and connected to a nearby Main Transmission Substation (MTS) in a region with high solar, wind or hydropower resources and sold to off-takers a few hundred kilometres away. Using two software simulation packages, technical and economic analysis have been conducted based on load data from two industrial sites, to determine the viability of wheeling energy between an IPP and off-taker. The viability will be evaluated based on levelized cost of electricity (LCOE); net present cost (NPC); DG technology; distance from the load; available renewable resources; impact on voltage profile, fault contribution, thermal loading of the equipment and power loss.

The results from both case studies show that the impact of DG on the voltage profile is negligible. The greatest impact on voltage profile was found to be at the site closest to the load. Asynchronous and synchronous generators have a greater fault contribution than inverter-based DG. The fault contribution is proportional to the distance from the load. Overall, thermal loading of lines increased marginally, but decreased based on distances from the load. Power loss on short lines is negligible but there is a significant loss on the line between the load and DG based on the distance from the load. Electricity generated from wind power is the most viable based on LCOE and NPC. For larger wind systems, as illustrated by the second case study, grid parity has already been reached. Wheeling of wind energy has already proven to be an economically viable option. According to future cost projection, large scale solar energy will become viable by 2019.

The concept of wheeling energy between an IPP and off-taker has technical and economic merit. Wheeling charges are perceived to be high, but this is not the case as wheeling tariffs consist of standard network charges.

In the future, renewable energy will continue to mature based on technology and cost. Solar energy, including lithium-ion battery back-up technology, looks promising based on future cost projections. Deregulation of the electricity market holds the key to the successful implementation of energy wheeling as it will open the market up for greater competition.

ACKNOWLEDGEMENTS

I would like to express my sincere gratitude to my supervisor, Dr. Marco Adonis, for the guidance during this research. Your help in making sure that the objectives of the research were well constructed and coherent is highly valued. I am very grateful for the time spent in reading the document and your valuable feedback and suggestions.

I would like to thank my employer, Actom Electrical Products for supporting my ambition to undertake this research. I want to especially thank my CEO for the financial support.

The financial assistance of the National Research Foundation towards this research is acknowledged as well.

Lastly, but most importantly, I want to thank my darling wife, Nikki, parents-in-law, and my two beautiful daughters, Bella and Sienna for the emotional and moral support when I needed it the most. I owe everything I've achieved to my loving wife and daughters.

DEDICATION

To

My darling wife, Nikki and

Our beautiful daughters, Bella and Sienna

TABLE OF CONTENTS

LIST OF FIGURES

LIST OF TABLES

GLOSSARY

List of abbreviations

CAPEX	Capital Expenditure
CSR	Corporate Social Responsibility
LCOE	Levelized Cost of Electricity
NPC	Net Present Cost
CO_2	Carbon dioxide
DG	Distributed Generation
DOE	Department of Energy
EIUG	Energy Intensive User Group of Southern Africa
Eskom	Electricity supply company of South Africa
GHI	Global Horizontal Irradiation
HFO	Heavy Fuel Oil
IEA	International Energy Agency
IPP	Independent Power Producer
IRENA	International Renewable Energy Agency
IRP	Integrated Resource Plan
kW	kilowatt
kW/m^2	kilowatt per square metre
kWh	kilowatt-hour
kWh/m^2	kilowatt-hour per square metre
MW	megawatt
NERSA	National Energy Regulator of South Africa
NREL	National Renewable Energy Laboratory
O&M	Operating and Maintenance
PPA	Power Purchase Agreement
RE	Renewable Energy
REFIT	Renewable Energy Feed-In Tariff Program
REIPPP	Renewable Energy Independent Power Producer Procurement
Solar PV	Solar photovoltaic
WASA	Wind Atlas for South Africa

CHAPTER ONE
INTRODUCTION

1.1 Introduction

This chapter provides a general introduction to the thesis. It starts with the background to South Africa's energy sector and its renewable energy potential. The research problem is presented and the objectives are stated. Finally, the outline of the thesis is presented.

1.2 Background

In the White Paper on the Energy Policy of the Republic of South Africa of 1998, then minister of minerals and energy, Dr. P.M. Maduna, highlighted the importance of renewable energy for economic growth and development. In this paper, the government made a firm commitment to the development and support of renewable energy in South Africa.

Eskom, which is the state-owned, vertically integrated generation and supply authority, owns and controls the national grid (Newbery & Eberhard, 2008). Since its establishment in 1923, Eskom has enjoyed the monopoly of power supply in South Africa. In 2008, Eskom's reserve margin was less than 10%, causing major disruption in power supply. The economy suffered, and the industrial sector was severely affected. Significant increases in electricity tariffs since 2008, and loss of supply prompted consumers to consider renewable energy as an alternative option for reliable electricity supply. One of these options to secure alternative energy at competitive pricing, is energy supplied from an Independent Power Producer (IPP), transported via the utility's grid.

It has been suggested that third party transportation of energy, commonly known as wheeling, could be a potential solution to unlock South Africa's renewable energy potential (Media Update, 2015). Wheeling could open up opportunities for IPP's to supply power via Eskom's transmission grid to a host of industrial consumers at very competitive tariffs. In contrast to South Africa's electricity structure, the global electrical power supply industry has changed since the 1980's from a regulated to deregulated market. In Great Britain, Spain, New Zealand, USA, Argentina, and Chile there has been a strong drive toward deregulation and wheeling of energy (Sood, Padhy, & Gupta, 2004). The practice has been very successful and it has resulted in greater efficiencies and price reduction as a result of competition.

South Africa is currently ranked 84 amongst 125 countries by the World Energy Council based on security, equity and environmental sustainability (World Energy Council, 2016). The World Energy Council's report acknowledges the investment and maintenance by the electricity supply utility and its ability to address load shedding, but questions South Africa's ability to diversify its energy sources. Until policy is reviewed and the energy balance is addressed, South Africa's ranking is unlikely to improve. Given this scenario, renewable energy potential, and the energy demand forecast by the Integrated Resources Plan (IRP), wheeling could be the answer to unlocking South Africa's energy potential.

Prior to the establishment of large centralized power stations, electricity was produced at or very close to the load (Jenkins, Ekanayake & Strbac, 2010). However, over the past 50 years, we have seen a shift towards large centrally located generating stations. At these large generators, voltages are increased via step-up transformers to higher voltages where it is transmitted over long distances via an interconnected transmission system. At the distribution level, voltages are step down via step down transformers and distributed via a radial system at medium voltage. Beyond this point, voltages are step down again to low voltage where it is distributed to the end consumer. In a conventional system, power always flows from the large generation stations to the end consumer. In recent years, there has been a shift back to generating power close to the load (Jenkins, Ekanayake & Strbac, 2010). These generation systems, typically connected to the medium or low voltage network are referred to as *Distributed Generation (DG).* The uptake of DG over the past years can in part be attributed to climate change, as governments aim to reduce greenhouse gasses; increased fossil-based electricity pricing; market liberalization and deregulation; falling prices of renewable energy and demand for reliable electricity supply.

Even though DG has a positive effect from an environmental and security of supply perspective and could potentially solve energy demands, connection to the network poses some technical challenges. In a conventional power system, power flows from the point of generation to the point of consumption. This *unidirectional* power flow is typical of traditional power systems as illustrated in figure 1.1. Connecting DG to the high, medium or low voltage network changes the power flow and impacts the stability of the system. With DG connected, power flows from the generating plant and voltage bus where the DG is connected. At high penetration levels, DG could be detrimental, affecting power system operations such as voltage, fault level, power quality, thermal limits of equipment and power losses. Technical limitations should be evaluated to determine safe operating levels of DG. The impact of wheeling to determine the most

viable path between an IPP and off-taker should be thoroughly assessed by means load flow analysis.

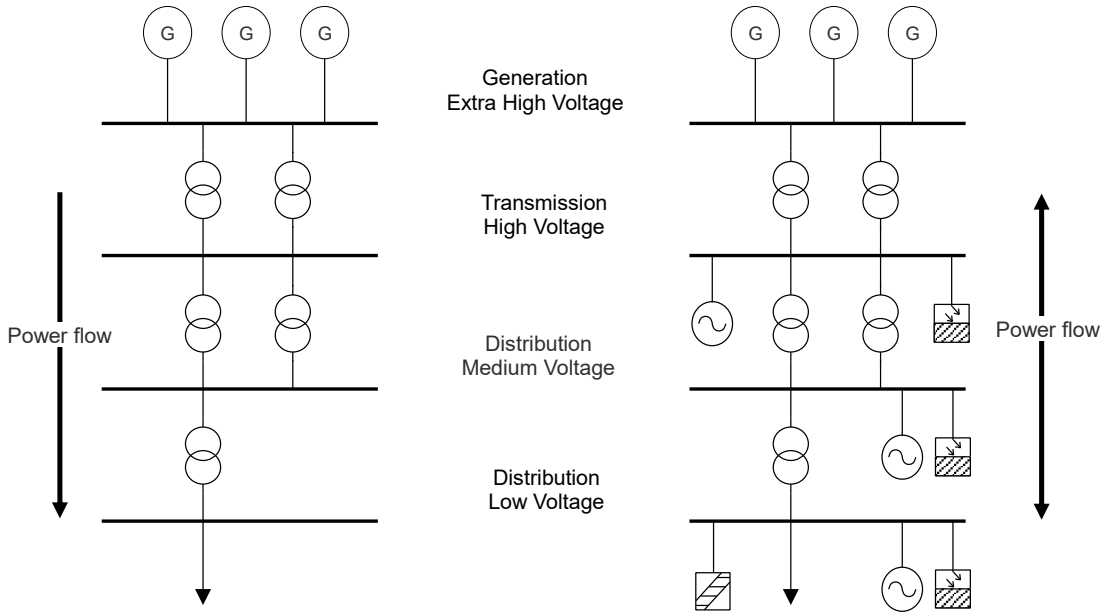

Figure 1.1: Traditional electric power systems (left) and electric power systems with distribution generation (right) (adapted from Jenkins, Ekanayake & Strbac, 2010)

1.3 Research problem statement

Industry, which forms the lifeblood of South Africa is under tremendous pressure due to escalating electricity prices and unstable supply in recent years. Various industry sectors are looking at alternative energy in the form of renewable energy. One of the mechanisms available to industry is third party transportation or wheeling of renewable energy. Wheeling has been successfully implemented worldwide in deregulated markets. In a regulated market like South Africa, only a few projects have been successful implemented. The transportation of energy, based on a bilateral agreement between an IPP and a private consumer using the supply authority's power grid, could be a viable option. DG, however alters the power flow in conventional distribution systems. Various factors such as technology, distance from the load, available renewable resources, impact on voltage profile, fault contribution, power quality, thermal limits of equipment and power losses could influence the viability of a wheeling agreement other than pure economic incentives.

1.4 Research questions

There are some challenges that could emerge when a private consumer selects a suitable IPP. Several questions emerge as a result

1. What is the optimal level of generation that can be absorbed without exceeding equipment thermal limits?
2. What is the impact of location on voltage profile, fault level and power losses on the network?
3. What is the impact of DG technology and size on above network parameters?

1.5 Significance of research

Whilst this study will focus on industry, the results could be applied as a reference to any sector of the economy including municipalities who wishes to enter into a wheeling agreement with an IPP. The study could be useful to determine the most suitable IPP based on size, location and technology.

1.6 Aims and objectives

The aim of this research is to determine the viability of energy wheeling between an IPP and a consumer.

The objectives are to:

1. Identify the potential for DG in the industrial sector
2. Present a cost analysis of DG technologies and determine the most viable option based on economic considerations.
3. Review international wheeling practice and South Africa's perspective on wheeling, including a few case studies
4. Investigate the impact of DG on voltage profile, fault contribution, thermal limits of equipment and power losses

1.7 Methodology

The research methodology applied involves:

- Review of DG technologies suitable for industry
- Collecting and modelling load data obtained from two industrial sites
- Collecting weather data from potential RE sites
- Develop a distribution model to test the research questions
- Use DIgSILENT PowerFactory to do load flow analysis to calculate the impact of DG on the network voltage profile, thermal limits of equipment, fault level and power losses.
- Use HOMER Energy to determine the optimal RE-grid solution based on LCOE and NPC

1.8 Outline of the thesis

Chapter 1 is the introduction to the thesis.

Chapter 2 gives an overview of the South African energy landscape, the industrial sector, different DG technologies, potential and technology cost. Barriers to DG entry are discussed as well. Secondly, literature reviews on international wheeling trends and cost allocation methods is presented. A local perspective of wheeling practice and successfully implemented case studies is discussed. Thirdly, power flow in conventional systems, including a mathematical analysis of the impact on these systems when DG is added to the network is discussed. Lastly, the effect on voltage profile, fault levels, thermal limits of equipment and power loss based on DG technology is discussed.

Chapter 3 is the development and simulation of a distribution model which illustrates the impact of DG on network parameters based on technology, size and distance from the load.

Chapter 4 is a presentation of the results and discussion

Chapter 5 presents the conclusion and recommendations

CHAPTER TWO
LITERATURE REVIEW

2.1 Introduction

This chapter provides a literature review of different distributed generation (DG) technologies available to industry. Secondly it provides an overview of energy wheeling and gives a global and local perspective of wheeling practice. Thirdly, a mathematical analysis of power flow in distribution systems with and without DG is presented. The objective is to determine the most suitable DG technology source to match an industry load based on location and demand.

2.2 The Industrial Sector

2.2.1 Overview

Economic activity, which is a measurement of gross domestic product (GDP) is generally divided into 3 activities, i.e. agriculture, industry and services, according to the International Standard Industrial Classification system (ISIC) (Napp, Gambhir, Hills, Florin, & Fennell, 2014). The breakdown of economic activity is illustrated in figure 2.1.

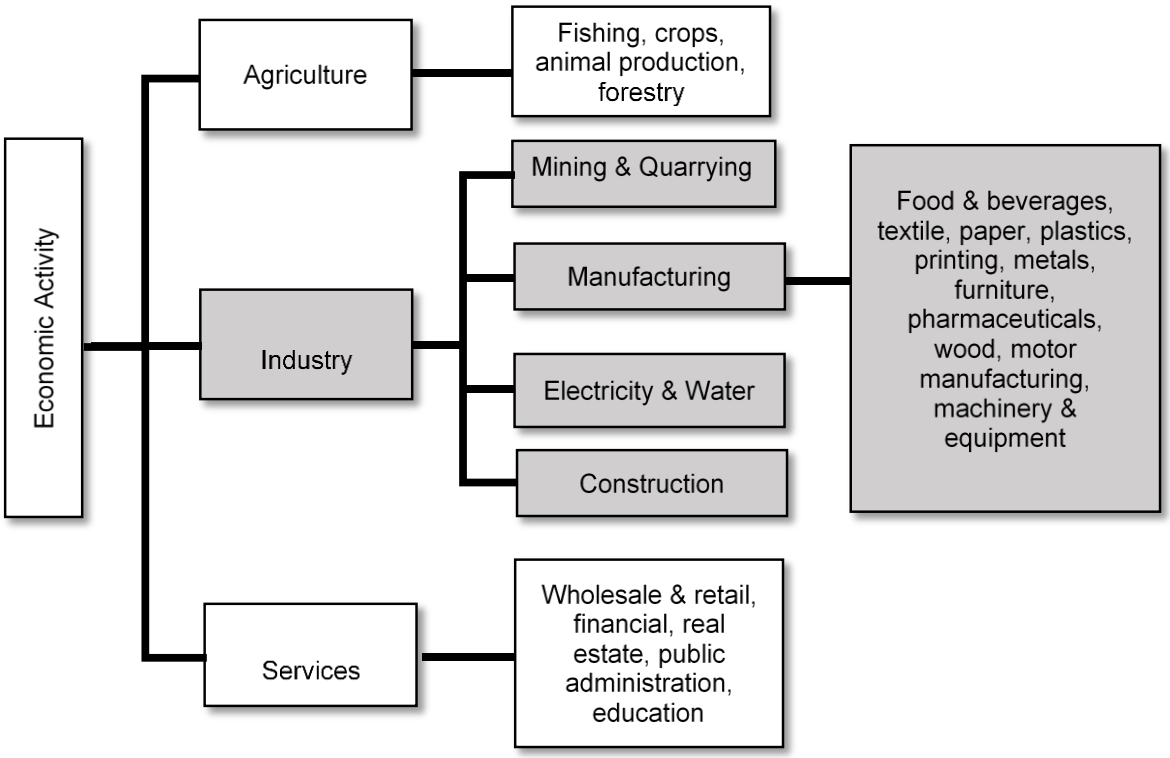

Figure 2.1: Breakdown of economic activity (Napp et al., 2014)

One-third of global energy is used for industrial processes (Napp et al., 2014). Fossil fuels account for approximately 70% of this energy. Industry, contributes to approximately 40% of global CO_2 emissions (Napp et al., 2014).

2.2.2 Energy Landscape

In 2015, South Africa's economy was the second largest in Africa with GDP of $314.6bn (World Bank, 2017). The South African energy consumption is divided into five sectors i.e. agriculture; commerce and public services; industry; residential; and transport. Approximately 41% of total energy is used for industrial processes. Industry, comprises of mining, iron and steel, chemicals, non-ferrous metals, non-metallic minerals, pulp and paper, food and tobacco, and other manufacturing (Department of Energy, 2015). The largest industrial consumers are iron and steel at 27%, followed by mining at 26% (Department of Energy, 2015). Figure 2:2, is an illustration of the electricity consumption per sector.

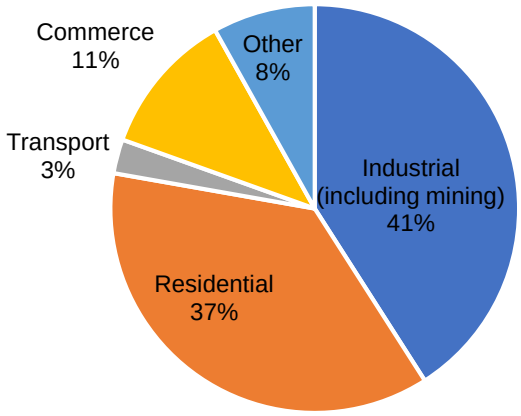

Figure 2.2: Electricity consumption (Department of Energy, 2015)

South Africa's electricity producing parastatal, Eskom, generates 95% of the country's electricity. Eskom sells electricity directly to certain large industrial customers and approximately 40% of electricity to municipalities of which 8 metros account for about 60% of total economic activity in South Africa (Department of Energy, 2015). The electricity tariff charged to industrial consumers varies depending on Eskom or municipal rates. The average blended Eskom price for industrial consumers based on megaflex rates was ZAR71.05 cents in 2017. This average is based on a transmission zone of ≤300km and voltage of ≥ 500 V & < 66 kV (Eskom, 2017). In 1990, Eskom's reserve margin was 55% and the utility was able to keep tariffs relatively low (Marquard et al, 2015). As a result of low prices, Eskom was able to strategically enter into long supply contracts with more than 25 major energy consumers like BH Billiton and Anglo

American (Yelland, 2011). In 2017, the Energy Intensive Users Group of South Africa (EIUG), a non-profit association of energy intensive consumers comprising of 31 companies, accounted for 20.3% of GDP (EIUG, 2017).

2.2.3 Mining

The mining sector is a big part of South Africa's economy and in 2016, contributed 8.0% of GDP (StatsSA, 2017). The electricity crisis in 2008 affected mining in a very adverse way when it was brought to a standstill as a result of load shedding. Eskom shut down AngloGold Ashanti, Gold Fields and Harmony, the three largest gold mines in 2008 (The Guardian, 2008). Despite the unstable electricity supply from Eskom, a study by Banerjee et al. (2015), shows that South Africa still has one of the most stable and reliable electricity supplies in Sub-Sahara Africa. It is projected that mining power requirements could triple by 2020 in relation to 2000 figures with growth rates of 3.5% per annum expected.

Table 2.1: Power sourcing typologies for mines (Banerjee at al., 2015)

Typology	Description	Generation drivers
Self-supply	Mine produces own supply	Diesel, HFO, Hybrid
Self-supply + CSR	Mine provides power to community	Diesel, HFO, Hybrid
Self-supply + sell to the grid	Produces own power and sells excess to the grid	Coal, Gas, Hydro, Hybrid
Grid supply + self supply back up	Grid connected but standby power when required	Diesel, HFO
Sell to utility	Investment in large power plant offsite connected to the grid	Diesel, HFO, Solar
Invest in own grid	Mines invest on their own or with utility in new grid	Hydro, Gas, Hybrid

The mining sector consumes approximately 15% of Eskom's annual generation. The demand in South Africa could potentially rise by an additional 15 GW by 2020 (Banerjee at al., 2015). Gold and platinum mining, consumes 47% and 33%

respectively. The remaining 20% is consumed by all other mining (Eskom, 2010.) Mines have traditionally sourced electricity from Eskom or alternatively produced their own supply based on network unavailability. The cost of electricity in South Africa has historically been cheaper when compared with international rates. Until Eskom experienced severe power shortages in 2008, electricity supply to mines has generally been very stable.

2.2.4 Iron and Steel

The steel industry is critical to infrastructure development and largely dependent on stable, cost-effective electricity supply. The iron and steel industry represent 1.5% of the country's GDP (Department of Trade and Industry, 2014). Over 190 000 jobs are created directly from the steel industry with an additional 100 000 jobs created indirectly. Approximately R600bn or 15% is added to the country's GDP by the top 5 steel industry consumers (Department of Trade and Industry, 2014). These are: a) building and construction at R157 billion, b) Structural steel at R7 billion, c) Cables and wire products contribute R4 billion, d) Automotive at R38 billion and e) Mining at R376 billion.

The consumption of energy in the steel and iron sector is dominated by fossil fuel at 60%, followed by electricity at 28% and natural gas at 12% (Department of Energy, 2015). Almost 60% of electricity is used for process heating for electric arc furnace applications. In South Africa, 43% of steel manufacturing uses the electric arc furnace method (Department of Energy, 2015). ArcelorMittal South Africa (AMSA), previously ISCOR, is the biggest steel manufacturer with a capacity of 6.1 million tonnes of liquid steel, accounting for 70% of domestic steel production. AMSA is one of Eskom's top 10 electricity consumers.

The impact of electricity price increase on AMSA's business model was highlighted at NERSA's public hearing on Eskom's multi-year price increases in 2013 (NERSA, 2013). The model in figure 2.3, illustrates the cross-over point between earnings before interest, taxes, depreciation, and amortization (EBITDA) as a percentage of turn-over and electricity as a percentage of turn-over. In order to cope with the increasing strain on the business model, AMSA have implemented energy efficiency measures and load shifting, but the latter leads to disruption of continuous production processes (NERSA, 2013). Own generation, whether diesel, gas or renewable will require vast capital layout. It is against this backdrop that AMSA have consulted IPP's with the intention of procuring electricity to meet current and future energy demands.

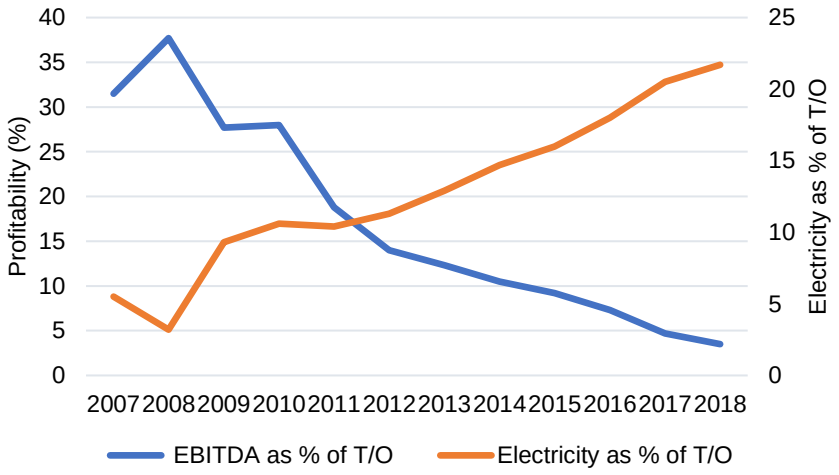

Figure 2.3: Influence of increased electricity prices of AMSA profitability (NERSA, 2013)

2.3 Distributed Generation

Renewable energy is defined as "*energy that comes from an energy source that's being replaced by a natural process at a rate that is equal to or faster than the rate at which that source is being consumed" (Doble & Kumar, 2007*).

Over the past decades there has been a drive to conserve energy and explore other forms of non-fossil based or renewable energy resources (Funabashi, 2016). This non-fossil-based energy resource can be generated from the sun, wind, water, geothermal or biofuels (Pali & Vadhera, 2016). It is expected that renewable energy will play an important role in future energy demands and will eventually replace fossil fuel over time (Funabashi, 2016). Distributed Generation (DG), in the context of this research, refers to renewable energy sources which are generated at low voltage, but connected to the high voltage network for transmission. South Africa has an abundance of renewable energy resources. It is estimated that by 2050, RE could contribute to more than 50% of South Africa's electricity demands (Banks & Schäffler, 2006).

2.3.1 Solar Photovoltaic

2.3.1.1 PV Systems

A solar cell is a simple solid-state device that converts solar radiation directly into electrical energy (Khartchenko, 2014). The following are the main technologies used commercially in PV modules:

- **Mono-crystalline** silicon cells are silicon wafers cut from a single homogenous crystal. The cells have a uniform look and an even colour. These *cells* have a conversion efficiency of up to 24.3%. This world record was achieved based on

Sunpower's Maxeon Generation III solar cell technology (Sunpower, 2017). Whilst the latter is at the top end of conversion efficiencies, the average commercial solar panel generally have conversion efficiencies of 17% (Fraas & Partain, 2010). Sunpower's commercial E-series solar panel has an average efficiency of 20.3% which is based on measured production values (Sunpower, 2017). The drawback of high efficiency cells and modules is that this technology is more expensive than other crystalline silicon types.

- **Poly-crystalline** silicon cells are manufactured from raw melted silicon. It is poured into a square mould, which is cooled and cut into perfectly square wafers. This technology is cheaper than monocrystalline cell production due to the simpler manufacturing process (Kalogirou, 2014). Poly-crystalline cells however have a lower efficiency conversion rate. Typical module efficiencies for commercially applications is 13-15% with 17% at the top end of the conversion rate (Kalogirou, 2014).

- **Thin film** solar cells are manufactured by depositing extremely thin layer of photovoltaic materials on a low-cost backing, such as glass. The cells have a conversion efficiency of 5-12%, though First Solar claims to have developed the most efficient cell of 20.4% in 2016 (Martin, 2016)

- **Multiple junction** cells use two or three layers of different materials on top of each other in order to improve the efficiency of the module. Cell efficiency could theoretically reach 33% (Khartchenko, 2014).

PV modules are made up of various solar cells connected in series or parallel, encapsulated to form a panel or module. An array is constructed from various modules connected in series or parallel (Khartchenko, 2014).

PV systems can be divided into stand-alone and grid connected:

- Stand-Alone Systems

Stand-alone systems can be divided into off-grid DC systems and AC systems where the former supplies DC loads and the latter supplies AC loads via an inverter. Both systems supply power to its respective load in the absence of a utility grid. Applications for off-grid systems range from residential, consumer products, commercial, rural to space (Luque & Hegedus, 2011)

- Grid Connected

Grid connected systems can be divided into decentralized and centralized systems. Decentralized systems are generally roof-mounted and range from a few Kilowatt to a few Megawatt. The systems consist of PV panels, suitably sized inverter and optional storage units (Goetzberger & Hoffmann, 2005). Energy is supplied during the day by the PV system and at night by the utility. Centralized systems have an installed capacity of several Megawatts. Applications range from large commercial rooftop installations to utility power plants (Goetzberger & Hoffmann, 2005). For this study, we will focus primarily on grid-tied systems. The main components of a grid-tied systems are:

- PV modules – PV modules are connected in series or parallel to form an array which convert solar radiation directly into DC power.
- An inverter – inverters are used to converts DC into AC power
- Mounting or Tracking system – these are used to secure PV modules to a fixed frame or sun tracking system
- Step-up transformers – for stepping up the voltage to utility export voltage
- Bi-directional meter – measuring nett power

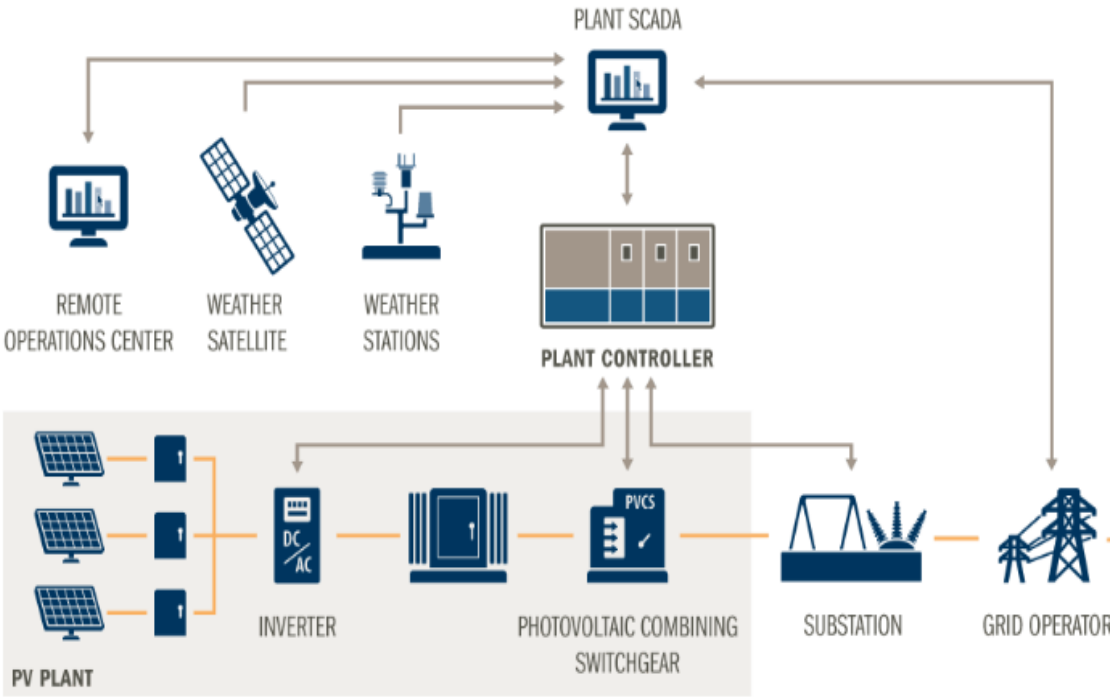

Figure 2.4: Large scale grid-connected solar PV plant (First Solar, 2017)

2.3.1.2 PV Potential

South Africa has one of the highest solar irradiance levels, with average daily levels between 4.5 and 7 kWh/m^2. South Africa enjoys 24% of the world's best winter

sunshine area and in some parts of the country, the daily average is more than 6.5 kWh/m^2 (Banks, 2006)

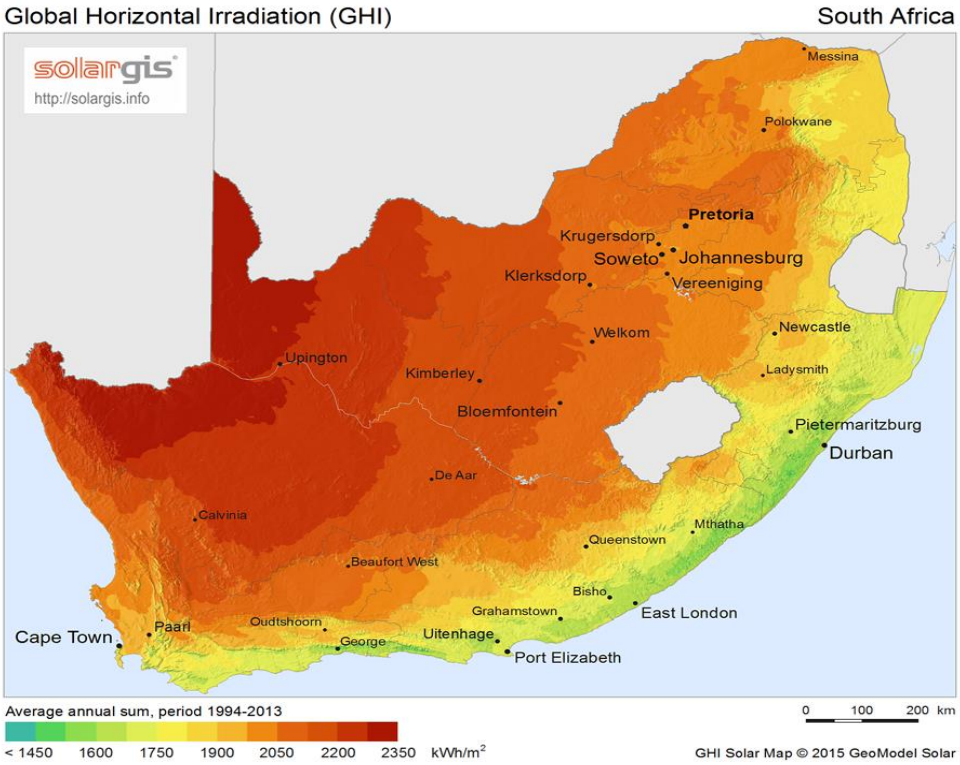

Figure 2.5: Global horizontal irradiation (Solargis, 2017)

2.3.2 Concentrated Solar Thermal Power

The first commercially viable concentrated solar plant (CSP) was built in 1984 in the USA. Between 1991 and 2005, the deployment stagnated, but after 2005, installed capacity increased by 50% per year with USA and Spain, the market leaders (World Energy Council, 2016). Concentrating Solar Power (CSP) plants generate electricity by using mirrors to concentrate the sun's rays (IRENA, 2013). The technology uses mirrors to reflect the direct normal component (DNI) of sunlight onto a single point to heat up a fluid to produce steam, which drives a turbine. CSP is ideal for supplying power during peak loads and is especially ideal in countries with high DNI (Zang et al., 2013)

There are four CSP technologies at present (Zang et al., 2013):

- Parabolic trough collector (PTC) – The receiving component is a group of curved reflectors that reflect the sunrays onto an absorber tube where a fluid is heated up to produce steam
- Solar power tower (SPT) – The receiving component are either flat or concave mirrors that concentrate the sunlight into a central receiver on a fixed tower.

- Linear Fresnel reflector (LFR) – Uses long rows of flat or slightly curved mirrors to reflect the sunrays onto a downward facing linear receiver.
- Parabolic dish systems (PDS) – Uses a dish to concentrate sunlight at a focal point

2.3.3 Wind Energy

2.3.3.1 Wind Systems

- Wind Turbine Structure

  The modern wind turbine consists of the tower, rotor blade and nacelle, which houses the gearbox and generator (Heier, 2014). Electrical power is generated by the force of the wind acting on the blades of the turbine. The rotation of the blades turns the armature of the generator, which creates a voltage (Rivkin, 2013). The rotor, made up of the blades and hub, rotates a drive train through the low-speed shaft connected to a gearbox, high-speed shaft and generator (or from the low-speed shaft to a direct-drive generator). The nacelle consists of the base frame and enclosure. It houses the drive train and electronics required to operate the turbine. Towers are made of steel or steel-reinforced concrete. Steel towers use either a tubular or lattice type construction (Kutz, 2007).

- Configurations

  Several turbine types exist, but presently the most common configuration has become the horizontal axis three bladed turbines (Kutz, 2007). The rotor may be positioned up or downwind. Modern wind turbines vary in size with two market ranges: small units rated at just a few hundred watts up to 50-80 kW in capacity, used mainly for rural and stand-alone power systems; and large units, from 150 kW up to 5 MW in capacity, used for large-scale, grid-connected systems.

- Power Plant System Components

  The main components of a wind power plant system consist of the:
  - mechanical power conversion which is made up of blades, nacelle, rotor hub, gearbox and generator
  - electrical power conversion which is made up of the controller and transformer
  - Tower

2.3.3.2 Wind Potential

In South Africa, meteorological data found that the best wind potential is along the coast. Figure 2.6 is an illustration of best wind source areas in South Africa. The uptake of wind energy in South Africa can be attributed to the Integrated Resource Plan (2010-2030). The revised policy has allocated 10.3% of total energy allocation to wind energy by end of 2030.

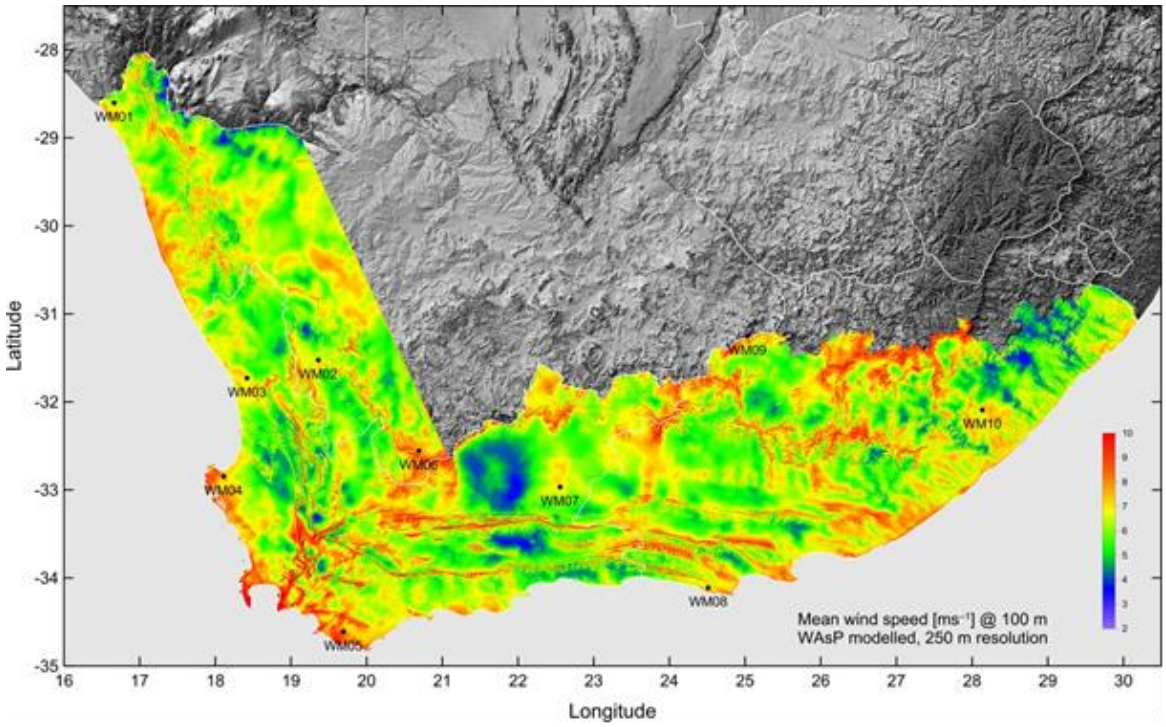

Figure 2.6: Best wind source areas in South Africa (WASA, 2017)

2.3.4 Battery Energy Storage Systems

Pumped hydro storage (PHS) is the most developed method of storing energy in the power sector and accounts for 96% of installed capacity.

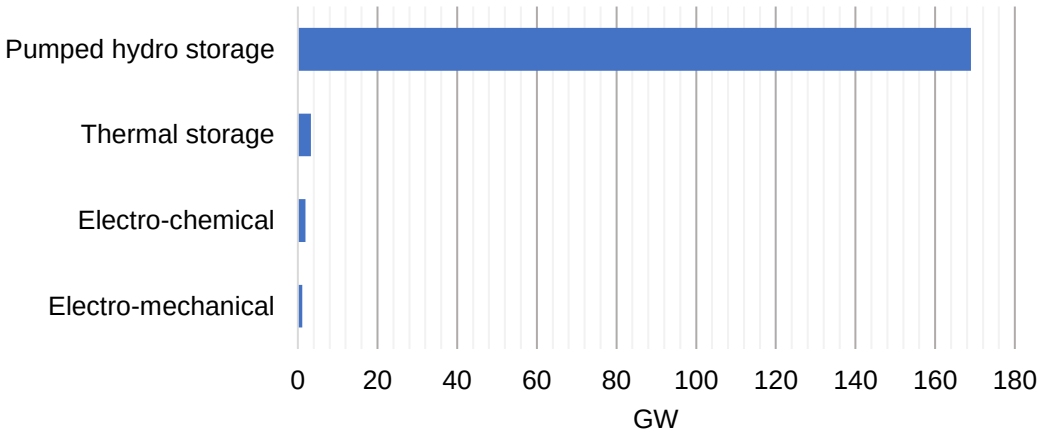

Figure 2.7: Global stationary energy storage capacity by 2017 (IRENA , 2017)

The total global electricity storage since mid-2017 is approximately 176 GW (IRENA , 2017). Hydro storage accounts for 169 GW, thermal, 3.3 GW, electro-chemical, 1.9 GW and electro-mechanical, 1.1 GW, as illustrated in figure 2.7 (IRENA , 2017).

Electro-chemical or battery electrical storage (BES) as depicted in figure 2.7, makes up a fraction of this composition at a mere 1.1%. Of this 1.1%, BES, accounts for a small fraction of utility scale storage potential. This, however, is starting to change with the integration of battery storage in solar and wind power applications (World Energy Council, 2016). Energy storage is an important component in the evolution of renewable energy deployment. It is predicted that 80% of global electricity could come from renewables by 2050 with wind and solar accounting for 52% (IRENA, 2017). Energy storage will be a key part of this transition.

2.3.4.1 Battery technologies

The most common types of rechargeable battery technologies in operation today are lithium iron and lead acid as depicted in figure 2.8 (World Energy Council, 2016). The other categories are Alkaline (Nickel) batteries and Silver batteries.

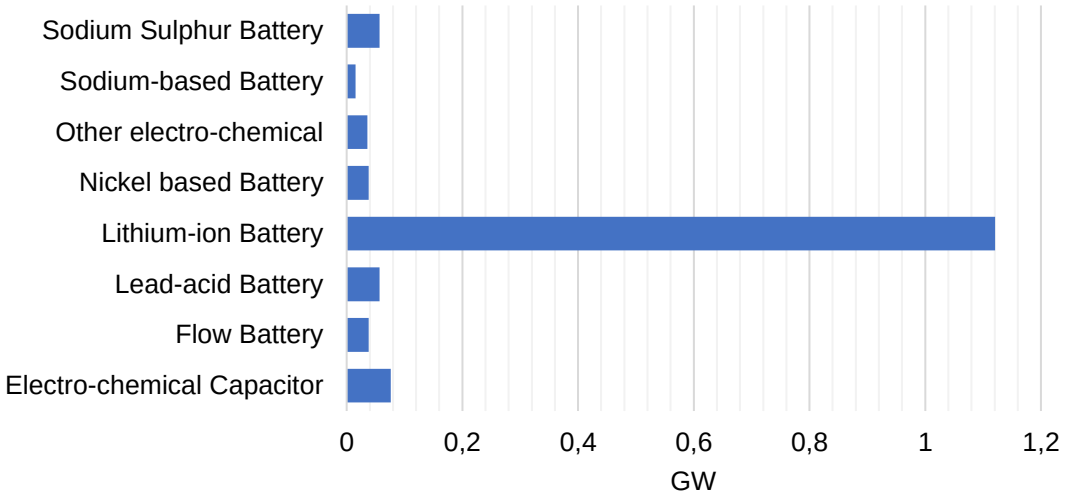

Figure 2.8: Battery technology by capacity (IRENA , 2017)

2.3.5 Hydropower

Hydropower is the generation of electricity through the movement of falling water. Electricity is produced by a generator from the action of water that moves a turbine from a definite height (World Energy Council, 2016). This technology has been designed to provide base-load power but is ideal to generate electricity at peak loads. Hydropower provided clean energy and at 90-95% efficiency, is the most efficient renewable energy source available. There has been a major growth of hydropower

development with an estimated growth of 39% between 2005 and 2015. The major drivers, which has seen 4% annual growth, has been clean energy and increased energy demand (World Energy Council, 2016). Hydropower contributes to 71% of global renewable electricity and 16.4% of global electricity. It is estimated that 10 000 TWh/year of hydropower potential is still unused worldwide (World Energy Council, 2016).

2.3.5.1 Hydropower Systems

Hydropower can be categorized as follows (World Energy Council, 2016):

- **Storage hydropower** – river water is captured in a dam and released when electricity is needed. Water is released through gates which turn a turbine and operates a generator.

- **Run-of-river hydropower** – water is channelled or diverted through a canal which drives a turbine to produce electricity. The natural flow of water and drop in elevation is used to channel water through a turbine that spins a generator, much like a conventional coal-fired power station which uses steam to drive a turbine. Unlike pump storage, where water is stored to be used during peak times, run-of-river schemes are subject to seasonal river flows. A typical scheme consists of:

    a) Weirs – barrier across the river to alter the water flow
    b) Canal – to direct the water from the river to the power chamber
    c) Forebay – to distribute the flow of water
    d) Power station intake structure - controls the transfer of water
    e) Power chamber – houses turbines and other electrical equipment. The Kaplan turbine, which is best suited based on head and flow characteristics for sites in South Africa
    f) Outlet works – the structure that returns water back to the river

- **Pumped-storage hydropower** – water is pumped from a lower to an upper reservoir during low demand. During peak demand, water is released from the upper reservoir which drives a turbine to produce electricity.

- **Offshore Marine and other new technologies** – a technology that uses wave action to generate electricity from seawater.

2.3.5.2 Hydropower potential

In South Africa, Eskom operates four large hydropower stations i.e. Drakenstein (1 GW), Palmiet (400 MW), Gariep (360 MW), Vanderkloof (240 MW) (Eskom, 2017). The City of Cape Town operates Steenbras Power Station which has a capacity of 180 MW. Various smaller stations are operated by independent operators. The potential for small hydropower power (SHP) in South Africa is estimated at 247 MW. As of 2016, only 50 MW has been installed (Klunne, 2016).

2.4 Generation cost

2.4.1 Introduction

Globally, the cost of RE has been decreasing and locally the cost of coal generation via Eskom's increased tariffs has increased year-on-year. The average cost of solar and wind in many countries is approaching grid parity. The cost of renewable energy technologies globally, has decreased dramatically during the past decade due to various factors such as technology advancement, local government policies, competition and demand. Solar PV has seen the most dramatic cost reduction of all the technologies. The cost of PV panels is 58% lower compared to 5 years ago (REN21, 2017). In regions with good resources such as Chile and Dubai, energy derived from solar PV farms produce electricity at a cost that is lower than fossil-based generation. The Renewables Energy Agency predicts a decline in PV by another 57% by 2025.

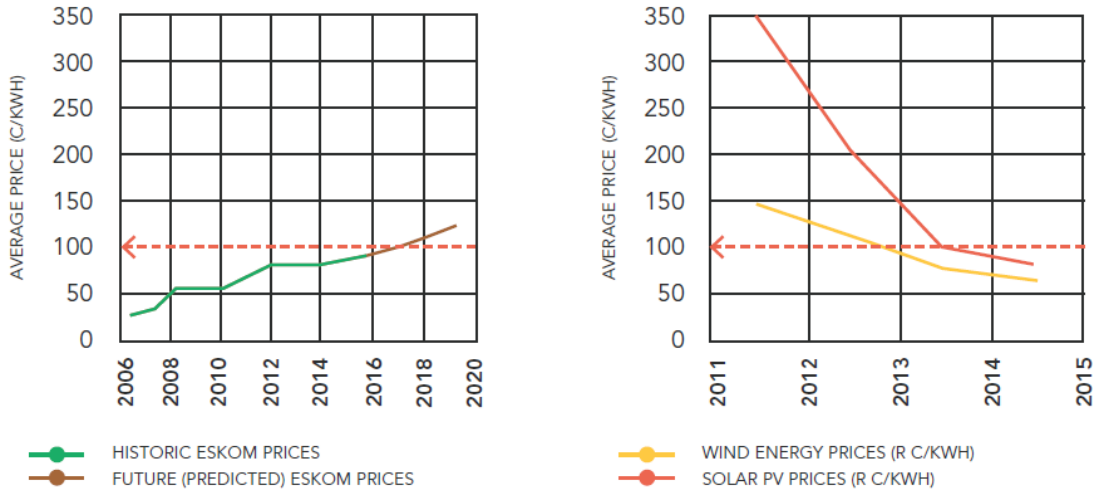

Figure 2.9: Blended average Eskom vs Utility scale tariffs (GreenCape, 2017)

The results from the last bidding window have seen prices for wind fall to R0.56/kWh and R0.77/kWh for solar compared to R0.76/kWh for fossil-based electricity for the same period. The trend in the decrease of renewable energy will continue to grow and eventually widen the gap between fossil- based energy and renewable energy.

2.4.2 Capital cost of Solar PV

The cost of solar PV modules has fallen by 81% between 2009 and 2017, which resulted in the global weighted-average LCOE of utility-scale solar PV projects in 2017 falling by 73% (IRENA, 2017b). The global weighted average fell by more than 300% from USD 4 394/kW in 2010 to USD 1 388/kW in 2017 % (IRENA, 2017b). The sharp drop is evident in recent PPA pricing in Mexico and Dubai, realizing pricing of 0.045 $/kWh and 0.03 $/kWh respectively (IRENA, 2016). In Africa, Zambia recently announced PPA tariffs of 0.06 $/kWh for a project under the World Bank's Scaling Solar programme (IRENA, 2016). Utility scale projects in Africa between 2014 and 2018 range from USD 1 200 to 4 900/kW (IRENA, 2016). South Africa has the lowest installed utility scale solar PV project in Africa at USD 1400/kW (IRENA, 2016).

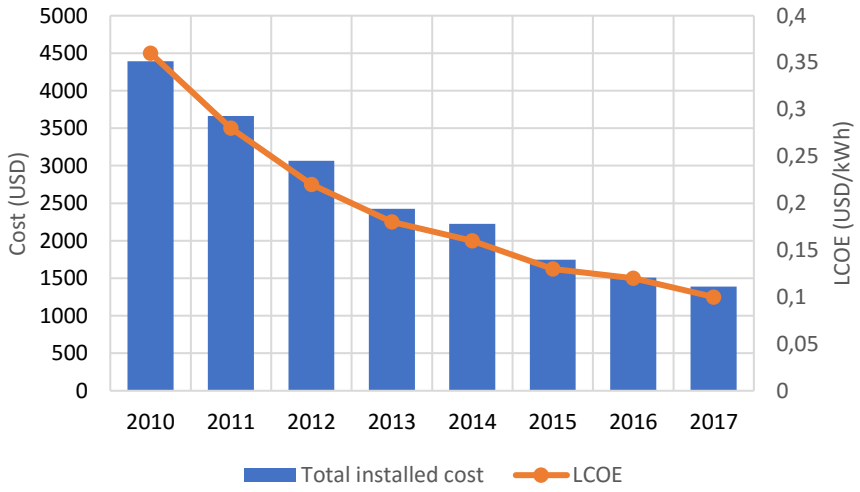

Figure 2.10: Global weighted average total installed costs and LCOE for solar PV, 2010-2017 % (IRENA, 2017b)

Figure 2.10 is an illustration of the capital cost of individual utility scale solar PV projects installed since 2011. Most of these projects are installed in South Africa, mainly as a result of the REIPPP.

2.4.3 Capital cost of Wind Energy

The major cost component in developing wind projects is the capital cost (CAPEX), which could be as much as 84% of the total cost. This cost consists of the wind turbine, including tower and installation (IRENA, 2015). The CAPEX can be broken down into the following cost:

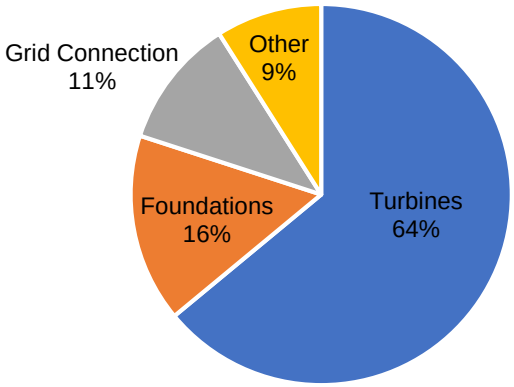

Figure 2.11: CAPEX breakdown of wind energy (IRENA, 2015)

- Turbine cost – includes the rotor, blades, gearbox, generator, converter, nacelle, tower and transformer
- Civil works – includes construction costs and foundation of the towers
- Grid connection costs – includes transformers, sub-stations and connection to local network
- Planning and project costs
- Other costs which include road construction and buildings

The average cost installed for wind energy based on data collected from 16 projects in the USA equalling 2 GW, is USD1 779/kW (Wiser & Bollinger, 2016). The cost of wind energy is affected by economies of scale. There is a substantial difference in cost for installations smaller than 5 MW compared to installations between 5-20 MW (Wiser & Bollinger, 2016).

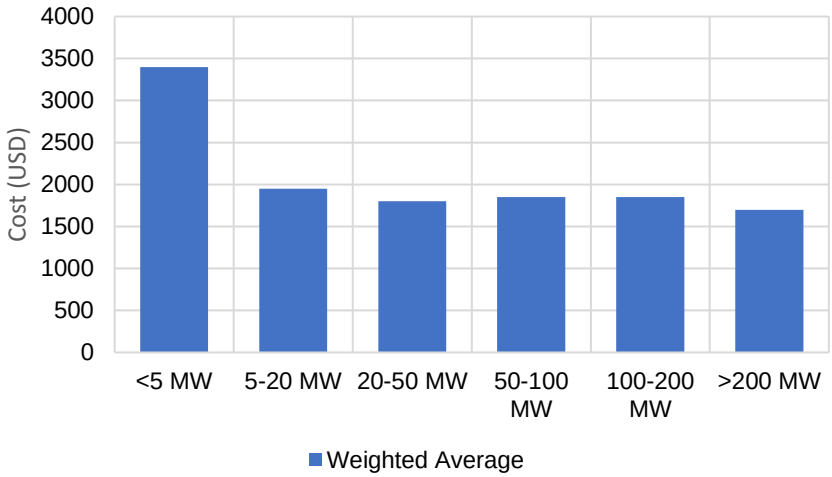

Figure 2.12: Installed wind power cost kW (Wiser & Bollinger, 2016)

In China and India where production costs are low, USD 1 320/kW was achieved in 2015, but in Eurasia and South America, cost average USD 1 720 and USD 2 200 respectively (Wiser & Bollinger, 2016). In Africa, the cost was around USD 2 210/kW which is steadily declining. In round 3 of REIPPP, wind projects above 100 MW had an average cost of USD 1 275/kW.

2.4.4 Capital cost of Battery storage

The installed cost of battery systems could fall by 50-66% by 2030. Based on the global installed capacity, Lithium-ion batteries has seen the most drastic reduction in price (IRENA , 2017). It is estimated that lithium-ion batteries could fall by 54-61% by 2030 as illustrated in figure 2.13, below (IRENA , 2017).

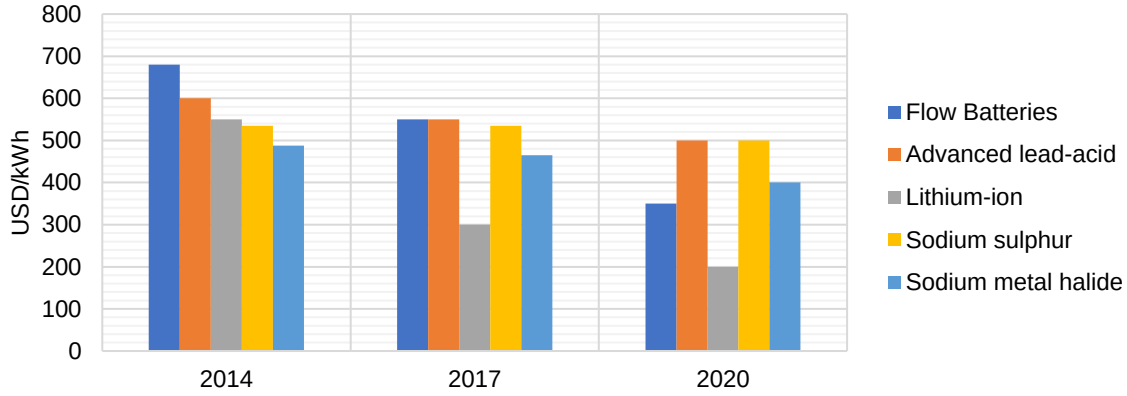

Figure 2.13: Current and projected battery cell price by type for utility-scale applications (IRENA , 2017)

2.4.5 Capital cost of Hydropower

Hydropower is the most mature, reliable, cost effective renewable energy source available and is the only cost-effective large-scale storage technology to date. The biggest drawback is that the technology is very cost intensive, due to planning, environmental impact assessment studies, design and construction of major civil works (IRENA, 2015). The largest cost associated with projects of this nature is the civil works, which range between 75-90% of total cost, followed by electro-mechanical equipment. Additional cost includes project development, pre-feasibility and feasibility cost (IRENA, 2015). The total installed cost of hydropower plants globally, range between USD 1 000/kW to around USD 3 500/kW. Figure 2.14 is an illustration of the average cost per region for small and large hydropower plants. The REIPPP remains one of the biggest drivers for SHP development with 19.1 MW being installed as part of this programme (Klunne, 2016). The average price submitted for PPA's for SHP in bidding

window Round 4 of REIPPP was R1.12/kWh (Klunne, 2016). The cost of generation and local water resources constraints, remains a challenge for hydropower projects in South Africa.

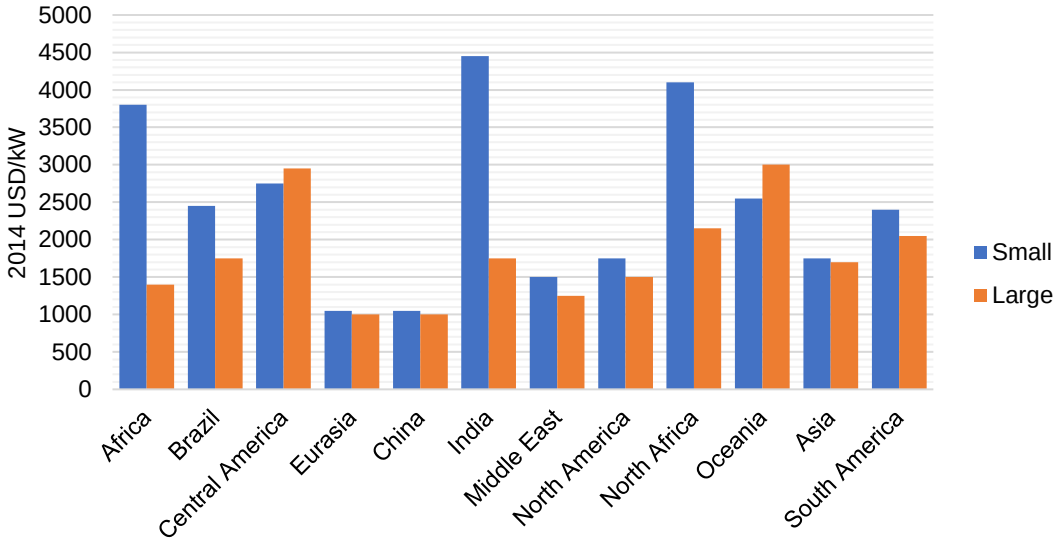

Figure 2.14: Capital cost of hydropower plants (IRENA, 2015)

2.4.6 Capital cost of CSP

The global CSP market is dominated by PTC, which accounts for 85% of the total market. This will decline however as one third of current construction is either STC or Fresnel systems (IRENA, 2015). The average cost of current PTC plants without storage is between USD 4 600 and USD 8 000/kW in Organization for Economic Co-operation and Development (OECD) countries and typically lower, between USD 3 500/kW and USD 7 300/kW in non-OCED countries (IRENA, 2015). The cost for PTC plants with 4-8hour storage is between USD 6 800 and USD 12 800/kW.

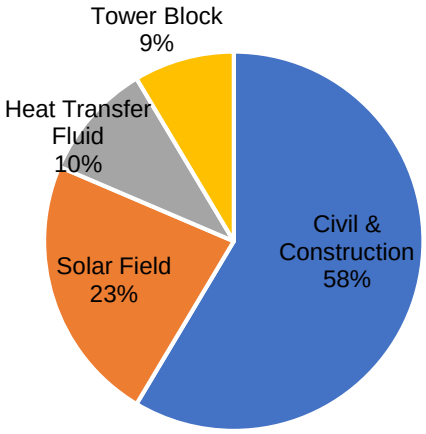

Figure 2.15: CAPEX breakdown of PTC plants (IRENA, 2015)

Figure 2:16, shows the cost of CSP by technology without storage by 2015 and projected cost by 2025. It is projected that the overall cost of Parabolic Trough Concentrator (PTC) and Solar Tower (ST) would decrease by 33% and 37% respectively by 2025 (IRENA 2017b). The average price submitted in the third bidding window of the REIPPP in South Africa was R1.62/kWh (NERSA, 2017).

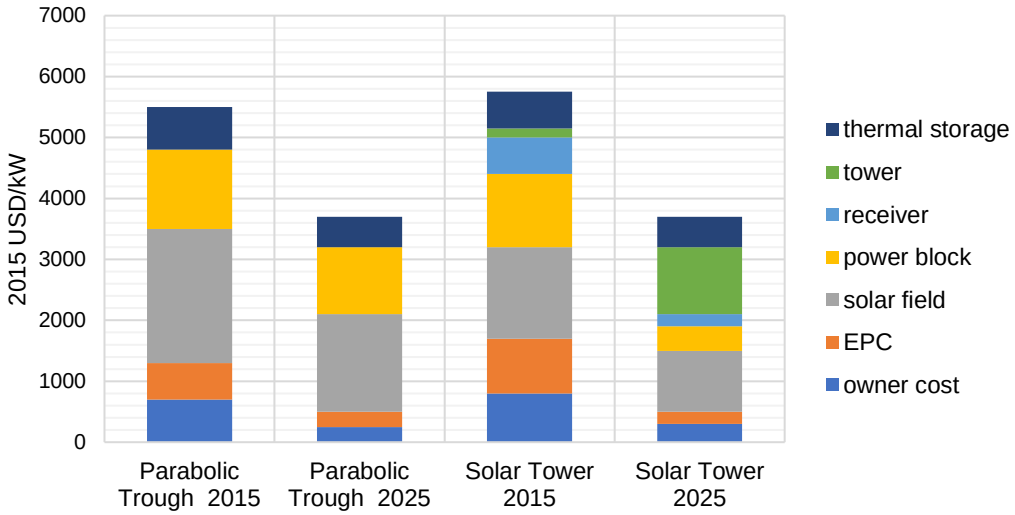

Figure 2.16: CSP installed cost breakdown by technology and storage (IRENA , 2017)

2.4.7 Capital cost comparison summary

Figure 2.17, represents a summary of the cost for various RE technologies for utility scale projects.

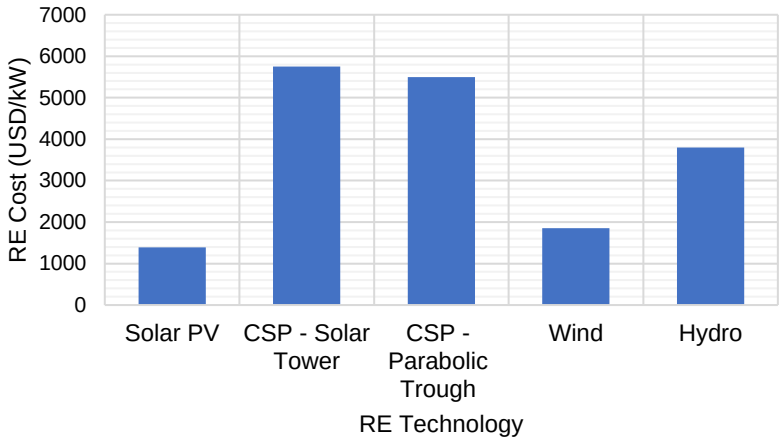

Figure 2.17: CSP installed cost breakdown by technology and storage (IRENA , 2017)

2.5 Barriers to DG entry

Whilst South Africa is blessed with natural resources, there are barriers to entry Department of Science and Technology, (2014); Pegels, (2014). Luthra et al (2015), gives an Indian perspective which mirrors some of the challenges faced in South Africa. These are technical, financial, awareness of information, geographical, market, cultural and behavioural and government issues. Gabriel, 2016, summarizes challenges for RE penetration which includes; securing investor/financier interest, grid distribution, preparedness & stability, technology price, lack of formal industry standards, competition and/or tension with fossil energy service providers, lack of policy, legislative and tax incentives. Some of these are discussed below:

- Institutional challenges – a lack of clear and coherent policy framework is needed to attract investor confidence. Government bureaucracy, which causes delays in implementation of projects due to lengthy delays in obtaining wheeling licenses

- Lack of innovation – Due to its dependence on coal for electricity generation and fuel, Eskom and Sasol spent significant investment on research and development. It would therefore not be inconceivable to suggest that these parastatals would have a bias towards their own technology and protect their investment

- Cost of technology – the cost of RE technologies is a major barrier to entry in South Africa. The price of fossil-based energy production is still relatively low when compared to industrialized nations. The cost of wind energy, which was the most cost-effective energy in round 4 of the REIPPP, was well below Eskom's blended average cost. Non-utility scale energy production has not reached grid parity yet. High initial capital cost is another major hurdle.

- Financial barriers – There is a clear disconnect between the demand and funding from government. Without initial funding for research and development and continued funding, RE projects will struggle to become commercially viable.

- Geographical – the majority of PV and wind projects are located in the Northern Cape due to excellent irradiation and along the coast due to good wind speed.

2.6 Energy Wheeling

2.6.1 Definition

There are various definitions of wheeling, as highlighted by Sood, Padhy & Gupta, (2002) in a comprehensive bibliographical survey, but in its simplistic form, it can be defined as the bilateral trading of electricity between a generator (seller) and consumer (buyer) under a long term PPA. Babu & Ashok, 2010, defines wheeling as the "*purchase of electricity by a customer from a source other than its own servicing utility*". Figure 3.1, illustrates the energy flow emanating from a wheeling arrangement between and IPP and an off-taker. In a wheeling agreement, energy flows from the IPP to the off-taker via the utility's network. The utility charges the buyer and a seller for costs incurred resulting from the use of the network.

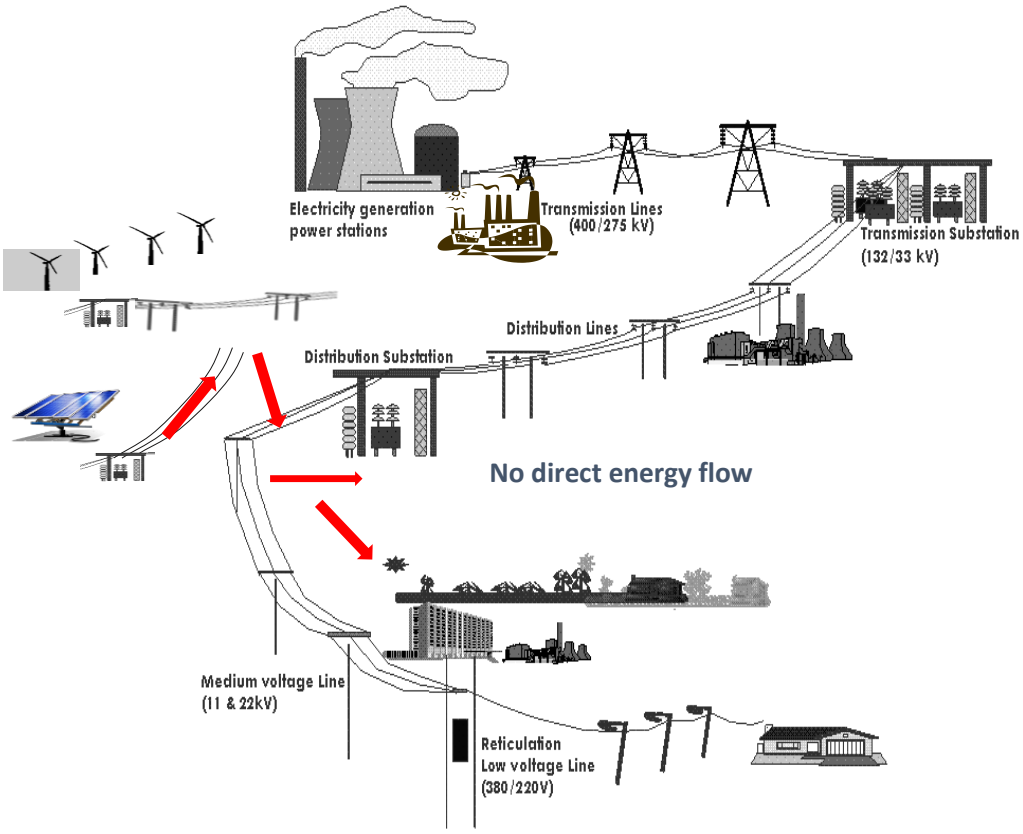

Figure 2.18: Wheeling Structure (Eskom, 2011)

2.6.2 Transmission cost allocations methods

Wheeling charges are an important part of power network operation. It is the price that IPP's and other users of the network pay owners of that transmission network for the use of their network and assets. The aim of applying transmission cost is to recover the cost incurred by transmission (Heeter et al., 2016). These costs can be attributed to:

- CAPITAL – cost recovery of network plant and equipment is based on the valuation of the existing network assets;
- OPERATION and MAINTENANCE (O&M) – typical cost varies between 2.5-5% of the capital cost per annum;
- NETWORK LOSSES – the cost of transmission losses is recovered; and
- CONGESTION – the cost is a result of transmission congestion

Some commonly used rates and cost allocation methods used by the wholesale electricity market are illustrated in table 2.2:

Table 2.2: Historic wheeling rates and cost allocation methods (Heeter et al., 2016)

Pricing methods	Description
Contract paths	The "contract path" is selected between the seller and the buyer without carrying out a load flow analysis. The buyer pays for the costs of any new investment along the contract path based on their use.
Postage stamp	This method uses a fixed cost, independent of the distance between the seller and buyer. Postage stamp is considered the simplest cost recovery method based on its flat transmission charge.
Distance-sensitive pricing (MW-km)	Charges are accrued based on the transmission capacity and total kilometers from the generator to the load. The distance between the generator and the load is based on a straight 'as the crow flies' concept
Load-flow based (MW-km)	This method calculates the cost per MW-km of the line. The total cost is determined by taking account of the power flow of transaction and transmission length. Transmission prices are determined in relation to the proportion of the transmission

	system used by individual transactions, as determined by load-flow studies
Nodal Pricing	Each origin and node have its own pricing

France, Spain, Mexico and the Philippines uses the MW postage stamp method, while South Africa used a zonal postage charge method until it was replaced by the distance sensitive pricing method in 2003. Brazil uses the load-flow based method.

2.6.3 Global perspective

2.6.3.1 United States of America

The USA's grid is quite unique in that it consists of three independently synchronized grids. The national grid is divided into the Western, Eastern and Electricity Reliability Council of Texas Interconnections and interconnected by direct current (DC) lines (Heeter et al., 2016). The electric power industry consists of more than 3200 entities that supply power to industrial, commercial and residential customers (Heeter et al., 2016). These electricity supply entities consist of a) investor-owned-utilities (IOU), which generate, transmit and distribute power to customers within the region b) locally public-owned systems c) rural electric cooperatives d) public joint access agencies e) Federal power agencies and f) co-generation and small power producers.

The energy regulatory body in the USA is the Federal Energy Regulatory Commission (FERC), which is an independent body that regulates electricity sales and transmission rates (Heeter et al., 2016). The FERC's mandate regarding wheeling is to ensure that the rates for wheeling is not discriminatory and that the same rates apply for all electricity generators. In April 1996, the FERC deregulated wholesale and bulk transmission and issued an order to provide open access of their systems under a regulated Open Access Transmission Tariff (OATT). Before 1990, many state utilities were vertically integrated, i.e. they were responsible for generating, transmission and distribution of electricity. During the subsequent years, these state utilities changed their structure to separate generating, transmission and distribution companies, forming what is today known as Independent System Operators (ISO's) and Regional Transmission Operators (RTO's) (Heeter et al., 2016). Energy wheeling from renewable energy sources can take place within one or multiple states. Wheeling charges accrue when the grid is accessed within an ISO and RTO grid. These charges are paid to Participating Transmission Owners (PTO's) by the ISOs/RTOs which covers the cost of all operating and capital costs (Heeter et al., 2016).

The state of California, which electricity tariffs were approximately 50% above the national average was the most aggressive in terms of deregulation. In March 1998, California became the first state to offer customers a choice of service providers. California Independent System Operator (CAISO), adopted the postage stamp wheeling method and has a uniform single access transmission charge rate for high and low voltage. California's wheeling charge as of July 2017 for voltages higher than 200 kV, is 11.6747 $/MWh including an additional LV wheeling charge where applicable (CAISO, 2017). New York Independent System Operator (NYISO) is another state that uses the postage stamp method. Wheeling tariffs varies, based on ISO's (Heeter et al., 2016).

The Sacramento Municipal Utility District (SMUD), offers wheeling services to generators within its borders subject to a) network availability, b) the generator has a signed PPA with an off taker, c) the generator is connected to SMUD grid d) power is wheeled outside the municipality's borders (SMUD, 2017). The municipality's wheeling charges are based on a cost per kilowatt. An additional fixed line loss cost is charged for wheeling electricity outside the municipal borders.

Table 2.3: Sacramento distribution wheeling rates (SMUD, 2017)

Charge	Distribution Voltage	
	12/21 kV	69 kV
Wheeling charge ($/kilowatt-month)	$9.452	$1.472
Line loss factor	4.06%	1.53%

2.6.3.2 Mexico

Wheeling of energy and the development of renewable energy in Mexico, was driven by the Renewable Energy Act of 2008, passed by the Ministry of Energy. The mandate when the act was passed, was to achieve 35% of electricity demand by renewable energy by 2024. Before 2013, Mexico's state-owned utility, Federal Electricity Commission (CFE) was responsible for the generation, transmission and distribution of electricity (Heeter et al., 2016). The state-owned utility did however allow self-generation, co-generation and procurement of electricity from IPP's.

In December 2013, the National Center for Energy Control (CENACE), separated from CFE to become an independent system operator. Under new legislation, CFE's

monopoly as a buyer and seller of electricity was limited, which opened the door for IPP's (Heeter et al., 2016). Wheeling rates for renewable energy projects in Mexico uses the postage stamp pricing method. The wheeling rates for renewable energy generators is more favourable when compared to traditional energy generators. Figure 2.19, illustrates Mexico's postage stamp model with corresponding rates according to voltage levels.

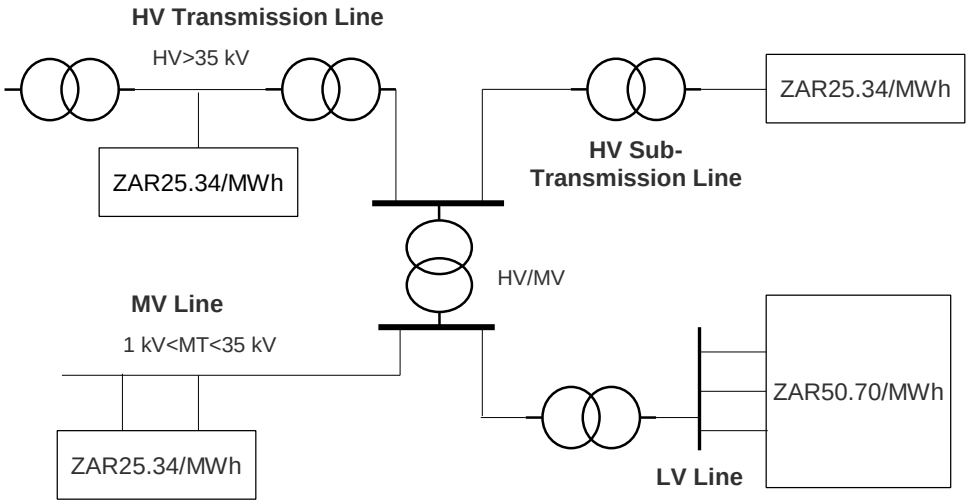

Figure 2.19: Postage stamp model wheeling charges (Heeter et al., 2016)

Wheeling charges are based on fixed rates and not on the distance between a generator and the load. The rates are calculated based on cost related to:

- The infrastructure
- Losses
- Services related to transmission
- Administration charges of the contract

The benefit of this wheeling cost method is that IPP's are not disadvantaged based on the distance from the load, as a fixed cost is used. This provides project developers with a sense of security regarding the transmission cost for the project. This method has particularly benefitted wind projects, which is located far from the load (Heeter et al., 2016).

2.6.3.3 India

Renewable energy accounted for 37 GW of the total installed generation capacity of 302 GW in India by 2016 (IRENA, 2017). As with many other countries, India's power sector consists of generation, transmission and distribution. Only generation has an

element of private investor ownership. Transmission is operated by the Power Grid Corporation of India Limited, a parastatal, which is 100% government owned (IRENA, 2017). The Electricity Act of 2003 provided a framework that allowed unrestricted access to the grid and encouraged competition amongst electricity suppliers. Consumers were empowered to select their choice of power source. Wheeling charges for the use of the transmission and distribution network are payable to respective operators. These charges are a) Cross Subsidy Surcharge, b) Transmission Charges & Transmission Loss ($/MW/month), c) Wheeling Charges & Wheeling Loss Compensation and d) Additional Surcharge (IRENA, 2017).

Table 2.4: Rajasthan equivalent wheeling charges (Rajasthan Energy, 2017)

Charge	Distribution Voltage		
	132 kV	33 kV	11 kV
Wheeling charge (kWh)	ZAR0.002	ZAR0.022	ZAR0.064
Line loss factor	-	3.8%	12.60%

Wheeling charges in the Indian states of Madhya Pradesh and Rajasthan applies to the end-user only and the cost recovered by the network provider is not related to network related costs, which is the norm in other markets. The cost charged to the end-user is based on the distribution voltage level which is 33 kV, 11 kV and Low Voltage (LV) as well as a separate line loss factor (Heeter et al., 2016). The equivalent rate per voltage level is shown in table 3.3.

2.6.3.4 Philippines

The Philippines power sector consist of generation, transmission, distribution and supply. The National Power Corporation (NPC) used to monopolize generation and transmission until the introduction of the Electric Power Industry Reform Act of 2001 (KPMG, 2014). The Act was instrumental in allowing consumers to procure electricity from private generators provided these generators are licensed by the Energy Regulatory Commission (ERC) (KPMG, 2014). Electricity is distributed to end-users by investor-owned utilities (IOU's), government-owned utilities and electric cooperatives.

2.6.4 South African context

Eskom, which is a government parastatal is responsible for more than 95% of power generation and transmission as illustrated in figure 2:20.

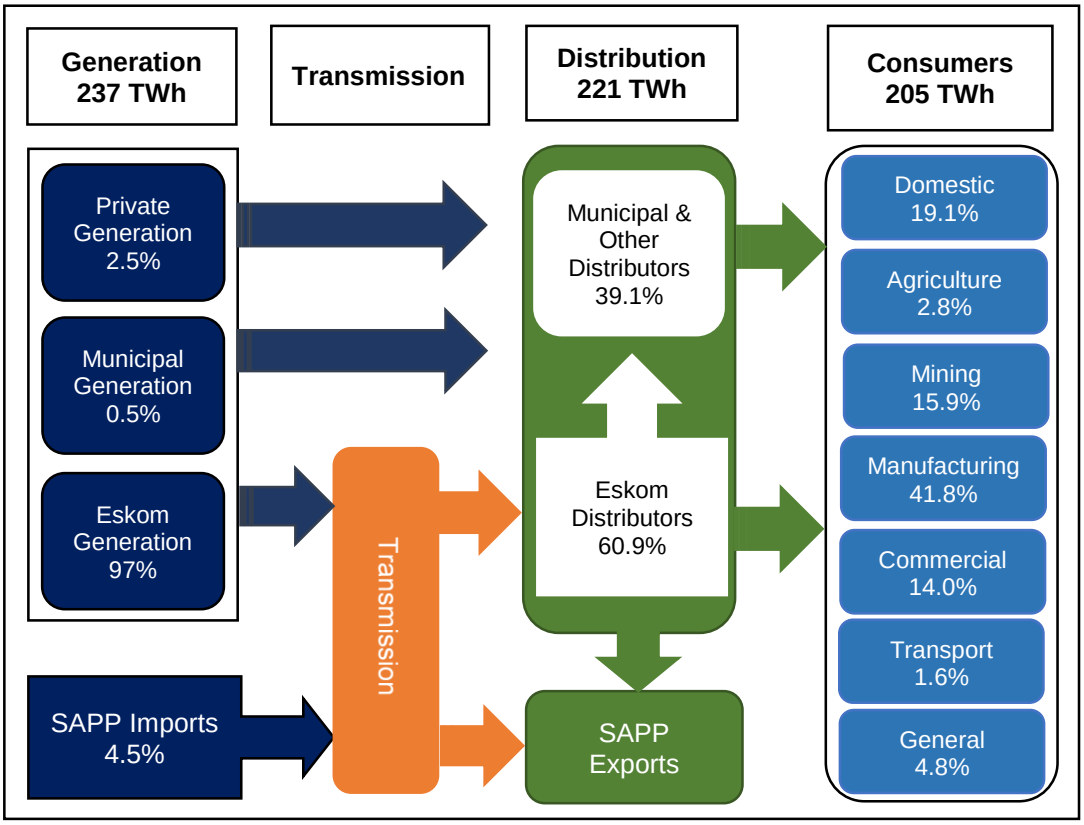

Figure 2.20: Energy flow in South Africa (Eskom, 2015)

Wheeling of power in South Africa therefore would require the use of Eskom's transmission network in the majority of cases. The Electricity Regulation Act (Act No. 40 of 2006), states that "*transmission or distribution function shall provide non-discriminatory network access to all users of the transmission or distribution system*". Wheeling in South Africa using Eskom or a municipal network is thus allowed, subject to NERSA's approval.

According to NERSA's "Process and pricing of wheeling" published in 2011, wheeling will be allowed based on the following conditions (NERSA, 2011):

- The generator must obtain a wheeling licence from NERSA
- Either the buyer or the generator must be an Eskom customer. Eskom will not be involved where its transmission network is not required
- A generator will be required to have signed a connection and use-of-system agreement with Eskom. If within a Municipal area of supply, a connection and use-of-system agreement will need to be concluded with the Municipality.
- The account(s) will be adjusted in terms of Eskom's policy on the reconciliation of accounts

- The buyer of the energy must agree to allow Eskom to do the wheeling reconciliation
- Generators will not exceed 300 MW (currently being revised)
- A generator will not connect at low-voltage (<1 kV)

Eskom recently changed its electricity retail tariff from a bundled, where all the charges were wrapped as one, into an unbundled tariff. The Wholesale Electricity Pricing System (WEPS) which provided a detailed cost breakdown was developed to give greater transparency (NERSA, 2011).

The WEPS consists of:

- A time and season differentiated energy charge
- A transmission use-of-system (TUOS) charge that recovers the cost of losses caused by the transmission of energy
- A geographic, voltage and urban/rural differentiated distribution use-of-system (DUOS)
- A customer service and administration charge

All wheeling charges are standard network related tariff charges. The generator is charged for what is exported and will pay NERSA approved standard general-use-of-tariff (GUOS) related charges. The consumer will pay for what is delivered at UOS charges based on the generator's location or voltage and the MW capacity. The detailed charges pertaining to a wheeling agreement between a generator and consumer is summarized below:

- Connection charges – once off distribution charges based on customer specific costs

- Network charges – Distribution network charges for consumers are based on the cost per kVA demand determined using notified annual maximum demand (NMD). Transmission network charges for consumers are charged in R/kVA per month, based on the customer's maximum demand with a surcharge differentiated into four zones based on the distance of the load in kilometres from Johannesburg. The transmission network charges for generators is charged in R/MW per month, based on the installed sent out capacity. The transmission network charge (TNC) for generators shall be differentiated into six tariff zones based on the concentration of power generation in South Africa.

- Losses – Generators and consumers are charged for losses. The cost of losses is based on calculated average loss factors for all consumers and generators. The transmission loss factors for consumers are calculated for the 0 to 3% geographic differentiation (and the loss factors for generators are calculated for the six generator zones

- Reliability charge – All loads and generators will be charged for reliability services based on the total energy exported or consumed into/from the network

- Subsidy charge – Users of the network from a load perspective pay only the electrification and rural component of the subsidy. Generators are exempted from paying the electrification and rural subsidy

- Service & Admin charge – Service and administration charges are independent of network operations or installed capacity and will be applied to both loads and generators to recover billing, meter reading and customer support costs.

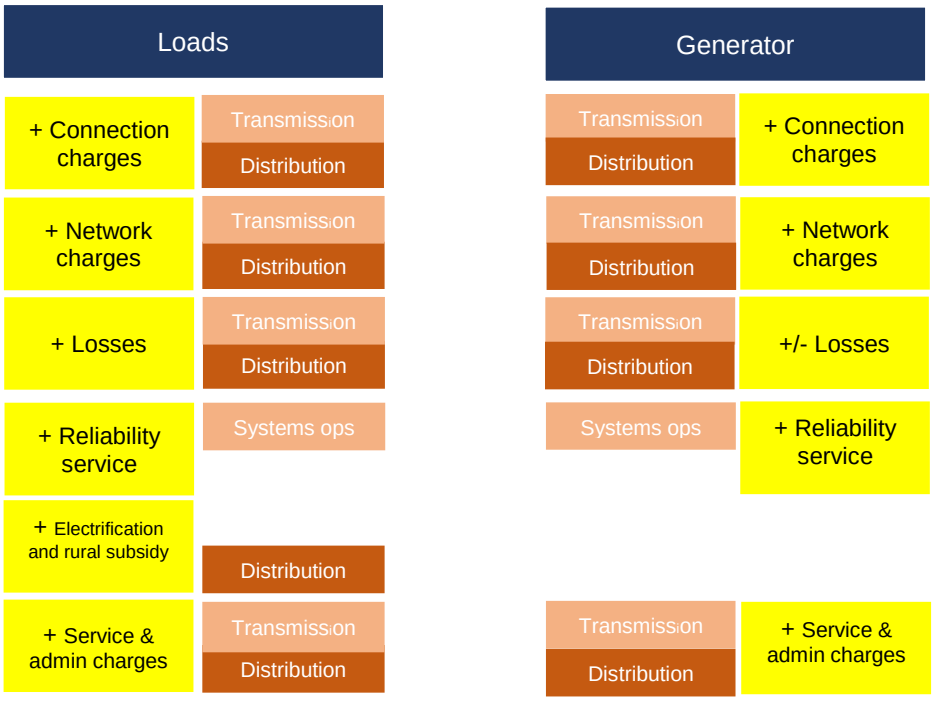

Figure 2.21: Wheeling charges for loads and generators (Eskom, 2011)

2.6.5 Case Studies

2.6.5.1 Power X (Amatola Green Power)

In 2008, Nelson Mandela Bay Municipality became the first municipality in South Africa to connect small scale embedded generators to the municipal network (ICLEI, 2015). Subsequently, the municipality adopted policies wherein it set a target of procuring 10% of total demand from renewable energy sources. This paved the way for the first wheeling contract in South Africa between PowerX (previously Amatola Green Power) and the Nelson Mandela Bay Metro Municipality (NMBMM) on a 20year non-exclusive PPA (ICLEI, 2015). The signing of this wheeling agreement in 2013, was a historical achievement as it paved the way for similar agreements.

The company's business model is to procure access energy from various renewable energy sources and to sell this to consumers, based on PPA's of up to 20 years (PowerX, 2017). Approximately 5 GWh are wheeled from Electrawind's Coega Wind Farm to BHB Billiton. PowerX's tariffs varies between R0.80 and R1.40 per kWh. IPP's are paid between R0.62 and R1.05 per kWh supplied. The wheeling agreement between NMBMM and PowerX as depicted below in figure 3.5 below, states that the wheeling charge payable to the municipality will be approximately 20% of the value of the energy wheeled, which covers all network costs. The agreement is a commercial agreement but all technical standards relating to renewable energy generators connecting onto the grid must be adhered to as stated in the Grid Connection Code for Renewable Power Plants (SEA, 2017).

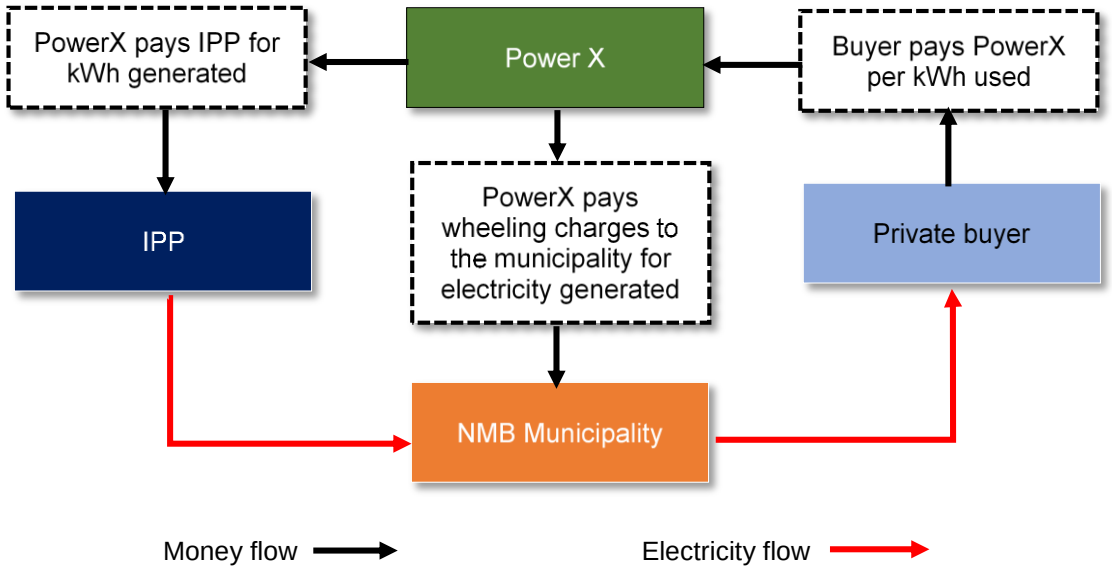

Figure 2.22: Schematic of wheeling arrangement (adapted from SEA, 2017)

2.6.5.2 The Bronkhorstspruit Biogas Project

South Africa's first animal-waste-to-energy plant was conceptualized in 2007, but only took full commercial operation in October 2015. The business model and the technology used during the project was new and many important lessons were learnt from this pioneering project. The Bronkhorstspruit Biogas Project is situated 40 km east of Pretoria on one of South Africa's largest feedlots.

Figure 2.23: Bronkhorstspruit Biogas Project (Bio2Watt, 2015)

The farm houses more than 25 000 cattle, which produce more than 40 000 tonnes of manure per annum (SEA, 2017). This waste is supplemented by an additional 20 000 tonnes of municipal and chicken waste obtained from a nearby abattoir. Methane and CO_2 is produced by this decomposed waste, which fuels a gas engine, which produces electricity. The project was conceptualized, developed and built at a cost of R135m by Bio2Watt (Pty) Ltd, an industrial scale waste-to-energy company.

The Industrial Development Corporation (IDC) provided 70% of the funding with the remaining 30% provided by equity finance funded by Bio2Watt and a host of other private investors (SEA, 2017). The project was initially earmarked to sell electricity to the municipality but due to a lack of regulations, another off-taker was approached. Bio2Watt obtained a generating licence from NERSA to export 4.2 MW based on the capacity of the plant with the option to increase this to 5 MW, depending on the available waste resources (SALGA, 2015). In 2009, Bio2Watt started negotiating a PPA with BMW manufacturing plant in Rosslyn, north of Pretoria. The terms of the agreement were to supply 3.3 MW based on a 10year PPA. The price of producing electricity from the Bronkhorstspruit site was higher than municipal tariffs, but the contract was signed based on the assumption that tariffs would increase over the next few years which would make the project viable. The developer signed two ten-year wheeling agreements with Eskom and the City of Tshwane whereby electricity would

be generated at the site and wheeled 40 km via Eskom's grid and the municipality's network to the end-user (SEA, 2017).

2.6.5.3 Darling Wind Farm

The Darling Wind Farm is situated between Darling and Yzerfontein, in the wind rich area along the west coast of South Africa. The project was developed in 2007 as a national demonstration project by the Darling Independent Power Producer, the Central Energy Fund, the Development Bank of South Africa, and the Government of Denmark and completed in 2008 (SEA, 2017). The farm comprises of four 1.3 MW turbines, producing 5.2 MW of electricity, was built at a cost R75-million. This was South Africa's first commercial wind farm.

The project and sites were identified in 1997 but was only completed in 2008 due to many delays, including a) additional environmental impact assessment (EIA) studies in 2004 b) negotiating a PPA with the City of Cape Town, the eventual off-taker and c) negotiating a wheeling agreement with Eskom (SEA, 2017). In 2006, The City of Cape Town council approved the signing of a 20year PPA with the Darling Wind Farm. The City intended to sell this renewable energy to consumers at R0.25 per kWh above the electricity tariffs of 2008 (SEA, 2017). Due to the cost of electricity produced at that time, the City was unable to sell this electricity to private customers. Almost 10 years later, electricity generated from this wind farm has reached grid parity which shows the progress made in technology and cost.

Figure 2.24: Darling Wind Farm (Darling windfarm, 2010)

2.7 Connecting Distributed Generation to the Distribution Network

2.7.1 Distribution System

Traditional power plants were designed to transmit real and reactive power at high voltages and transported to load centres at lower voltages via a network of transmission lines (Jenkins, Ekanayake & Strbac, 2010). In most industrialized nations, power plants were designed to generate electricity at a central location some distance away from the consumer (Baggini, 2008). These centralized power plants, whether fossil fuel based, hydro or nuclear are located away from the end consumer.

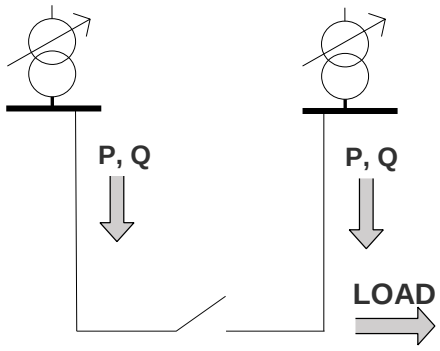

Figure 2.25: Conventional power flow (Jenkins, Ekanayake & Strbac, 2010)

Generation, transmission and distribution was designed based on a passive system with unidirectional energy flow (Baggini, 2008). With an increase penetration of distributed generation, the conventional power distribution system has been transformed into an active system (Jenkins, Ekanayake & Strbac, 2010). Power is assumed to flow from the secondary transformer side to the load as illustrated in figure 2.25 (Jenkins, Ekanayake & Strbac, 2010). Any addition of distributed generation to the network, typically close to the load, would alter the flow of power. The resultant flow of power would be bi-directional as depicted in figure 2.26 (Jenkins, Ekanayake & Strbac, 2010).

Where,

P = Real Power (W)

Q = Reactive Power (var)

A = Asynchronous Generator

S = Synchronous Generator

CHP = Combined Heat and Power

PV = Photovoltaic

CONV = DC-AC Converter

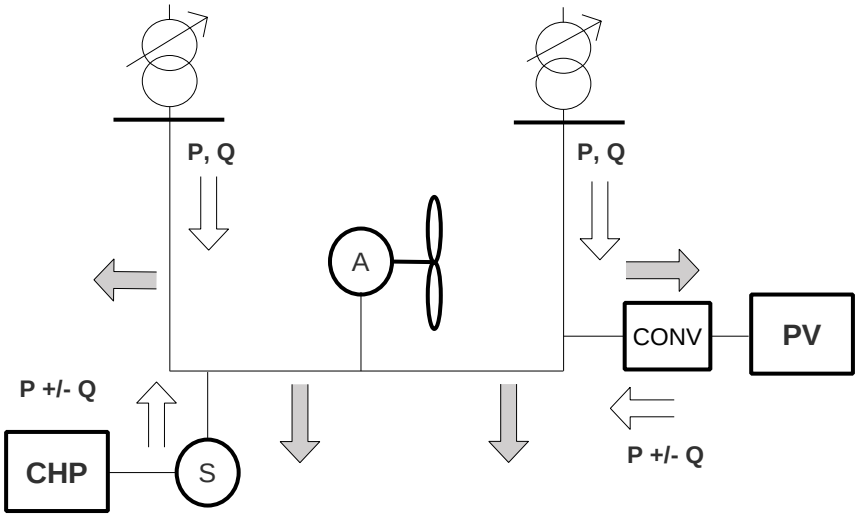

Figure 2.26: Distribution system with Distributed Generation (Jenkins, Ekanayake & Strbac, 2010)

When originally designed, distribution networks did not have to consider technical issues as a consequence of external generators connected to the grid, as the network was passive and stable (Dulau, Abrudean & Bica, 2014). Any addition of distributed generation to the network would naturally lead to technical issues as a result of bi-directional power flow (Baggini, 2008). These technical issues include:

- *Voltage profile changes along the network*
- *Increase in network fault levels*
- *Steady state voltage limits*
- *Protection issues*
- *Technical losses*
- *Thermal loading*
- *Power quality*

The level of generation that can be absorbed onto the distribution network is determined by many factors according to Masters (2002):

- *Voltage level*
- *Voltage at the primary substation*
- *Distance from the primary substation*
- *Size of conductor*
- *Demand on the network*
- *Other generation on the network*
- *Operating regime of the generation*

- *The location where the generator is connected (a strong or a weak distribution network)*

According to Funabashi, 2016, the potential to connect DG to a specific part of the network is determined by:

- *The minimum and maximum voltage limits with respect to the rated value;*
- *The maximum current allowed to circulate in the network branches in steady-state conditions; and*
- *The fault level, usually defined by the rating of existing switchgear*

2.7.2 Impact of DG on voltage profile

One of the primary objectives of supply authorities is to keep voltage levels of distribution networks within their prescribed limits (Gaonkar, 2007). These limitations vary between +/-2.5% and +/-10% of sending voltage, depending on the country and standards adopted. The rise in steady state voltage when connecting DG to the distribution network is a major concern for supply authorities (Gaonkar, 2007).

2.7.2.1 Conventional Distribution System

The voltage in traditional unidirectional distribution systems reduces as the distance from the distribution transformer increases (Dulau, Abrudean & Bica, 2014).This voltage drop is caused by line impedances and load currents flowing through the distribution transformer to the point of connection of the customer. These variations are usually compensated for at the original design stage or by substation and distribution transformer tap settings, fixed capacitor banks or voltage regulators on the distribution feeders (Walling et al., 2008). A basic two-bus system volt drop is illustrated by figure 2.27 (Viawan, 2008).

Where,

V_S = sending voltage (V)

V_1 = voltage at the transformer secondary side (V)

V_2 = voltage at the load busbar (V)

P = real power flowing though the network (W)

Q = reactive power flowing through the network (var)

P_L = real power at the load (W)

Q_L = reactive power at the load (var)

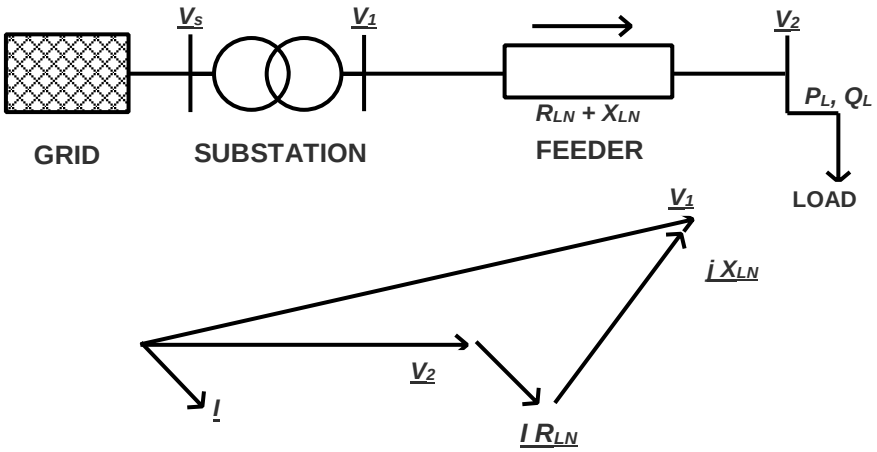

Figure 2.27: Conventional two-bus distribution feeder and corresponding phasor diagram for a voltage drop (Viawan, 2008)

The current I as a function of the apparent power S and the voltage at V_2 is given by:

$$I = \frac{S}{V_2} = \frac{PL - jQL}{V_2}$$

(Equation 4.1)

The volt drop on the feeder is given by,

$$V_1 - V_2 = I(R_{LN} + jX_{LN}) = R_{LN} P_L + X_{LN} Q_L - \frac{j(X_{LN} P_L - R_{LN} Q_L)}{V_2}$$

(Equation 4.2)

For a small power flow, the voltage angle between $V_1 – V_2$ is small and the imaginary part can be neglected. The voltage drop therefore can be approximated by

$$\Delta V \approx \frac{R_{LN} P_L + X_{LN} Q_L}{V2}$$

(Equation 4.3)

2.7.2.2 Distribution systems with DG

DG can be connected to the grid by synchronous, induction generators or power electronic interface whereby it either generates or absorbs reactive power (Viawan, 2008). Induction or asynchronous generators always consumes reactive power whereas synchronous generators can supply and absorb reactive power depending on the excitation (Dulau, Abrudean & Bica, 2014). The behaviour of the network changes when DG is connected to the grid. Active power from the generator flows to the load

and similarly reduces the power flow from the substation. If the penetration of DG increases beyond the load size, power will flow towards the substation, which will cause an increase in the volt drop along the feeder (Gaonkar, 2007).

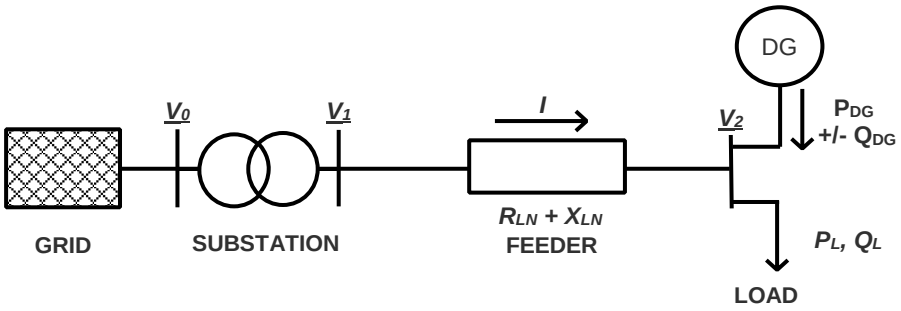

Figure 2.28: Conventional two-bus distribution feeder diagram with DG (Viawan, 2008)

A two-bus distribution system with DG connected is illustrated in figure 2.28. The volt drop on the feeder can be represented by

$$\Delta V = V_1 - V_2 \approx R_{LN}(P_L - P_{DG}) + X_{LN}(Q_L - (+/-Q_{DG})/V_2$$

(Equation 4.4)

Where,

P_{DG} and Q_{DG} are the real and reactive power produced by the DG. From above, the level of DG that can be connected to the network is influenced by:

- voltage at the primary distribution system
- voltage level of the receiving end
- size of the conductors as well distance from the primary distribution system
- load demand on the system
- other generation on the system

For the maximum allowable DG penetration, the utility must ensure the voltage limits are not exceeded for the worst operating conditions (Viawan, 2008). These are:

- no generation and maximum load
- maximum generation and maximum load
- maximum generation and minimum load

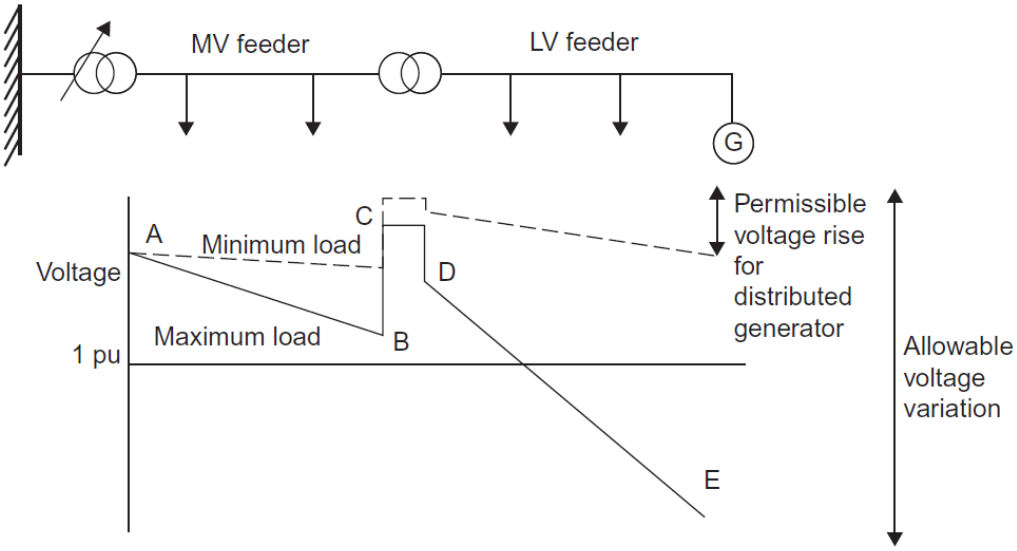

Figure 2.29: Voltage variation along a feeder (Jenkins, Ekanayake & Strbac, 2010)

Figure 4.5, above is an illustration of the voltage variation along a typical feeder which is typically allowed by network operators to be +/- 5% of nominal voltage where:

- A: voltage held constant by tap-changer of distribution transformer
- A–B: voltage drop due to load on medium voltage (MV) feeder
- B–C: voltage boost due to taps of MV/LV transformer
- C–D: voltage drop in MV/LV transformer
- D–E: voltage drop in LV feeder

2.7.3 Impact of DG on fault level

Conventional distribution networks are designed to address normal operating conditions such as breakdown of insulation or mechanical damage (Jenkins, Ekanayake & Strbac, 2010). When a fault current occurs at any point on the network, the current will naturally flow towards the point where the fault occurred. The increased penetration of DG provides an additional source to the fault current. An increase in fault current is detrimental to switchgear and cables (Jenkins, Ekanayake & Strbac, 2010). Fault current contribution is determined by:

- The type of DG
- Distance of the DG from the fault
- Whether or not a transformer is present between the fault location and the contributing DG
- The configuration of the network between the DG and the fault

- The method of coupling the DG to the network (direct or inverter based)

2.7.3.1 Short circuit in a conventional network

The fault current in a network will be the vector sum of all the contributions of the upstream grid, impedance of the line and other equipment such as large motors connected to the distribution network as illustrated in figure 2.30 (Zabava et al., 2015). The maximum fault current is calculated using three-phase faults when the network neutral is earthed. The three-phase symmetrical short current using the equivalent voltage source is given by:

$$Ik = \frac{cVn}{\sqrt{3Zk}} = \frac{cVn}{\sqrt{3}(Z_T + Z_L + Zs)}$$

(Equation 4.5)

Where,

Zk = equivalent short-circuit impedance of the electric network at the short-circuit location F (Ω)

Zs = impedances of the network feeder (Ω)

Z_T = impedance of the transformer (Ω)

Z_L = impedance of the load (Ω)

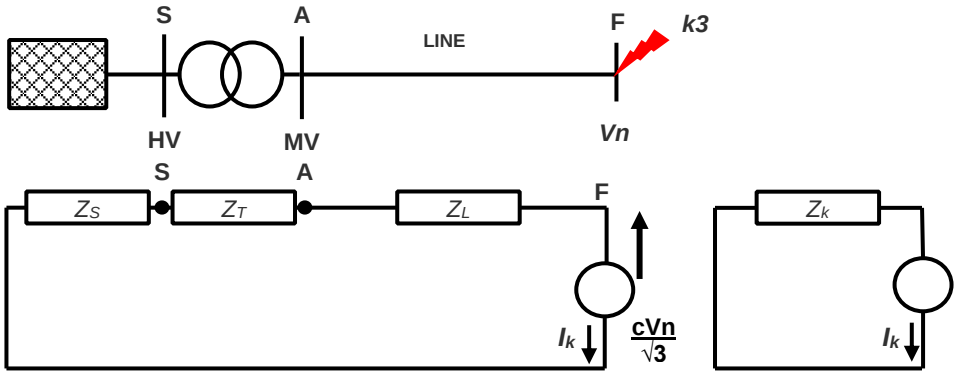

Figure 2.30: Symmetrical short circuit current using equivalent voltage source (Zabava et al., 2015)

2.7.3.2 Short circuit with DG connected

In a circuit with DG, the fault current at any point in the network is the vector sum of the fault from the grid, transformers and connected DG. Figure 2.31, is an illustration of a three-phase symmetrical fault, simulated on a two-bus system using the equivalent voltage source method (Zabava et al., 2015). The short circuit current is given by:

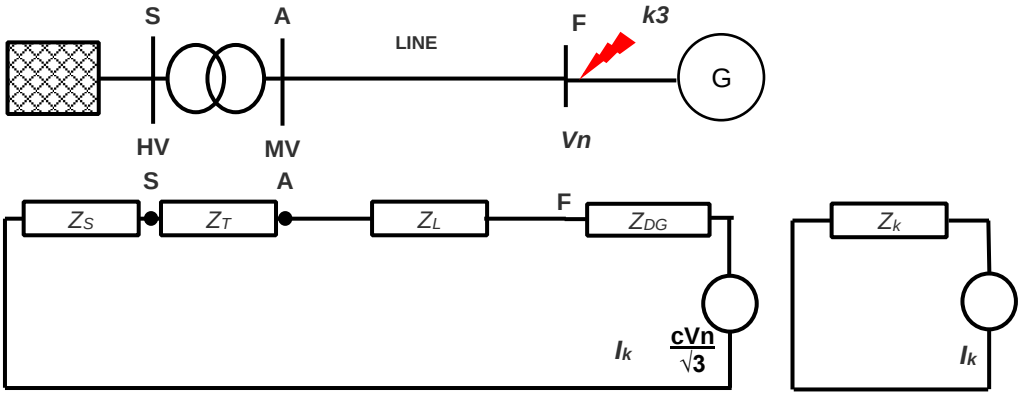

Figure 2.31: Symmetrical short circuit current with DG connected (Zabava et al., 2015)

$$Ik = \frac{cVn}{\sqrt{3Zk}} = \frac{cVn}{\sqrt{3}(Z_{DG} + Z_T + Z_L + Zs)}$$

(Equation 4.6)

Where Z_{DG} is the equivalent impedance of the distributed generation (Ω)

The fault current contribution by synchronous generators to a three-phase fault can be expressed as:

$$I(t) = E_F[\frac{1}{X} - \left(\frac{1}{X'} - \frac{1}{X}\right)e^{-\frac{t}{T'}} + (1/X'' - 1/X')e^{-t/T''}]\cos(\omega t + \lambda) - E_F/X''e^{-t/Ta}\cos\lambda$$

(Equation 4.7)

Where,

X = synchronous reactance (Ω),

X' = transient reactance (Ω),

X'' = sub-transient reactance (Ω),

E_F= pre-fault internal voltage (V),

T' = transient short-circuit time constant (s),

T'' = sub-transient short circuit time constant (s),

Ta = armature (DC) time constant (s),

λ = angle of the phase at time zero (°),

ω = system angular velocity (m/s)

When compared to distribution circuits, synchronous machine impedances have a higher X/R ratio which result in an armature time constant (Ta) and DC component that last much longer for a fault close to the generator (Jenkins, Ekanayake & Strbac, 2010). Conventional power systems behave in an opposite way where the DC offset has a rapid decay and constant AC component (Jenkins, Ekanayake & Strbac, 2010). The time response of a synchronous generator is illustrated in figure 2.32.

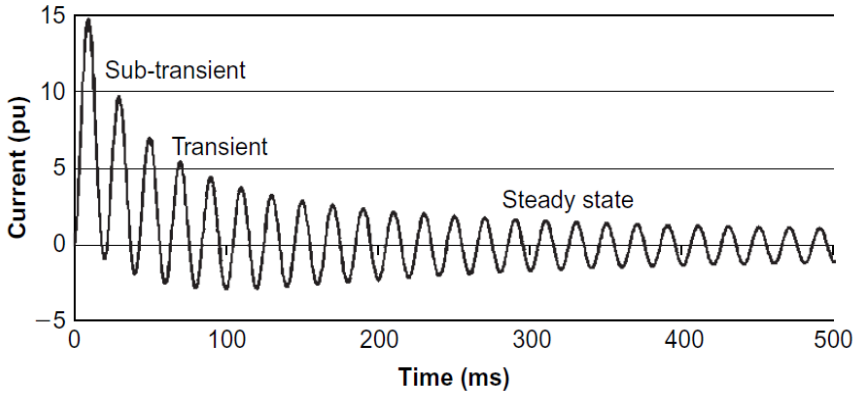

Figure 2.32: Synchronous generator close-up fault
(Jenkins, Ekanayake & Strbac, 2010)

The fault contribution of an induction generator is different to that of a synchronous generator. The transformer equivalent circuit is used to describe the behaviour of an induction generator under fault conditions (Jenkins, Ekanayake & Strbac, 2010).

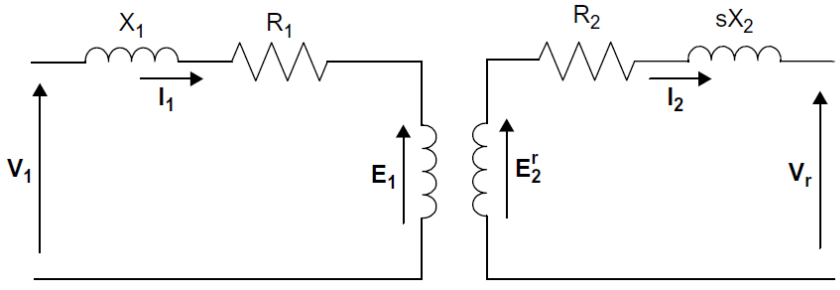

Figure 2.33: Induction generator equivalent circuit
(Jenkins, Ekanayake & Strbac, 2010)

In figure 2.33, the rotor is short circuited and Vr becomes zero. The value of $V_{1,}$ will be reduced when a fault occurs in the network, making the magnetic field and

subsequently E_1 the same as before the fault occurred. This causes the stator current to be reversed and the generator to feed into the fault. The size of the fault is proportional to the value of E_1 and V_1 (Jenkins, Ekanayake & Strbac, 2010). The rotor current is given by,

$$I_2 = \frac{E_2^r}{R_2 + jsX_2}$$

(Equation 4.8)

Where,

E_2^r = sωøk (ø = magnetic field at the air gap; k = proportional constant)

If a fault occurs at the terminals of the generator, V_1, becomes zero. The magnetic field collapses as illustrated in figure 2.34 as magnetising current cannot be sustained. The magnetic field will not diminish immediately after the fault, but the fault current will decay to zero over time (Jenkins, Ekanayake & Strbac, 2010).

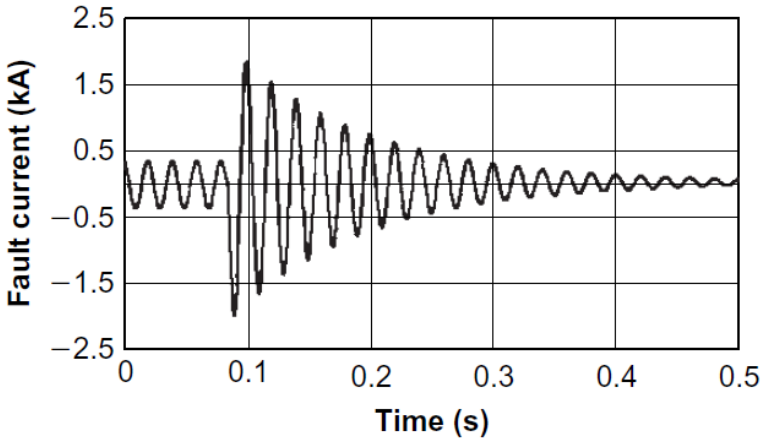

Figure 2.34: Fault current of Induction generator at its terminals (Jenkins, Ekanayake & Strbac, 2010)

The rotor current for a three-phase fault at the terminals of the generator is given by,

$$I_{2\_fault} = \frac{E_{2\_fault}^r}{R_2 + j(^{\omega_r}/_{\omega_s})X_2}$$

(Equation 4.9

$(^{\omega_r}/_{\omega_s})X_2$ = rotor reactance (Ω)

With r/ωs ≈ 1, the rotor current for a three-phase fault at the terminals can be rewritten as:

$$\frac{I_{2\_fault}}{I_2} \approx \frac{1/_S}{1 + j\left(X_2/_{R_2}\right)}$$

(Equation 4.10)

The fault current contribution of an induction generator to a three-phase fault at its terminals may be expressed as,

$$I(t) = \frac{V_1}{X^{"}\left[\cos(\omega t + \lambda)e^{-t/T^{"}} + \cos(\lambda)\, e^{-\frac{t}{Ta}}\right]}$$

(Equation 4.1)

Where,

$X^{"}$ = $X_1 + X'_2X_m/X'_2 + X_m$ *(Ω)*

$T^{"}$ = $X"/\omega R'_2$ *(s)*

T_a = $X"/\omega R_1$ *(s)*

X'_2 = *stator-referred rotor reactance (Ω)*

R'_2 = *stator-referred rotor resistance (Ω)*

Inverter based DG (IBDG), uses power electronic devices such as DC-AC inverters and DC-DC converters to connect to the utility's grid. Inverters and converters are static electronic devices which do not develop inertia, therefore the fault current is different from rotating machines. Figure 2.35 is an illustration of grid connected DG with power electronic interfacing.

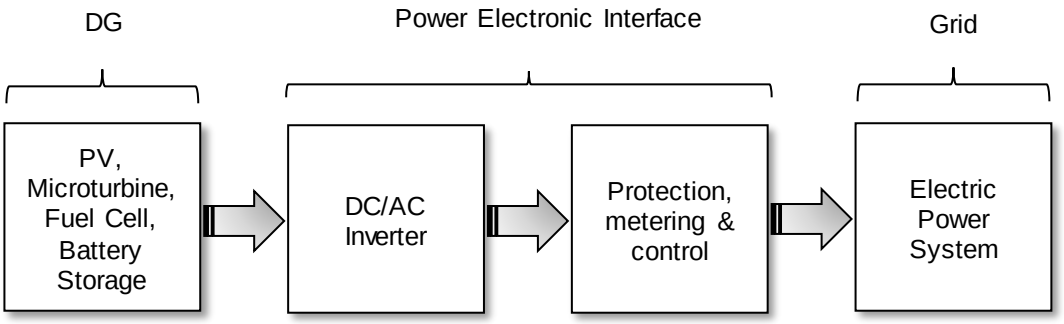

Figure 2.35: Inverter based DG block diagram (Keller & Kroposki, 2010)

The maximum fault level contribution, which is typically 200% of rated current and decay time of a fault of power electronic interfaces is much smaller than rotating machines (Masaud & Mistry, 2016).. The length of time IBDG take to respond to fault

currents, can be controlled, which minimizes the fault current contribution to the system. The effect on the network's protection devices is therefore negligible.

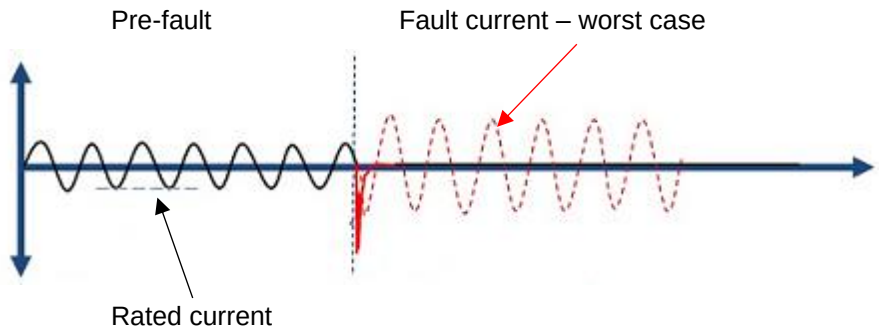

Figure 2.36: Three phase fault current waveform of IBDG (Keller & Kroposki, 2010)

2.7.4 Power loss

Electrical line losses occur in any network. The magnitude of the losses is dependent on the line resistance and the value of the current. One of the advantages of connecting DG close to the load is that it can reduce the power loss in a network as it decreases the current flow in that part of the network (González-longatt, 2007). The utility passes charges incurred by network losses onto the generator and buyer.

Line losses in a conventional network can be calculated by the following equation

$$P_{Loss1} = 3\ x\ I_L^2\ x\ r\ x\ L$$

(Equation 4.1)

where,

P_{Loss1} = electrical line losses (W)

r = line resistance (Ω)

L = distance between substation and load (km)

I_L = line current (A)

With the addition of DG to the network, the resultant line losses are the sum of losses between the substation and the DG represented by (P_{LS_G}) and the losses between the load and DG represented by (P_{LG_L}).

$$P_{LS\_G} = \frac{r\ x\ G}{3V_L^2}\ (P_L^2 + Q_L^2 + P_G^2 + Q_G^2 + 2P_L\ P_G - 2Q_L\ Q_G\ )$$

(Equation 4.13)

$$P_{LG\_L} = \frac{r\ x\ L}{3V_L^2}\ [(P_L^2 + Q_L^2) + (P_G^2 + Q_G^2 - 2P_L\ P_G - 2Q_L\ Q_G)\left(\frac{G}{L}\right)]$$

(Equation 4.14)

The sum of the line losses can be calculated by the following equation

$$P_{LT} = \frac{r\ x\ (P_L^2 + Q_L^2)}{3V_L^2}\ (L - G)$$

(Equation 4.15)

Where,

P_G = DG real power (W)

P_L = load real power (W)

Q_G = DG reactive power (var)

Q_L = load reactive power (var)

V_L = load voltage (V)

G = distance between substation and DG (km)

The change in line losses is calculated by the following equation

$$\Delta P_{Loss} = \frac{r\ x\ G}{3V_L^2\ L}\ (P_G^2 + Q_G^2 - 2P_L\ P_G - 2Q_L\ Q_G)$$

(Equation 4.16)

Where,

ΔP_{Loss} = difference in line losses (W)

The cost of an increase in line losses will be passed on to the buyer and seller, whilst a decrease in losses means the utility will benefit.

2.8 Chapter Summary

This chapter presented an overview of different DG with specific reference to technology, resources and cost. The developments in DG technology and downward trend in cost over the past decade makes DG an increasingly viable alternative source of electricity generation for industry. According to global figures, wind energy is the most cost effective, followed by solar PV. CSP is still a relatively expensive technology but offers the benefit of storage. Lithium-ion battery technology is the most widely used battery storage technology and have been installed as back-up power in large solar farms recently. According to cost projections, the technology is maturing and could be

a viable option by 2020. South Africa's scarce water resources and geography makes hydropower a limited option to industry.

Secondly, the concept of energy wheeling was introduced. Various countries around the world have deregulated their electricity market and have adopted different wheeling and cost allocation methods. These methods can be complex or as simple as the postage stamp method, which uses a fixed cost regardless of the distance between the IPP and the off-taker. South Africa used the postage stamp method but adopted the distance sensitive pricing method in recent years. The common perception regarding wheeling charges is that the cost is too expensive, but according to Eskom, charges are based on standard network charges, which is clearly defined by NERSA. Despite various challenges, a few projects have been commercially viable and successfully implemented.

Thirdly, a mathematical analysis of power flow in conventional networks and the impact of DG on these networks was introduced. The effect on voltage profile, fault levels, thermal loading on equipment and power loss was discussed. The effect on network parameters based on the type of technology and distance from the load was highlighted. Asynchronous and synchronous generators have a greater effect on fault contribution than inverter-based DG. DG can have a positive or negative effect on voltage profile. The point of injection is a major determining factor.

CHAPTER THREE
MODELING AND SIMULATION

3.1 Introduction

This chapter is based on a qualitative analysis using two simulation software tools to determine the viability of DG for industry in South Africa. The aim of this chapter is: firstly to give an overview of the software tools that were selected for simulation; secondly to present the renewable energy resources based on selected sites; thirdly to plot load profiles of the selected industries; fourthly, to do a technical grid evaluation by means of simulation of the passive and active network based on DG technology, voltage profile, fault current, thermal loading of equipment and transmission line loss.

3.2 Simulation Software

3.2.1 HOMER

HOMER Software is an optimisation package which was developed by the National Renewable Energy Laboratory (NREL) in the USA in 1993 (NREL, 2017). The software requires various inputs such as technology options, component cost and resource availability to simulate different configurations on the basis of technical and economic feasibility. The inputs and outputs are summarized in figure 5.1, below. HOMER uses concepts like net present ost (NPC) and levelized cost of electricity (LCOE) to illustrate the economic viability of renewable energy systems (Firinc, Mircea, Hiyasat, & Mircea, 2015). HOMER performs three functions, (Srivastava & Giri, 2016) i.e.:

a) Simulation – An hourly power consumption profile is inserted. The renewable energy generation is then matched to the required load. It simulates the systems for each hour for the year and compares the thermal and electric load for that hour and determine its technical feasibility and life cycle cost.

b) Optimization – After simulation, HOMER optimizes the best feasible systems based minimum life cycle cost. The cost of various energy project scenarios can be determined.

c) Finally, a sensitivity analysis is done to compare the results with a change in inputs.

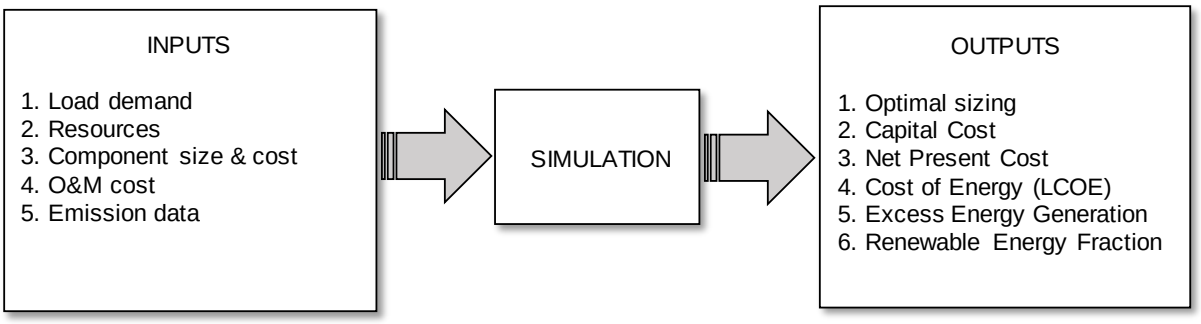

Figure 3.1: Homer inputs and outputs schematic (NREL, 2017)

3.2.2 DIgSILENT Power Factory

This software programme was selected to do load flow simulation and calculations. The software was design for power systems analysis with the objective of grid planning and network optimization. The programme uses load flow analysis for short circuit calculations, harmonic analysis, protection coordination and stability analysis.

3.3 Modelling and Simulation

The test system is based on a modified network which consist of 7 buses and 5 loads. Two loads are based on actual data received from industry based along the west coast of South Africa. These sites are located in an industrial zone close to above average wind resources with mean wind speed above 8m/s measured at 100m above ground level. Additional growth is forecasted for this industrial zone. Key economic activities are based on manufacturing with steel processing playing a major part, mineral mining, agro-processing, tourism industry and harbour industries. Steel and iron and mining was selected as case studies.

Technical and economic simulation is done in DIgSILENT PowerFactory and HOMER Energy software respectively. Two case studies will be conducted to determine the technical and economic viability of wheeling. The components modelled in HOMER Energy for the first case study is a conventional grid, solar PV (modelled as a PV array), wind turbines, hydro turbines and battery back-up (modelled as a battery and converter system). The components for the second case study is a conventional grid, solar PV and wind turbines. The renewable distributed energy resources available to the west coast of South Africa are wind and solar. Other than run-of-river hydropower for the first case study, other renewable resources will not be considered based on economic analysis presented in Chapter 2. Based on the location of renewable resources, the complexity of multiple wheeling agreements with one off-taker, hybrid systems will not

be considered. Each renewable energy source will be modelled separately. Sites, which generate the best yield based on available resources have been considered. Based on renewable resources, three scenarios will be simulated in DIgSILENT PowerFactory. The scenarios will be based on DG technology and distance from the load. The impact on voltage profile, contribution to fault level, equipment loading and power loss will be analysed.

3.4 Test Distribution System

The system below is a test distribution network which represents a section of an actual distribution network. This section of the distribution network will be the focus of this case study. The system consists of a Main Transmission Substation (MTS), which feeds various substations in the area. The MTS feeds two substations, which consist of one 80 MVA transformer, which supplies a 24hour industrial site. The site is approximately 25 kilometres from the MTS. The other substation consists of two 20 MVA transformers feeding other industrial loads. The MTS is 35 kilometres away from the second substation. All loads are modelled as general loads. The detailed specification of the test distribution network is given in table 3.2. The calculations will be limited to voltage regulation, fault level, thermal loading of equipment and power losses in the network as discussed in Chapter 2.

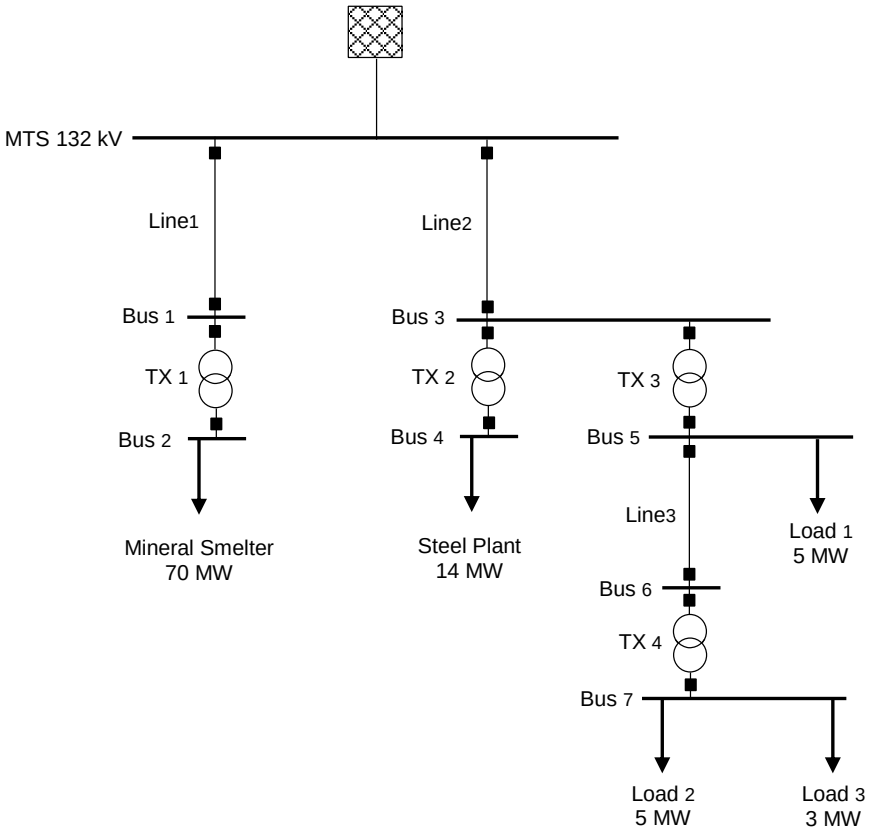

Figure 3.2: One-line diagram of test distribution system

Table 3.1: Specification of test system

Component	Specification
Transmission Line (Wolf)	r = 0.182 Ω/km, x = 0.52 Ω/km, I_r = 269 A,
Distribution Lines	$Line_1$= 25 km, $Line_2$ = 35 km, r = 0.253 Ω/km, x = 0.139 Ω/km, I_r = 262 A, $Line_4$ = 5 km
Substation transformers	TX_1 = 132/33 kV, 80 MVA, x/r = 10, OLTC at HV side, Dyn11 TX_2 = 132/33 kV, 20 MVA, x/r = 10, OLTC at HV side, Dyn11 TX_3 = 132/33 kV, 20 MVA, x/r = 10, OLTC at HV side. Vector group = Dyn11
Distribution transformers	TX_4 = 33/11 kV, 10 MVA, x/r = 10, OLTC at HV side, Dyn11
Load	$L_{smelter}$ = 70 MW with 0.95 pf, V(pu) = 1 L_{steel} = 14 MW with 0.95 pf, Vpu = 1 L_1= 5 MW with 0.9 pf, V(pu) = 1 L_2 =5 MW with 0.85 pf, V(pu) = 0.95 L_3 = 3 MW with 0.85 pf, V(pu) = 0.95
External grid	S_{Sc} = 1000 MVA, x/r = 10

3.4.1 Impact on voltage profile

The network is designed to achieve continuous network voltage at the user's connection. The design limit must not exceed 1.05pu and 0.95pu of nominal voltage during normal operating conditions.

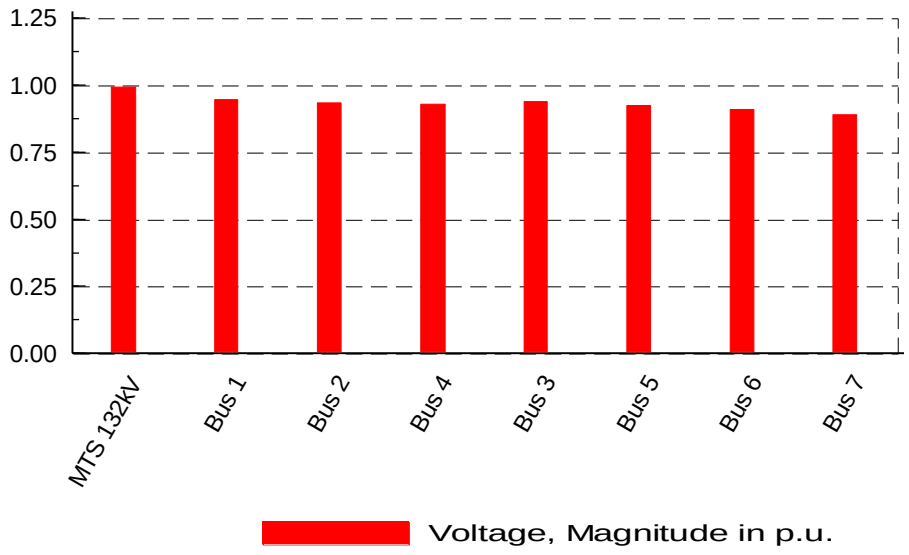

Figure 3.3: Voltage profile at various buses

The voltage profile of the conventional network is typical where the voltage decreases as the distances from the substation increases. The voltages as depicted in figure 3.3 ranges from 0.95pu to 0.89pu at the greatest distance away from the MTS. The voltage at all the buses, except bus 1 violates the lower limit specification which should not exceed 0.95pu of the nominal voltage.

3.4.2 Impact on fault level

Short circuit calculations are an important part of network design. These calculations determine the short circuit capacity which is the maximum allowable fault currents that determine the thermal and mechanical capability of the electrical equipment used at that point in the network. The load flow analysis which shows the fault level at various buses in the network is given in figure 3.4. A requirement for the IPP's connecting DG to the network is that the combined fault contribution from the exiting network and DG should not exceed the designed value.

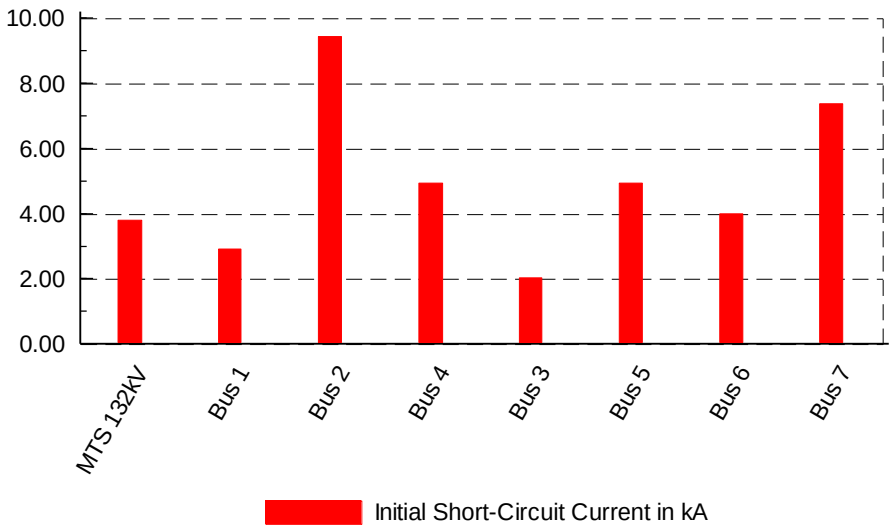

Figure 3.4: Fault level at various buses

3.4.3 Impact on thermal loading of equipment

Distribution and transmission equipment like overhead lines, underground cables and transformers have design limitations with regard to their current carrying capability. If these design limits are exceeded, equipment may be overloaded which can have a severe impact on voltage drops which negatively affects bus voltages along a feeder or transmission line. Exceeding equipment ratings can cause insulation breakdown. It is therefore critical that thermal limits of equipment should not be exceeded. Load flow analysis reveal the loading of the networks equipment. Cables and transformers loading are within design specification.

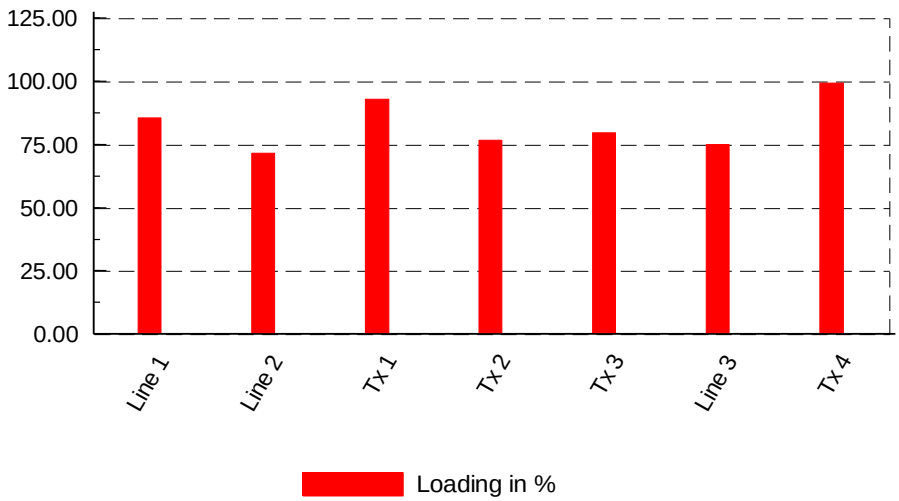

Figure 3.5: Thermal loading of equipment

3.4.4 Impact on power loss

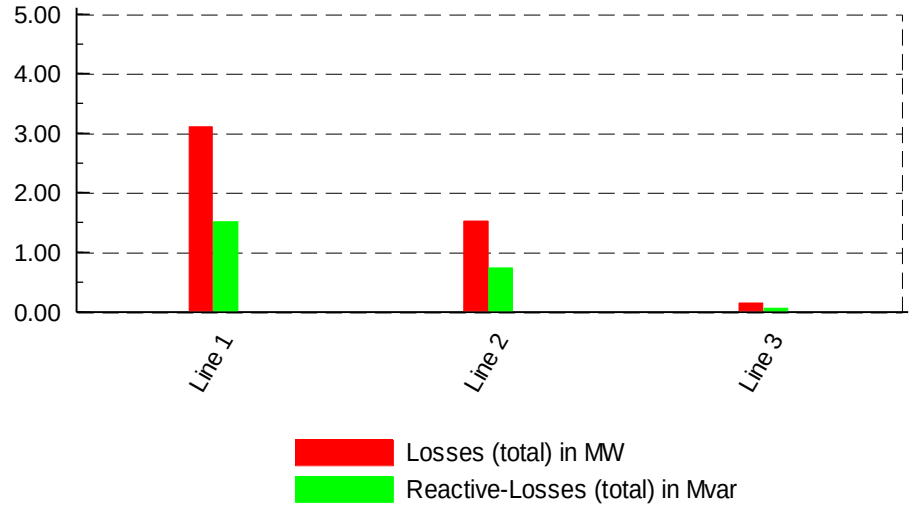

Figure 3.6: Line losses

3.5 Case Study 1 - Steel Plant

3.5.1 Network specification

The first case study is illustrated in figure 3.7. The plant is fed from a 132-kV transmission line by two 20 MVA, 132/33 kV transformers from a nearby MTS substation. Some of the loads are directly supplied by 33 kV and some are supplied via 33/0.4 kV step down transformers. Three DG systems, as illustrated in figure 3.8, will be connected at various distances from the load and connected to the nearby MTS. Energy will be injected at the point of production and transported to the point of consumption via a high voltage overhead conductor.

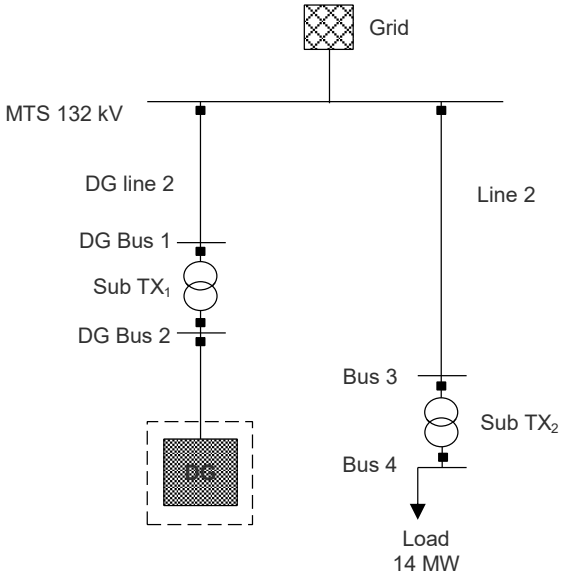

Figure 3.7: Single line diagram of IPP supplying 14 MW load

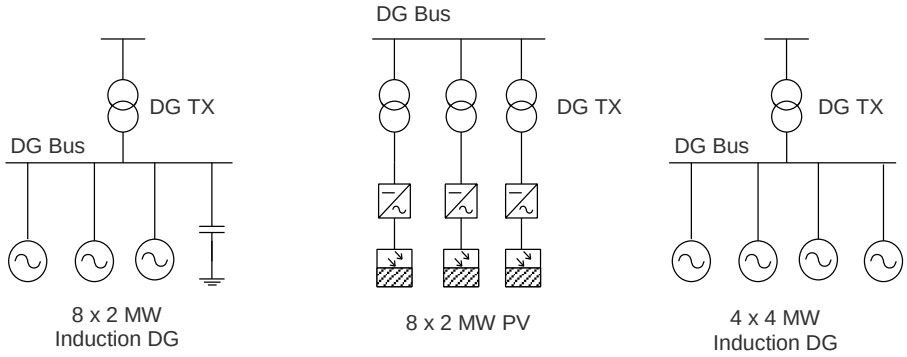

Figure 3.8: Single line diagram of wind system (left) solar PV system (middle) and hydro system (right)

Table 3.2 The specification for case study 1

Components	Specification
Transmission Line (Wolf)	r = 0.182 Ω/km, x = 0.52 Ω/km, I_r = 269 A, Line$_1$ = 25 km
DG transformer (TX)	Dry type cast resin – 11/0.69 kV, P = 2.5 MVA, x = 10%, x/r = 10, Dyn11
Substation transformer (TX_1)	132/33 kV, 20 MVA x/r = 10, OLTC at HV side. Vector group = Dyn11
Load	14 MW with 0.95 pf
Wind Turbine (induction generator)	S = 2.4 MVA, P = 2.05 MW, V = 0.69 kV, pf = 0.855, η = 97%, Rs = 0.01pu, Xs = 0.15pu, Xm = 4pu, Rm = 0.019pu, Xm = 4pu, Rm = 0.019pu, Xm" = 0.199pu,
Hydro Turbine (synchronous generator)	S = 4.5 MVA, P = 4.01 MW, V = 0.69 kV, pf = 0.96, η = 97%, xd = 1.5pu, xq = 0.75pu, rstr = 0.0504pu, Td" = 0.03, Td' = 0.53, xd' = 0.256, xq' = 0.3
DG (PV)	*S=P=2 MVA, V=1000 V*
External grid	S_{Sc} = 1000 MVA, x/r = 10

The detailed specification of the network and DG components is given in table 3.2.

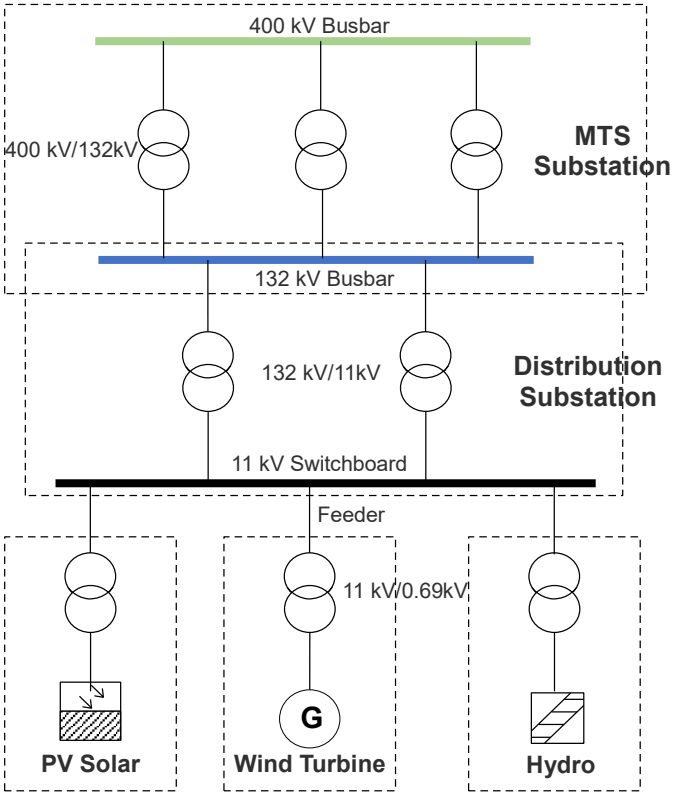

Figure 3.9: Single line diagram of DG interconnection to substation

3.5.2 Load Profile

The steel processing plant is a 24hour industrial facility with notified maximum demand of 20 MVA. The loads range from arc furnaces to light and heavy motor loads. The average monthly electricity consumption of the plant is 5.567 GWh. The average monthly power consumption is 13 MW with a maximum and minimum range of 14.6 MW and 10.5 MW.

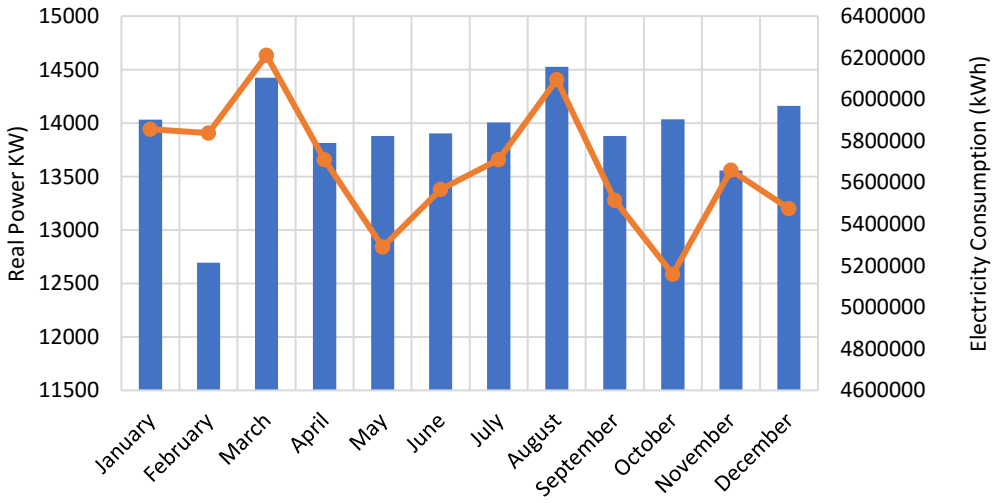

Figure 3.10: Monthly load and consumption profile of Steel plant for 2017

3.5.3 DG Components and Resource Input Data

Four 16 MW DG systems will be simulated and compared to the existing supply in terms of impact of voltage, fault contribution, thermal loading and power loss. These DG systems are a) 16 MW Wind b) 16 MW Solar PV c) 16 MW Hydro d) 16 MW PV + 5 MW, 3hour Lithium-ion battery back-up system. DG systems will be located at various distances from the load as illustrated in table 3.3. The sites were selected based on available wind, PV and hydro resources as illustrated in chapter two. The selected solar sites have good average irradiance and clearness index during the summer months. The clearness index is a measurement of the clearness of the atmosphere express as number between 0 and 1. Due to limited hydropower resources closer to the load, one site, approximately 625 km away, was identified as a potentially suitable site. This limits the viability of hydropower, but still presents an insight into its economic and technical merits.

Table 3.3: Summary of renewable site locations

System	Distance from load (km)		
	Site A	Site B	Site C
16 MW Wind	60	120	270
16 MW Solar	100	485	650
16 MW Solar + 10 MW Battery	100	485	650
16 MW Hydro	625	-	-

The renewable components for each DG system are discusses below:

3.5.3.1 Induction generator (Wind Turbine)

For the first scenario, the impact of wind turbines (induction generators) on the network will be analysed. The Vestas V90-2.0 MW wind turbines, manufactured by Vestas Wind Systems A/S of Denmark is selected for this study. Each turbine has a power rating of 2000 W. The power curve is illustrated in figure 3.11. This technology is established and used worldwide in various wind energy projects. Detailed electrical data is given is given in appendix A. The best wind resources are located along the west and eastern coast of South Africa as shown in Chapter 2. Table 3.4 is a summary of the average wind speed per site.

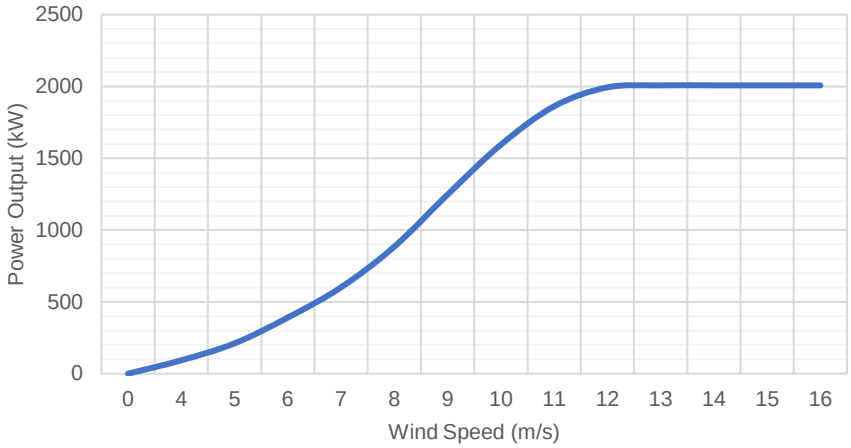

Figure 3.11: Turbine Power curve

Table 3.4: Average wind speed per site (NASA, 2017)

Month	Average wind speed (m/s)		
	Site A	Site B	Site C
Jan	7,08	6,42	5,81
Feb	6,97	6,33	5,90
March	6,55	6,07	5,81
April	6,14	5,79	5,73
May	6,11	5,87	5,96
June	6,75	6,36	6,38
July	6,75	6,37	6,50
Aug	6,55	6,21	6,15
Sept	6,60	6,12	5,94
Oct	7,15	6,56	6,15
Nov	6,92	6,30	5,87
Dec	6,68	6,15	5,82

3.5.3.2 Solar PV

For the second scenario, the impact of solar PV on the network will be analysed. Sunpower E20 327 monocrystalline 327-Watt Peak PV modules will be used for this application. Each module has a nominal power of 327 W with a rated voltage of 72.9 V and a maximum system voltage of 1000 V. This high efficiency PV technology is well established and used in various utility scale projects worldwide. The standard central 2200 kVA inverters will be used. The detailed specification of the solar components is given in appendix B. The average monthly solar irradiance data per site is given in table 3.5.

Table 3.5: Monthly average solar GHI of site A (NASA, 2017)

Month	Clearness index	Daily Radiation ($kWh/m^2/day$)
Jan	8.201	0,685
Feb	7.363	0,672
March	6.061	0,654
April	4.464	0,615
May	3.402	0,606
June	2.863	0,591
July	2.949	0,570
Aug	3.937	0,603
Sep	4.992	0,591
Oct	6.640	0,643
Nov	7.774	0,666
Dec	8.343	0,682

Table 3.6: Monthly average solar GHI of site B (NASA, 2017)

Month	Clearness index	Daily Radiation ($kWh/m^2/day$)
Jan	8.327	0,698
Feb	7.346	0,667
March	6.337	0,670
April	4.892	0,648
May	3.950	0,664
June	3.337	0,642
July	3.586	0,650
Aug	4.544	0,665
Sep	5.754	0,663
Oct	6.920	0,663
Nov	7.976	0,684
Dec	8.441	0,694

Table 3.7: Monthly average solar GHI of site C (NASA, 2017)

Month	Clearness index	Daily Radiation ($kWh/m^2/day$)
Jan	8.411	0,706
Feb	7.629	0,691
March	6.527	0,686
April	5.171	0,676
May	4.084	0,673
June	3,497	0,658
July	3.749	0,665
Aug	4,629	0,667
Sep	5,865	0,670
Oct	7.125	0,680

Nov	8.159	0,700
Dec	8,537	0,704

3.5.3.3 Run-of-river Hydropower

For the third scenario, the impact of hydro turbines on the network will be analysed. Run-of-river hydropower system will generate 16.04 MW, comprising of 4 x horizontal pit Kaplan 4010 W turbines and associated electrical infrastructure. The net head and rated flow is 15.34 m and 30 m^3/s respectively. The maximum and minimum operating flow of each turbine is 30 m^3/s and 5 m^3/s respectively. The rated efficiency is 98.6%. The average monthly rainfall and stream flow is given in figure 3.8.

Table 3.8: Monthly average rainfall (NASA, 2017)

Month	Rainfall (mm)	Days
Nov'16	6,9	5
Dec'16	0,3	2
Jan'17	19,9	8
Feb'17	13,3	7
March'17	4	6
April'17	11,2	5
May'17	2,5	2
June'17	3,4	3
July'17	0,5	1
Aug'17	0,2	1
Sept'17	0	0
Oct'17	6,9	3
Nov'17	5,6	4

Table 3.9: Monthly average stream flow (NASA, 2017)

Month	Flow (m/s)
Jan	140
Feb	175
March	200
April	180
May	115
June	100
July	60
Aug	40
Sept	75
Oct	60
Nov	90
Dec	150

3.5.3.4 Lithium-ion batteries

5 MW system with 3-hour use per day was selected for this study. This equates to 15 MWh per day. The average hourly consumption is 6.1 MWh. Back-up batteries can help with energy demand and load shifting during peak times when the electricity cost is at a premium. Loads can be shifted to match with supply and to assist in the integration of variable supply resources.

3.5.7 Economic Model inputs

The system component inputs in HOMER are capital cost, replacement cost, O&M cost and expected lifetime. The project is assumed to run over 25 years. The discount and inflation rates are 10% and 3.5% respectively. The capital cost of each system is given in table 3.10.

Table 3.10: Capital cost of energy system

Components	Capital Cost ($m)	Replacement Cost ($m)	O&M Cost ($/kW-year)
16 MW Wind	33 600	11 760	640 000
16 MW Solar PV	31 200	6 240	480 000
16 MW PV+5 MW li-ion battery, 5hour back-up	31 200 15 000	6 240 7 500	480 000 150 000
16 MW Hydro	48 000	0	320 000

3.5.7.1 Wind System inputs

Vestas 2 MW wind turbines will be used for this case study. The turbine has a rated output power of 2 MW, and rotor diameter of 82 m. The cut-out wind speed is 28-34 m/s. The turbine has a 20year lifespan. The average cost of wind turbines globally rated between 2 400-2 800 W was USD 1 000.00 (IRENA, 2017). The replacement cost of wind energy will be 15-20% of the wind turbine.

3.5.7.2 PV System inputs

Sunpower E20 327-Watt peak PV modules will be used for simulation. The efficiency of the modules is 20.4%, the life expectancy is 25 years and the derating factor is assumed to be 88%. The cost all other components including the inverter is included in the solar PV system. The average capital cost of the solar PV system for 16 MW, as

discussed in chapter 2 is $2500/kW. During the 30-year lifetime of the solar PV plant operation, it is assumed that 35% of the equipment which includes PV modules and inverters would be replaced. The price of CSP with 5.5 hour storage in round 3 of REIPPP was USD 8 800.00/kW and LCOE was 0.128 $/kWh (GreenCape, 2017). This is considered not economically viable for industry at present.

3.5.7.3 Hydropower System inputs

Homer is restricted to one hydro turbine of maximum 10 MW. The cost of the system will however be adjusted to reflect the full cost of a 16 MW system. The net head and rated flow is assumed to be 15.34 m and 30 m^3/s respectively. The maximum and minimum operating flow of each turbine is 30 m^3/s and 5 m^3/s respectively. The rated efficiency is 98.6%. The global average operation and maintenance cost for small hydropower plants is 2.5% of the total investment cost per annum (IRENA, 2017). Electro-mechanical equipment for hydropower plants are designed to last for 30 years. Replacement of hydropower equipment is not frequent (IRENA, 2017)

3.5.7.4 Lithium-ion Batteries

A generic lithium-ion battery will be used in this modelling. The biggest battery in the HOMER library is 1 MWh. The nominal capacity and voltage is 1.67 MAh, and 600 V respectively and roundtrip efficiency is 90%. The maximum discharge current is 1.67 mega ampere. The cost of lithium-ion batteries is approximately USD 3 000.00/kW (Olson, Allen & Sawyer, 2017). A 5 MW system with a 3hour use per day was selected for this study. The system would be able to generate 15 MWh per day, which would be adequate for peak shaving. The lifespan of Lithium ion batteries is 5-15 years. The batteries therefore need to be replaced once to match the lifespan of solar PV. NREL's predicted fixed O&M cost for li-ion batteries in 2018 is USD 17 000/MW/year. Each system is modelled in HOMER.

3.6 Case Study 2 – Mineral Smelter

3.6.1 Network Specification

The second system under study is illustrated in figure 3.12. The plant is a mineral smelter, which operates 24 hours a day. The loads consist of one 28 MW and one 35 MW direct-current furnace where ilmenite is smelted to produce titanium slag and pig iron. The auxiliary plants consume some electricity, which makes up the total electricity usage. The plant is supplied from a nearby substation by two 80 MVA, 132/11 kV transformers. The detailed electrical parameters of the system are given in table 3.11.

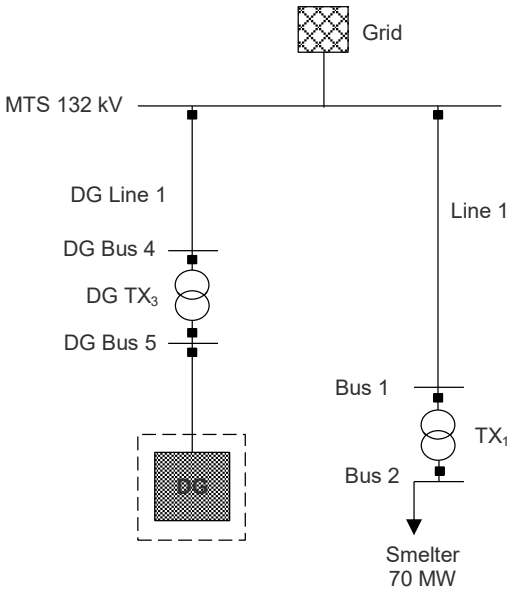

Figure 3.12: Single line diagram of IPP supplying 70 MW load

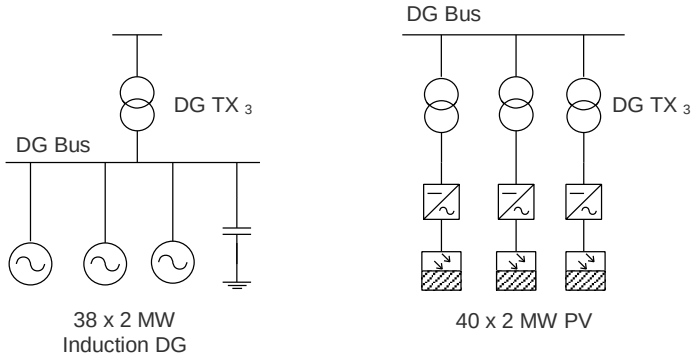

Figure 3.13: Single line diagram of wind system (left) solar PV system (right)

Table 3.11: The specification for case study 2

Components	Specification
Transmission Line (Wolf)	r = 0.182 Ω/km, x = 0.52 Ω/km, I_r = 269 A, Line$_2$ = 35 km,
DG transformer (TX_4)	Dry type cast resin – 11/0.69 kV, P = 2.5 MVA, x = 10%, x/r = 10, HV tapping +/- 2 x 2.5%. Vector group = Dyn11
Substation transformer (Sub TX_3)	132/33 kV, 80 MVA x/r = 10, OLTC at HV side. Vector group = Dyn11
Substation transformer (TX_1)	132/33 kV, 80 MVA x/r = 10, OLTC at HV side. Vector group = Dyn11
Load	70 MW with 0.95 pf, Vpu = 1

DG (induction generator)	*S* = 2.4 MVA, *P* = 2.05 MW, *V* = 0.69 kV, pf = 0.855, *η* = 97%, Rs = 0.01pu, Xs = 0.15pu, Xm = 4pu, Rm = 0.019pu, Xm = 4pu, Rm = 0.019pu, Xm" = 0.199pu,
DG (PV Solar)	*S = P = 2 MVA, V = 1000 V*
External grid	S_{SC} = 1000 MVA, x/r = 10

Three 76 MW DG systems will be simulated and compared to the existing network in terms of impact of voltage profile, fault contribution, thermal limits and power loss. These DG systems are a) 76 MW wind energy b) 76 MW PV c) 76 MW PV with 10 MW, 5-hour Lithium-ion battery back-up system. DG systems will be located at various distances from the load. The renewable components for the wind energy system are comprised of Vestas V90-2.0 MW wind turbines and associated electrical components. The solar PV system consist of Sunpower PV models, single axis trackers, 2 MW central inverters and associated electrical components.

Table 3.13: Summary of renewable site locations

System	Distance from load (km)		
	Site A	Site B	Site C
76 MW Wind Power System	60	120	270
76 MW PV System	100	485	650
76 MW PV Power System + 10 MW Lithium-ion batteries	100	485	650

Renewable components and resource input data for the second case study has been introduced and discussed in the previous case study. The location of the sites remains the same but the size varies.

3.6.2 Load Profile

The notified maximum demand of the smelter is 72 MVA with an average monthly electricity consumption of 39.5 GWh. The off-peak, standard and peak consumption for a month is 22 GWh,12.5 GWh and 5 GWh respectively. Large consumers within this region are supplied by Eskom, based on the megaflex tariff.

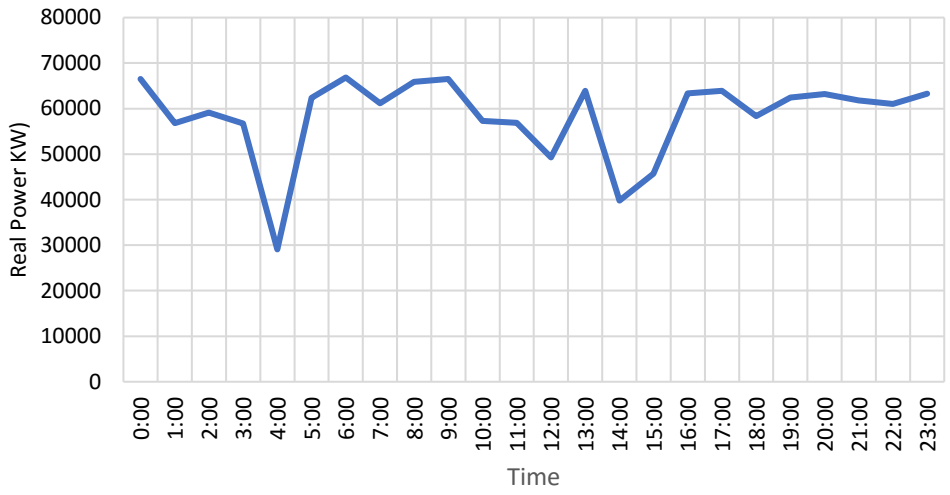

Figure 3.14: Typical average daily load profile of smelter plant

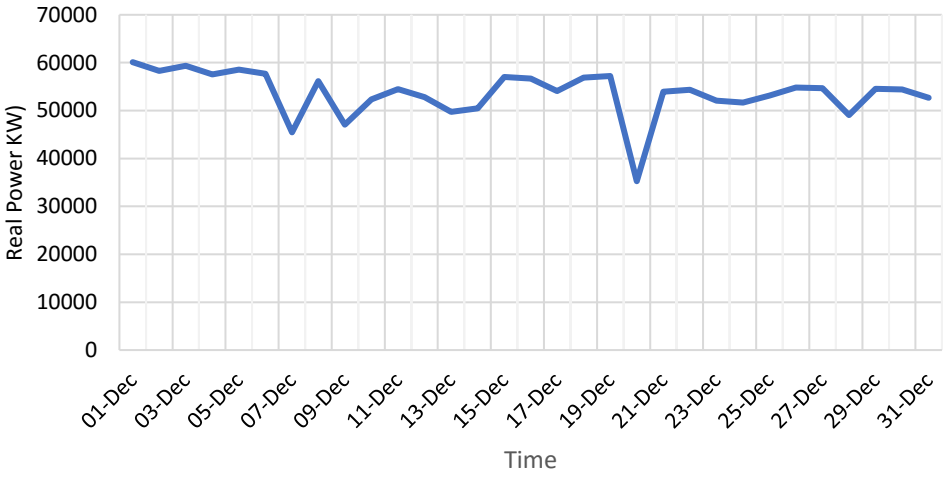

Figure 3.15: Typical average monthly load profile of smelter plant

3.6.3 Economic Model Input

The capital cost of each system is given in table 3.14. Each system is modelled in HOMER

Table 3.14: Capital cost of energy system

Components	Capital Cost ($m)	Replacement Cost ($m)	O&M Cost ($/kW-year)
76 MW Wind	155 800	54 530	3 040 000
76 MW Solar PV	101 250	20 250	1 292 000
76 MW PV	101 250	20 250	1 292 000
10 MW li-ion battery,3hour back-up	60 000	30 000	600 000

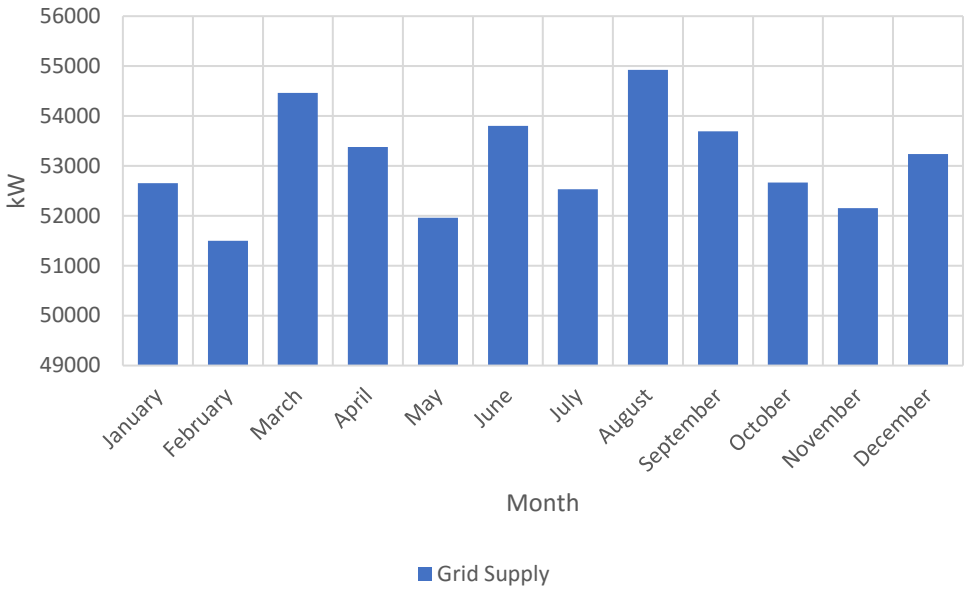

Figure 3.16: Grid supply results

The optimization results obtained from HOMER for the system without DG is given in figure 3.16.

3.7 Chapter Summary

In this chapter, two case studies were conducted to evaluate the technical and economic merits of transporting energy between an IPP and off-taker via the utility's network. The case studies focused on two industrial consumers. The first part of the study focused on the technical aspects.

Firstly, the parameters of the base case, i.e. the network without DG were calculated and presented. Secondly, 16 MW wind, solar PV and hydro power systems were injected into the network to supply the steel plant. Thirdly, 76 MW was injected at various distances to supply the load at the mineral smelter. Load flow simulations were conducted to determine the effect on network parameters after DG was injected into the network.

The second part of the analysis focused on economic viability of DG for wheeling. Simulations were conducted in HOMER to determine the optimal grid-RE system size. Considering the intermittent nature of wind, solar and hydro, grid and RE combination was selected. HOMER calculated the optimal system based on input parameters such as size, capital and O&M cost. HOMER presented the best RE fraction for all the sites.

CHAPTER FOUR
RESULTS AND DISCUSSION

4.1 Introduction

This chapter presents the results of the technical an economic simulation in DIgSILENT PowerFactory and HOMER respectively. Firstly, it starts with the presentations of results for the voltage profile, fault contribution, thermal loading and line losses for wind, solar and hydro systems at specific busbars, equipment and lines. Secondly, the economic results obtained from HOMER is presented and discussed. Thirdly, future cost projections and comparisons of grid and RE sources are presented and discussed.

4.2 Case Study 1 - Steel Plant

4.2.1 Wind system – Technical Results

Based on electrical component inputs, simulations were conducted in DIgSILENT PowerFactory. A load flow analysis on the network was conducted to determine the effect DG technology has on voltage profile, fault contribution, thermal loading of equipment and losses in network. The results for each technology based on site location is given below.

4.2.1.1 Impact on voltage profile

The results after 16 MW wind energy was injected into the network at three sites is tabulated below. According to international standards, voltage level must be kept within 0.95pu and 1.05pu at the customer's point of connection. According to NERSA's Grid Connection Code for Renewable Power Plants to the Distribution Systems in South Africa, the minimum and maximum operating voltage for DG at point of common coupling (POC) should between 0.9pu and 1.0985pu (NERSA, 2014). From the initial results voltage levels were within the prescribed limits, except at POC of site C.

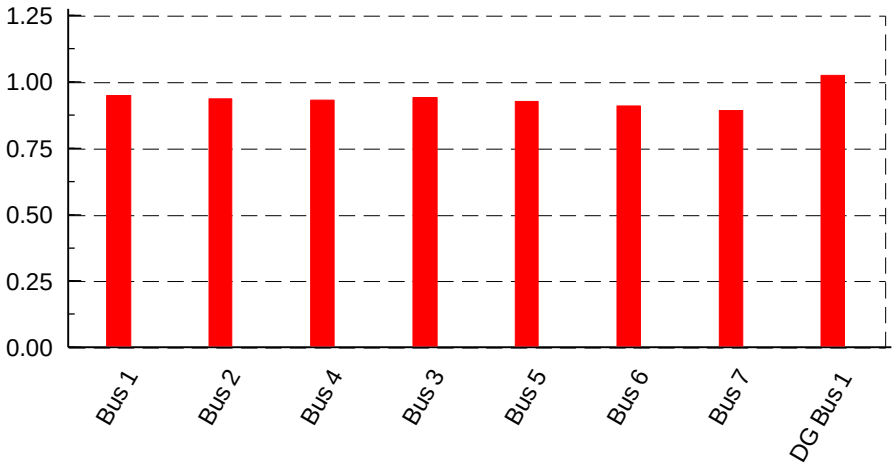

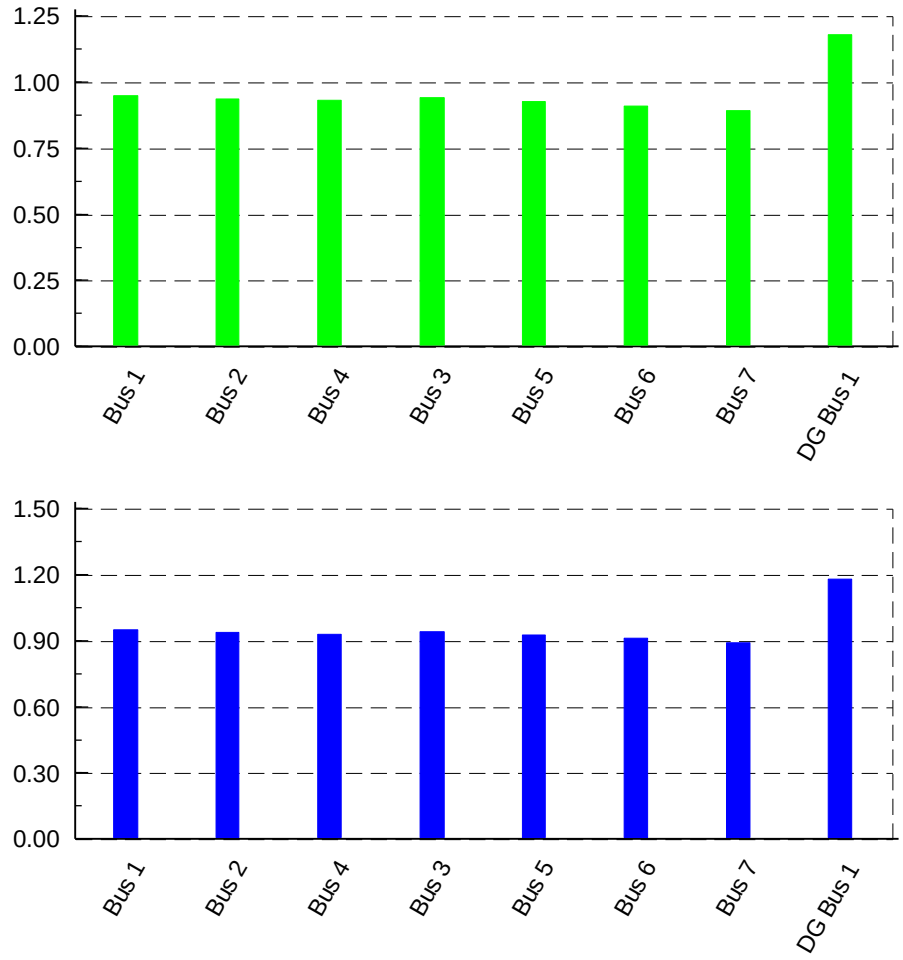

Figure 4.1: Voltage (pu) profile at site A (top), B (middle) & C (bottom)

4.2.1.2 Impact on fault level

The results for fault level contribution is tabulated in figure 4.2. The preliminary results show minimal impact the fault contribution.

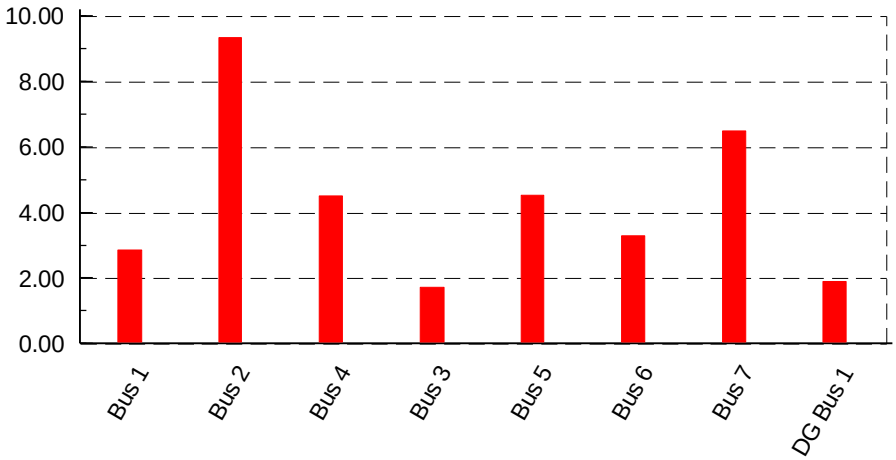

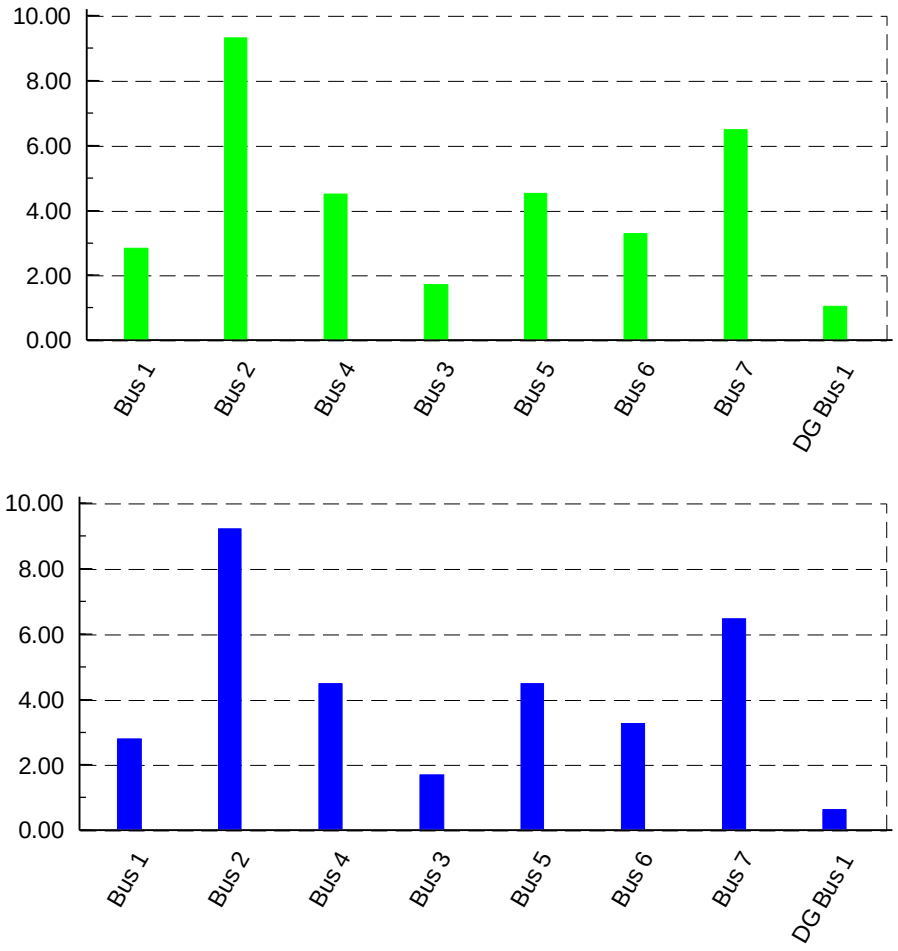

Figure 4.2: Fault level (kA) at site A (top), B (middle) & C (bottom)

4.2.1.3 Impact on thermal loading

DG should not have an adverse effect on equipment loading when connected to the network. Simulations results below, show the effect of injecting 16 MW wind energy at various sites. Results shows that equipment is operating within safe technical limits.

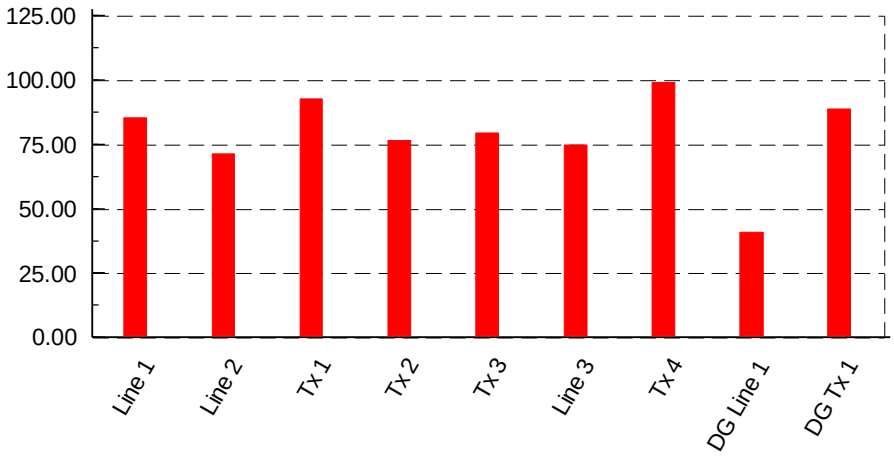

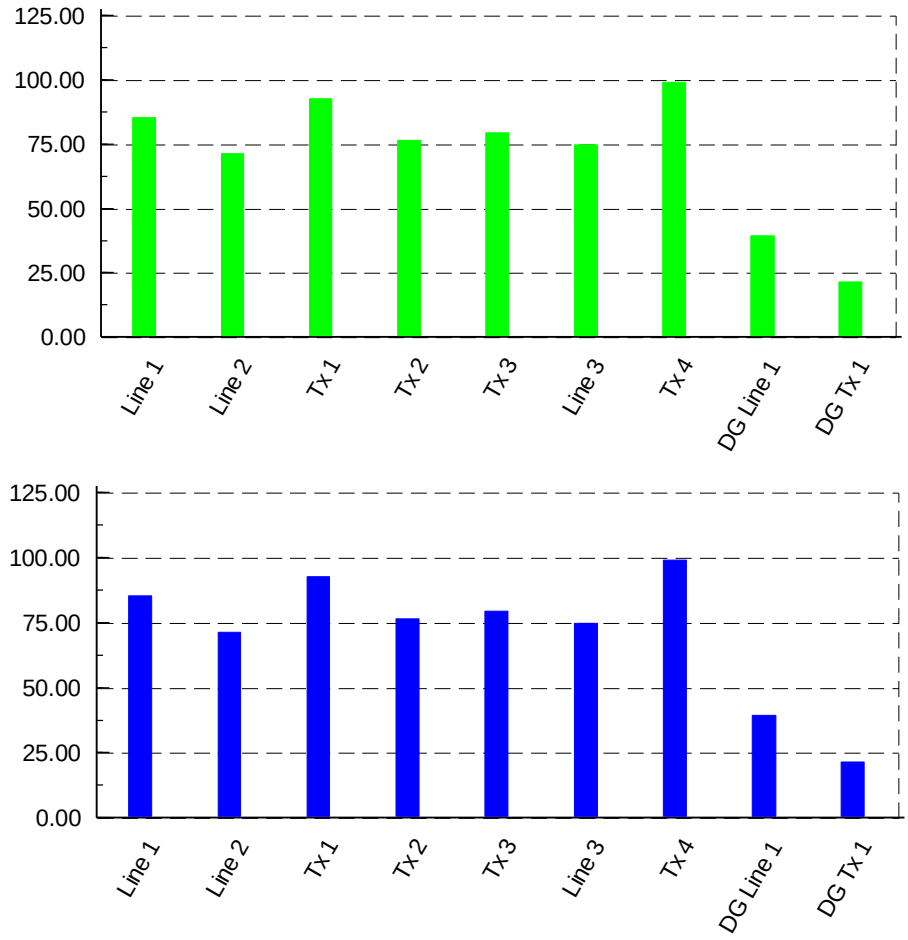

Figure 4.3: Thermal loading (%) of equipment at site A (top), B (middle) & C (bottom)

4.2.1.4 Impact on power loss

The results below show the impact of power loss on the overhead conductors and underground cables.

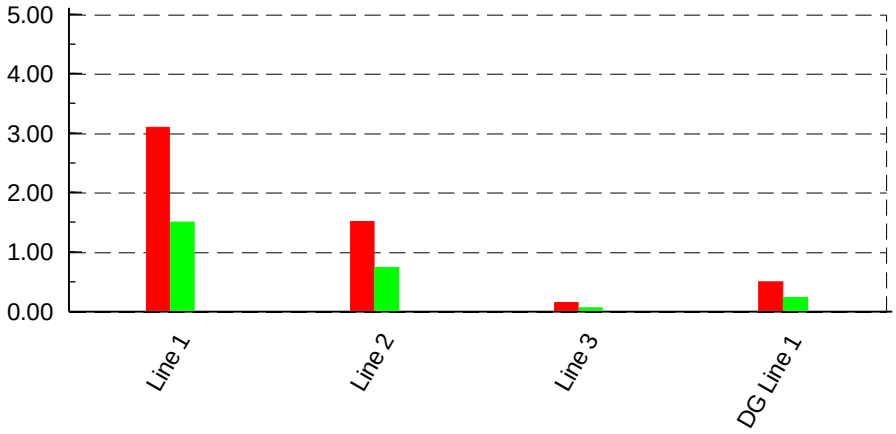

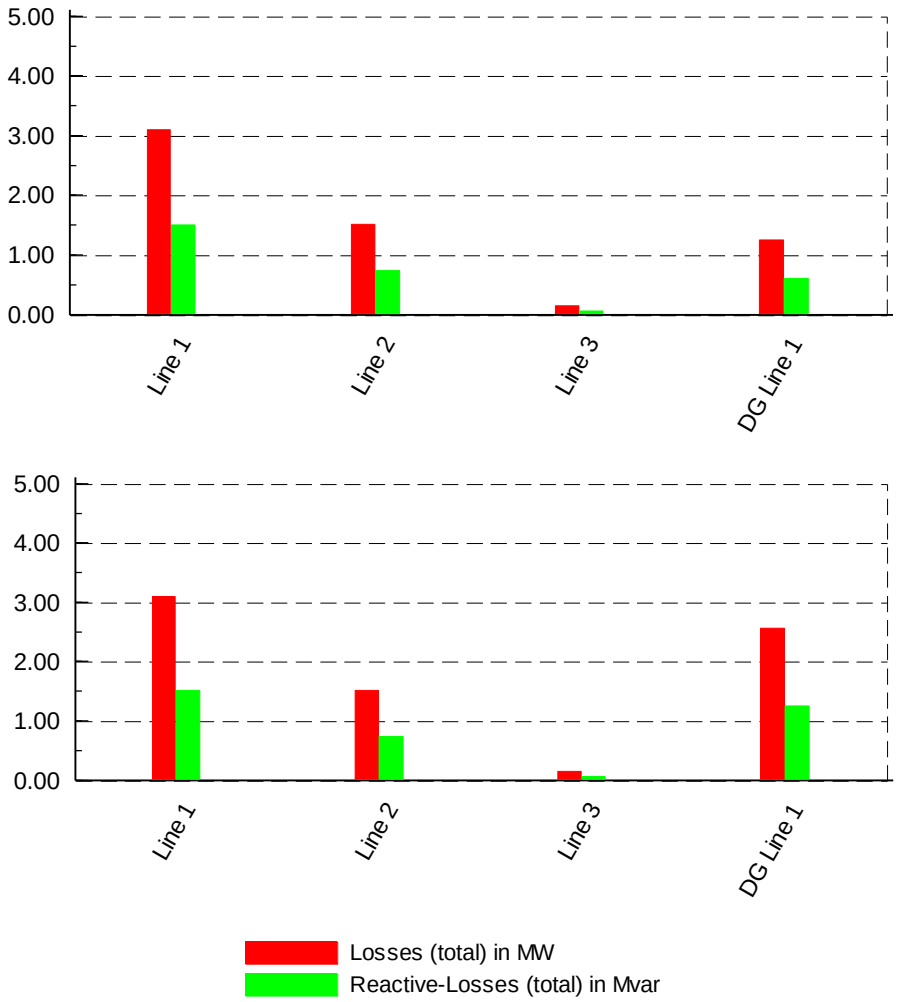

Figure 4.4: Line losses at site A (top), B (middle) & C (bottom)

4.2.2 Solar Power Technical Results

16 MW Solar Energy was injected into the network at various sites. The results on voltage profile, fault contribution, thermal loading and power loss is illustrated below.

4.2.2.1 Impact on voltage profile

The results show the impact on voltage profile on various buses in the network. The voltage profile remains within acceptable limits. The voltage at POC however has exceeded the limits.

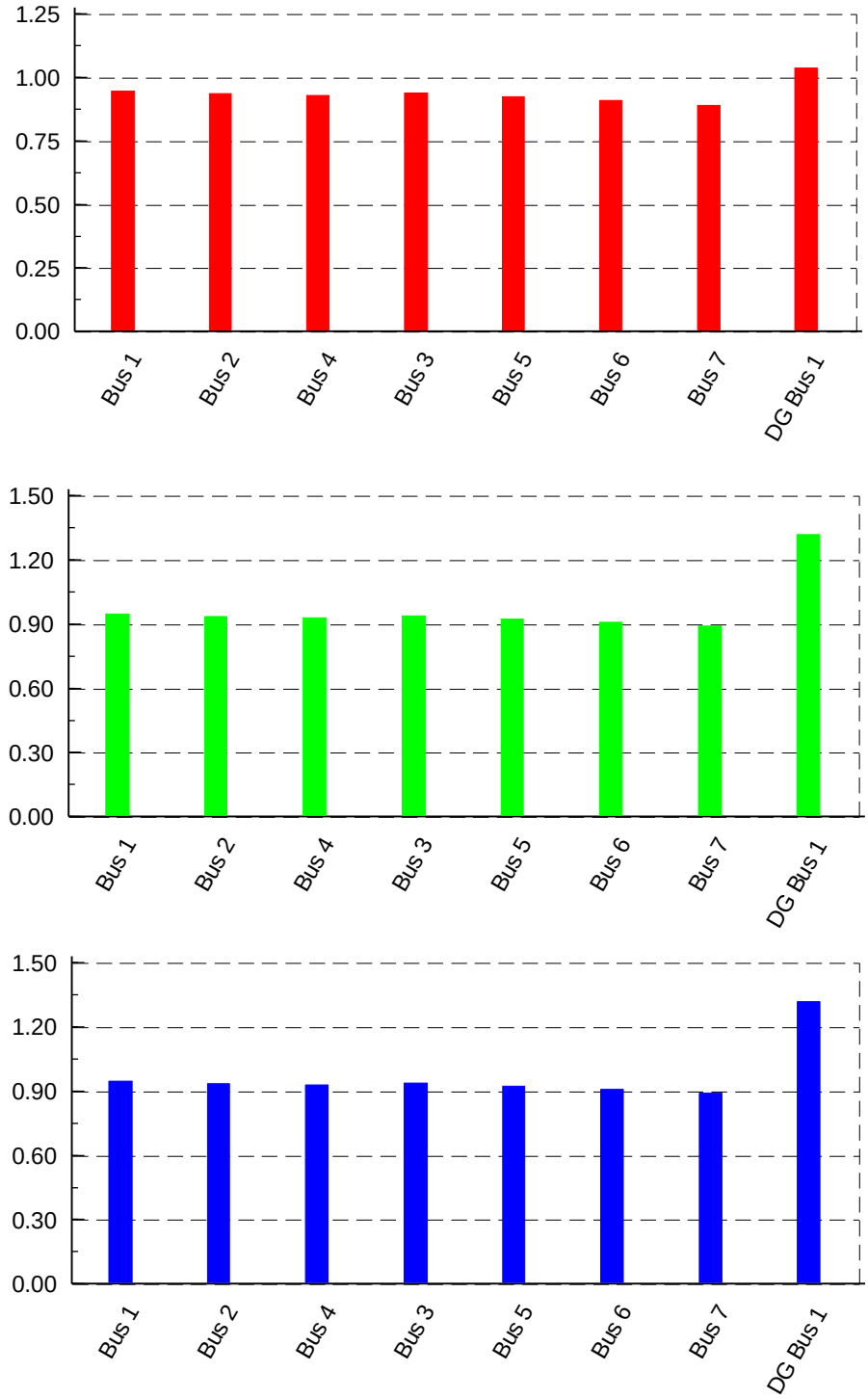

Figure 4.5: Voltage (pu) profile at site A (top), B (middle) & C (bottom)

4.2.2.2 Impact on fault level

Inverter-based DG has a marginal effect on fault contribution. From the results below, it can be seen that the fault contribution to the network does not increase significantly regardless of the distance from the load.

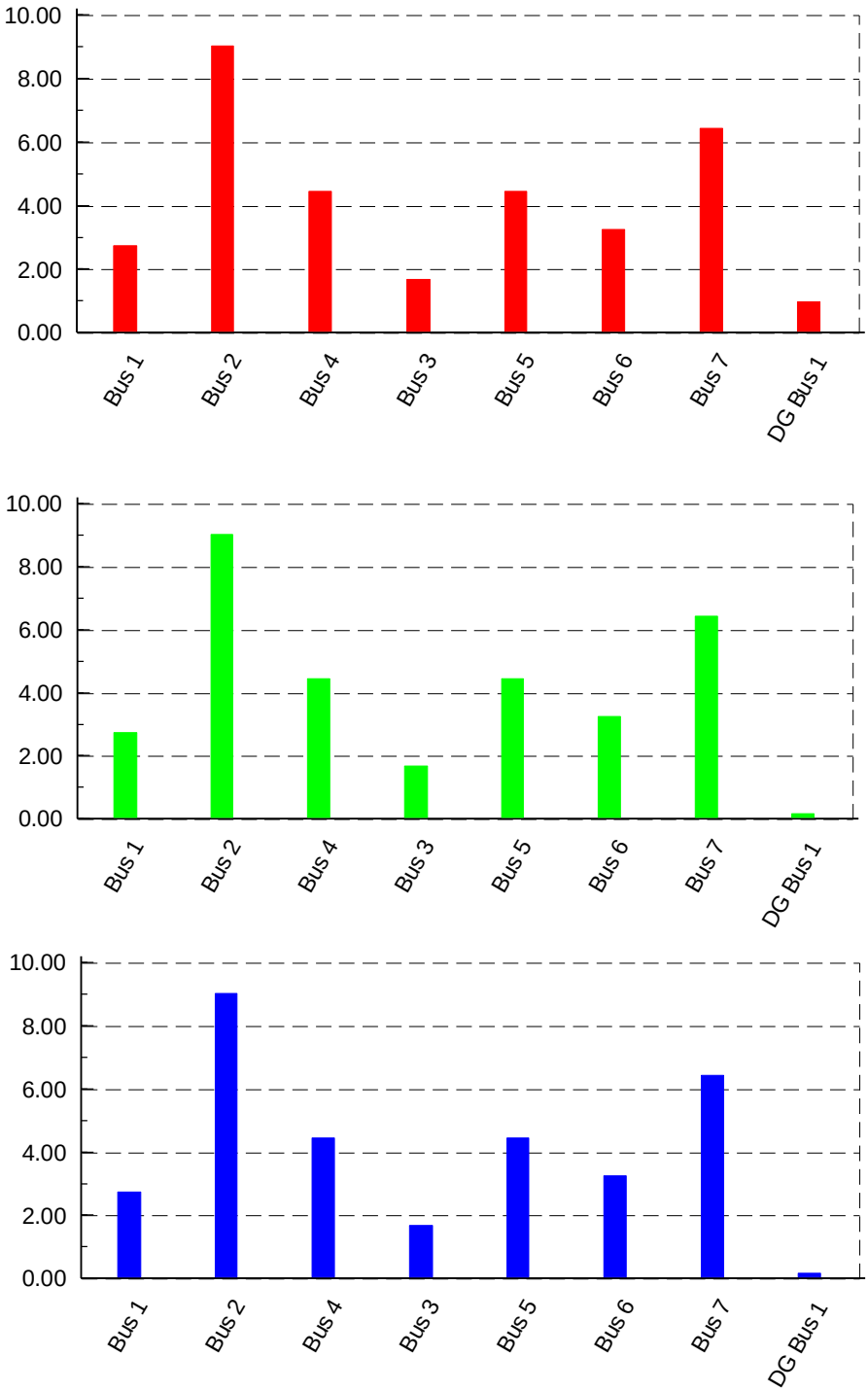

Figure 4.6: Fault level (kA) at site A (top), B (middle) & C (bottom)

4.2.2.3 Impact on thermal loading

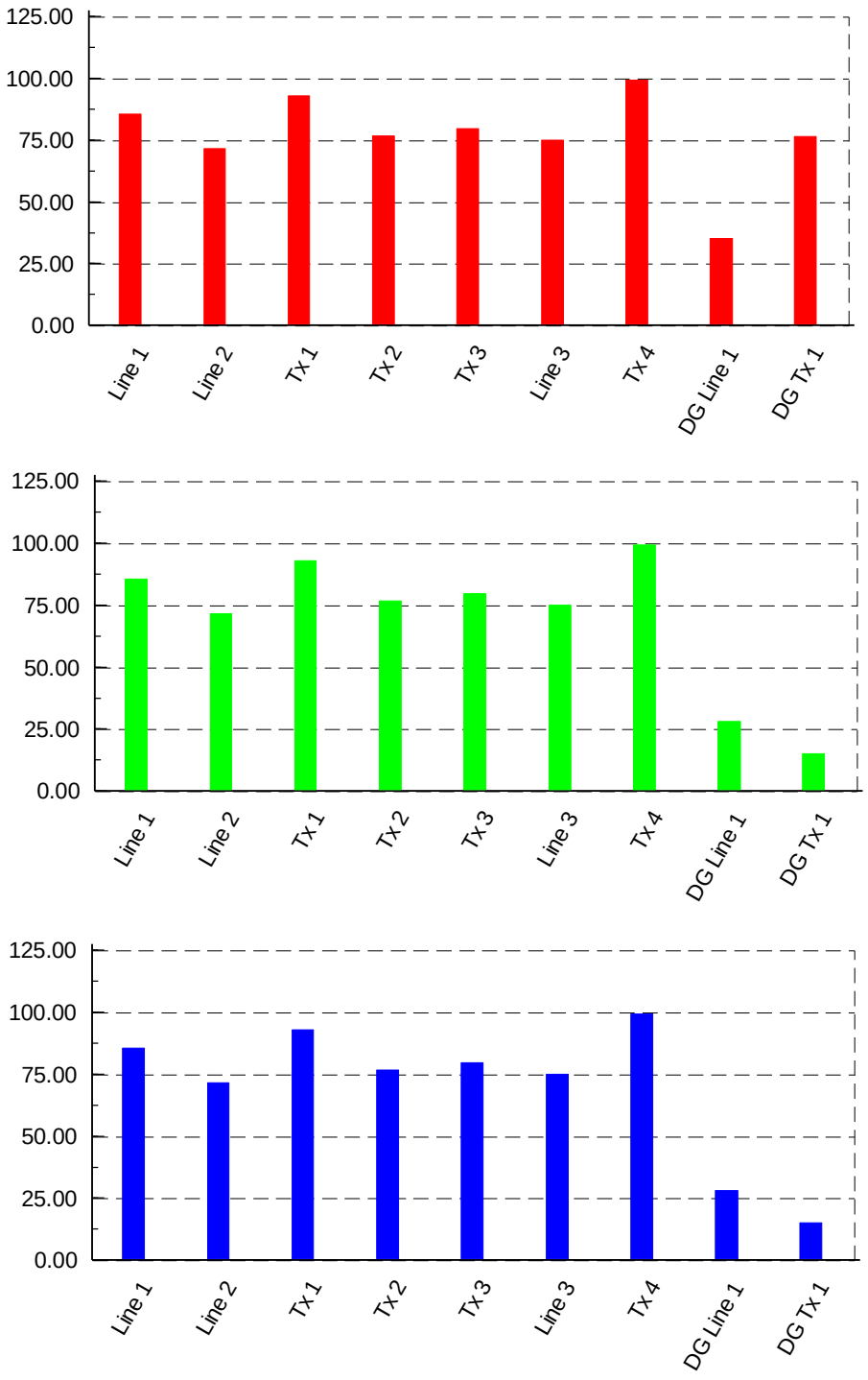

Figure 4.7: Thermal loading (%) of equipment at site A (top), B (middle) & C (bottom)

4.2.2.4 Impact on power loss

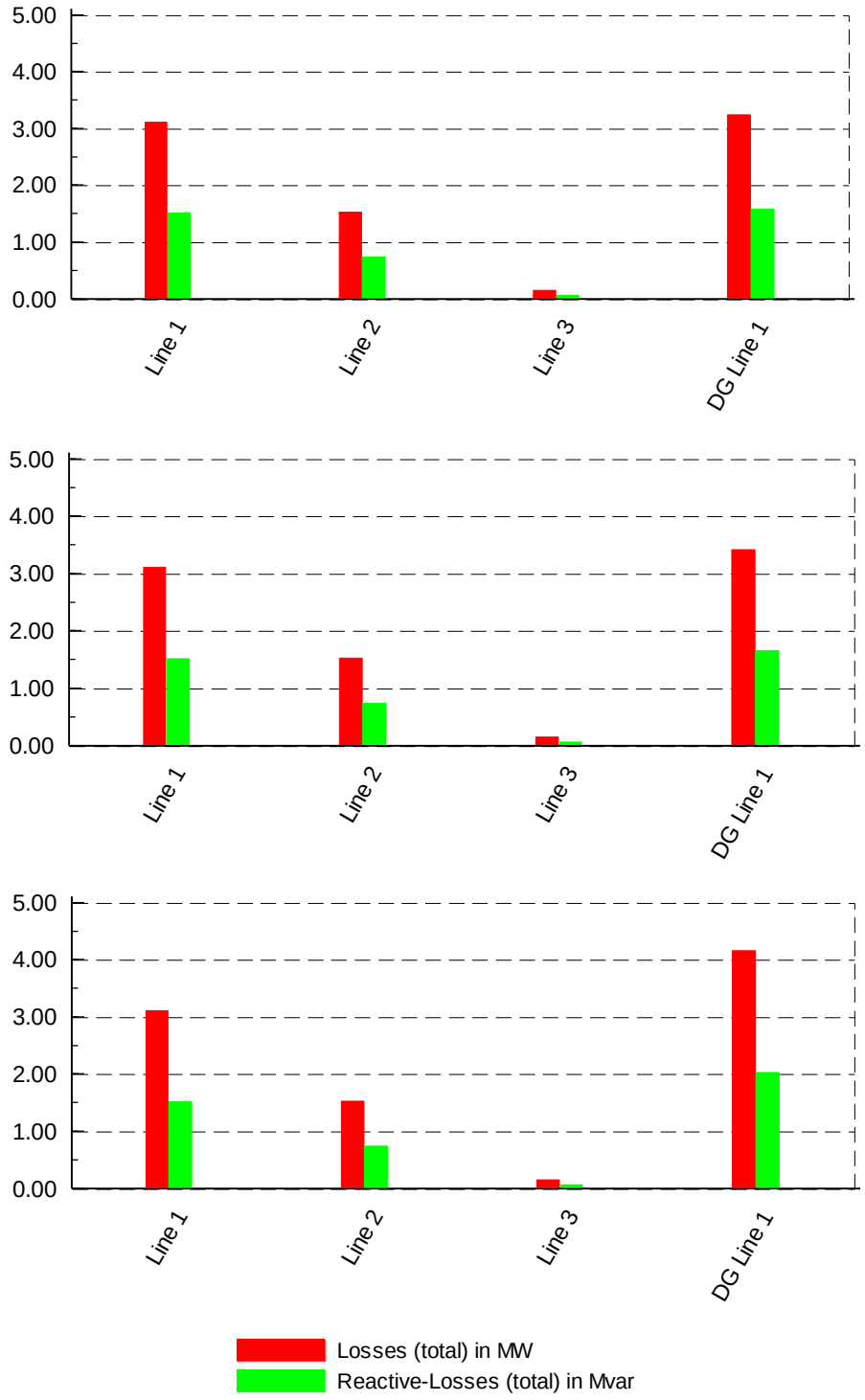

Figure 4.8: Line losses at site A (top), B (middle) & C (bottom)

4.2.3 Hydropower Technical Results

The hydropower system consists of four 4 MW synchronous generators. The effect on voltage profile, fault contribution, thermal loading on equipment and line losses were simulated. The results are given in figures 4.9 - 4.12.

4.2.3.1 Impact on voltage profile

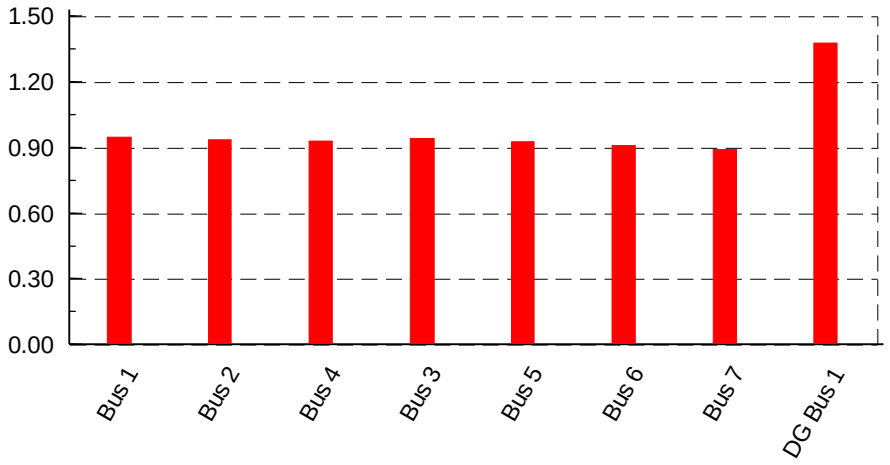

Figure 4.9: Voltage profile (pu) for hydropower

4.2.3.2 Impact on Fault level

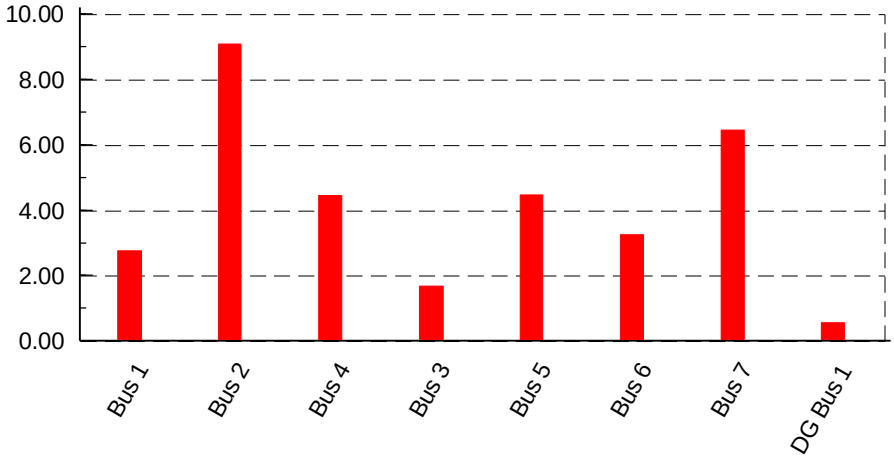

Figure 4.10: Fault level (kA) at various buses for hydropower

4.2.3.3 Impact on Thermal loading

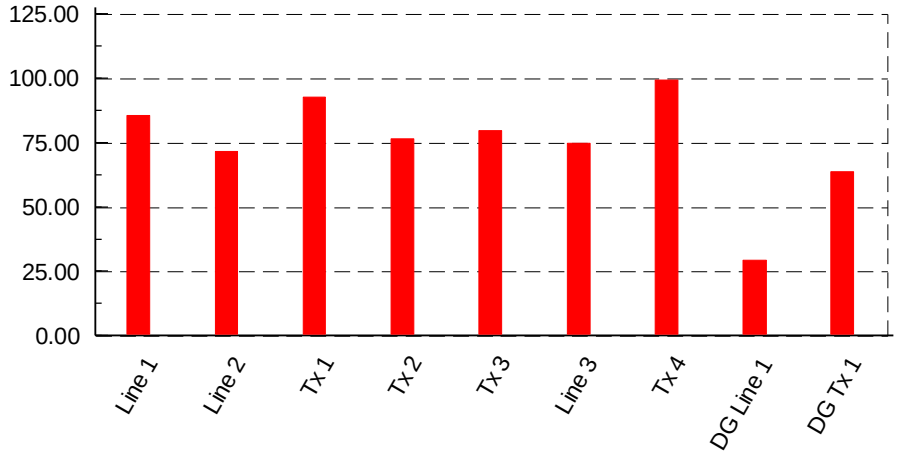

Figure 4.11: Thermal loading (%) for hydropower

4.2.3.4 Impact on Power loss

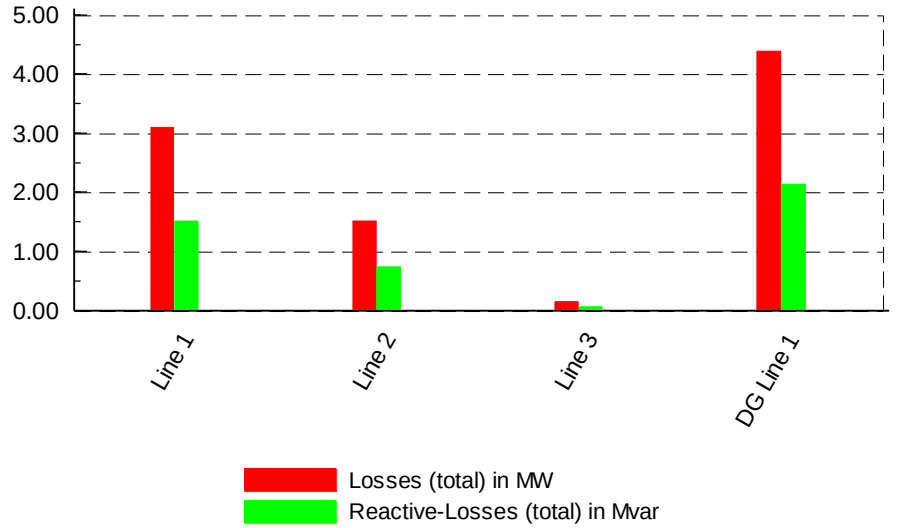

Figure 4.12: Line losses for hydropower

A detailed analysis of the results for the first case study is provided below. For the first case study, the effect on bus 4 is of particular interest as this is the bus where the steel processing plant is connected. The results for the voltage profile analysis show that injecting 16 MW of wind energy at all the sites, independent of distance has no effect on the voltage profile when compared to the base case. The voltage at bus 4 is below the minimum prescribed limit of 0.95pu. The voltage profile at DG bus 1, for site A and B, however, which is the point of common coupling (POC), is within the prescribed limit. The voltage at site C, however has exceeded the prescribed limit of 1.095pu.

Table 4.1: Analysis of voltage profile for Wind Systems

Bus No.	Base Case	Site A	Variation (%)	Site B	Variation (%)	Site C	Variation (%)
4	0.928	0.930	0.75	0.930	0.75	0.930	0.75
MTS	0.992	0.994	0.20	0.994	0.20	0.994	0.20
DG 1	-	1.025	-	1.075	4.65	1.178	12.98

Table 4.2: Analysis of fault contribution for Wind Systems

Bus No.	Base Case	Site A	Variation (%)	Site B	Variation (%)	Site C	Variation (%)
4	4.419	4.517	2.17	4.503	1.87	4.478	1.32
MTS	3.659	3.946	7.27	3.913	6.49	3.844	4.81
DG 1	-	1.914	-	1.047	45.29	0.627	67.24

Table 4.3: Thermal loading of selected equipment

Line No.	Base Case	Site A	Variation (%)	Site B	Variation (%)	Site C	Variation (%)
1	85.40	85.30	0.11	85.30	0.11	85.30	0.11
2	71.50	71.30	0.28	71.30	0.28	71.40	0.14
DG 1	-	41.20	-	39.40	4.37	36.00	12.62

Table 4.4: Line losses (MW)

Line No.	Base Case	Site A	Variation (%)	Site B	Variation (%)	Site C	Variation (%)
1	3.106	3.090	0.52	3.095	0.35	3.095	0
2	1.522	1.516	0.39	1.516	0.39	1.517	0
DG 1	-	0.510	-	1.253	59.29	2.599	80.37

The overall results for the wind system show that the profile remains virtually unchanged. Asynchronous generators fault contribution ranges from 7.3% to 3.8% at bus 4 where the steel mill is connected. The maximum fault contribution at the POC is 1.9 kA. Interestingly, the fault contribution decreases as the IPP distance away from the load increases. The thermal loading of the lines remains virtually unchanged for all sites. The loading on the DG line connecting the DG to the MTS increased to maximum by 12.6% at site C. All lines and network equipment remain within safe limits.

Table 4.5: Analysis of voltage profile for Solar Systems

Bus No.	Base Case	Site A	Variation (%)	Site B	Variation (%)	Site C	Variation (%)
4	0.928	0.928	0.0	0.928	0.0	0.928	0.0
MTS	0.992	0.992	0.0	0.992	0.0	0.992	0.0
DG 1	-	1.056	-	1.246	15.25	1.316	19.76

Table 4.6: Analysis of fault contribution for Solar Systems

Bus No.	Base Case	Site A	Variation (%)	Site B	Variation (%)	Site C	Variation (%)
4	4.419	4.435	0.36	4.434	0.34	4.433	0.32
MTS	3.659	3.686	0.73	3.693	0.92	3.693	0.92
DG 1	-	0.970	-	0.208	78.56	0.162	83.29

As with the wind energy system, the voltage profile remains unchanged. The voltage at bus 4 is below the minimum acceptable limit of 0.95pu. The voltage at DG 1 for site A is within the acceptable limit, but exceeded the limit of 10.95 at site B and C, which represents the POC. Fault level contribution of inverter-based generators is marginal. The results for thermal loading remain the same as the base case, which is not surprising as the line distance, remains constant. The loading of the DG line decreased by 20% at site C. As expected the line losses increase as the distance from the load increases. IPP's are charged for losses as part of the standard wheeling cost.

Table 4.7: Thermal loading of selected equipment

Line No.	Base Case	Site A	Variation (%)	Site B	Variation (%)	Site C	Variation (%)
1	85.40	85.40	0.00	85.40	0.00	85.50	0.12
2	71.50	71.50	0.21	71.50	0.00	71.50	0.00
DG 1	-	35.20	-	29.50	16.19	27.90	20.74

Table 4.8: Line losses (MW)

Line No.	Base Case	Site A	Variation (%)	Site B	Variation (%)	Site C	Variation (%)
1	3.106	3.106	0.0	3.106	0.0	3.106	0.0
2	1.522	1.522	0.0	1.522	0.0	1.522	0.0
DG 1	-	0.793	-	3.409	76.74	4.154	80.91

Table 4.9: Analysis of voltage profile for Hydropower System)

Bus No.	Base Case	Site A	Variation (%)
4	0.929	0.929	0.10
MTS	0.992	0.993	0.0
DG 1	-	1.378	-

Table 4.10: Analysis of fault contribution for Hydropower Systems

Bus No.	Base Case	Site A	Variation (%)
4	4.419	4.446	0.61
MTS	3.659	3.750	2.43
DG 1	-	0.599	-

The results for the voltage profile, fault contribution and thermal loading of equipment are marginal. As with solar and wind technology, for hydro power, the voltage at bus 4 is below the limit of 0.95pu. The lines loss on the DG line is 4.4 MW.

Table 4.11: Thermal loading of selected equipment

Line No.	Base Case	Site A	Variation (%)
1	85.40	85.30	0.12
2	71.50	71.40	0.14
DG 1	-	29.40	-

Table 4.12: Line losses (MW)

Line No.	Base Case	Site A	Variation (%)
1	3.106	3.098	0.26
2	1.522	1.518	0.26
DG 1	0.0	4.425	-

4.2.4 Economic Results

The industrial plant is currently supplied by Eskom on a megaflex tariff basis. The tariff is based on a time-of -use principle where the seasonal and daily rates apply based on peak, standard and off-peak rates. This makes supply from an alternative energy source interesting, especially during peak times where load shifting may not be possible.

Table 4.13: Eskom megaflex tariff breakdown ($/kWh) (Eskom,2017)

High Demand Season (June – August)			High Demand Season (June – August)		
Peak	Standard	Off-peak	Peak	Standard	Off-peak
0.223	0.067	0.037	0.073	0.050	0.032

The simulation results in HOMER for a grid application based on the current blended tariff of 0.062 $/kWh is given in figure 4.14.

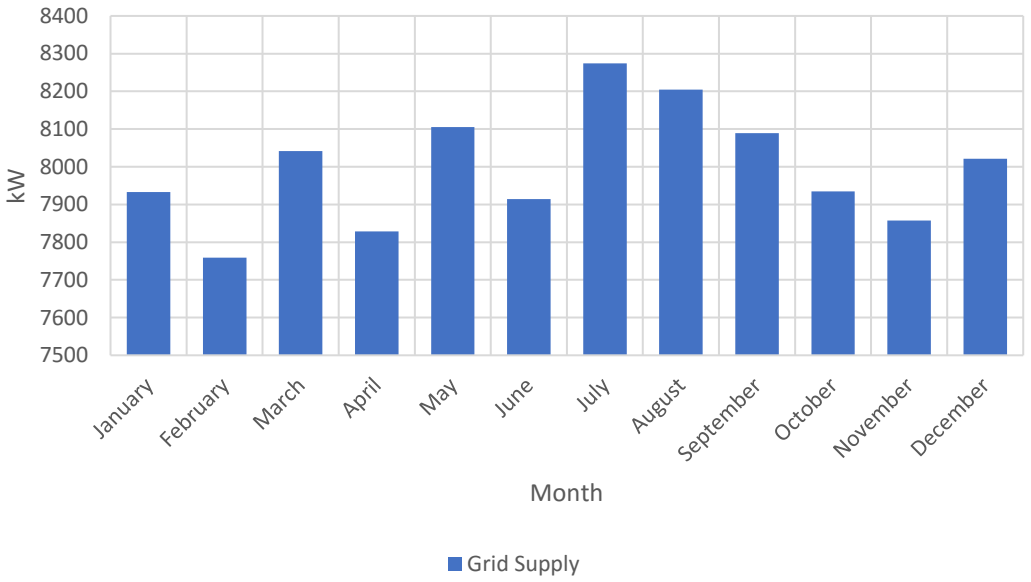

Figure 4.14: Grid supply results

4.2.4.1 Wind Energy

HOMER simulated various scenarios based on cost, technology inputs and size of the system. The following shows the optimal results for the wind energy system at the site previously selected. Site A, which has the best wind resources offers the best energy yield. More than 60% of energy is supplied by wind energy.

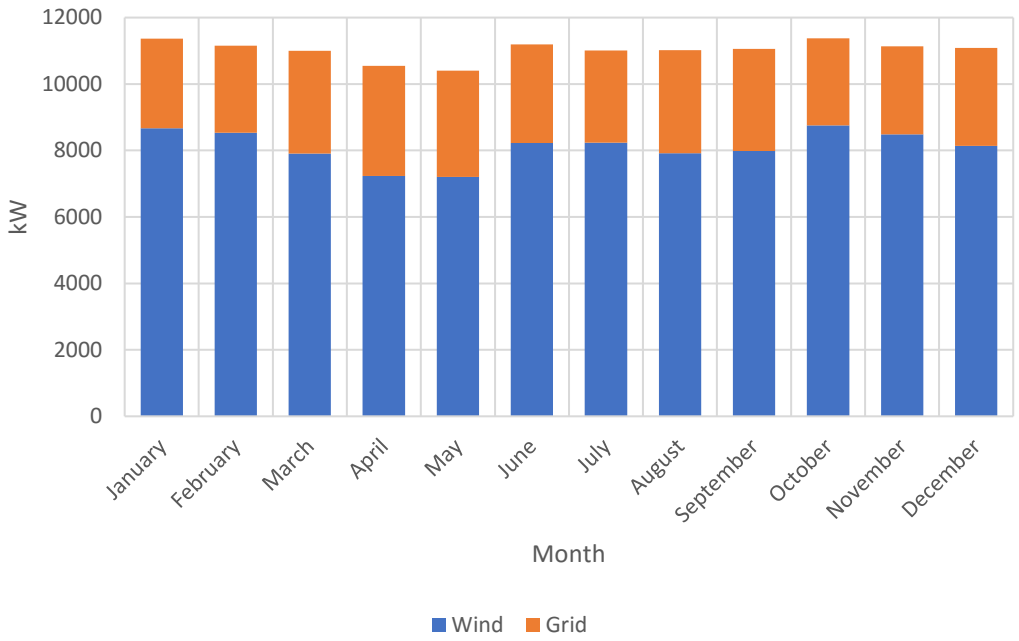

Figure 4.15 Grid-wind results for site A

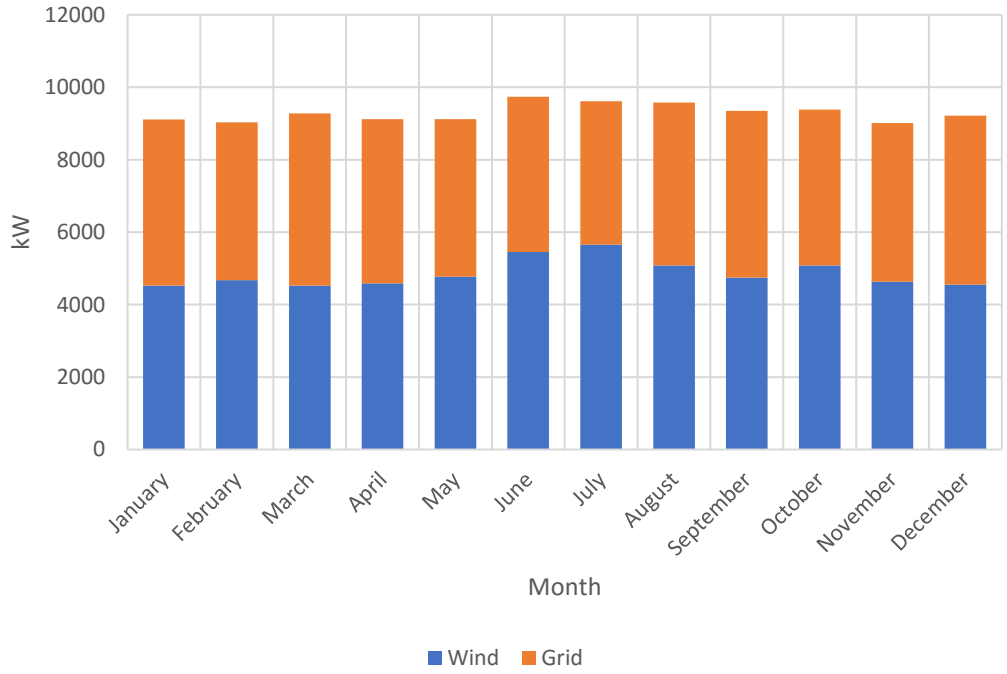

Figure 4.16 Grid-wind results for site B

The grid-wind system energy results for site B is tabulated in figure 4.16. The renewable fraction is 51%.

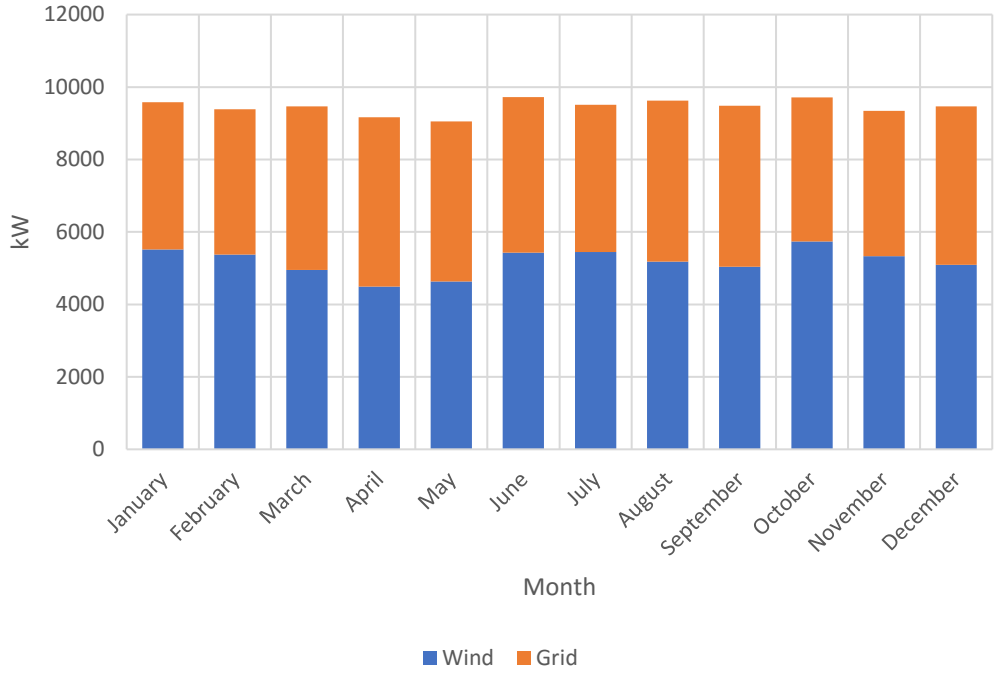

Figure 4.17 Energy results for site C

The grid-wind system energy results for site C is tabulated in figure 4.17. The renewable fraction is 55%. This site is located in an area with good wind resources. The mean wind speed is above 7 m/s measured at 100 m above ground level which is considered above good for wind energy production.

4.2.4.2 Solar Energy Results

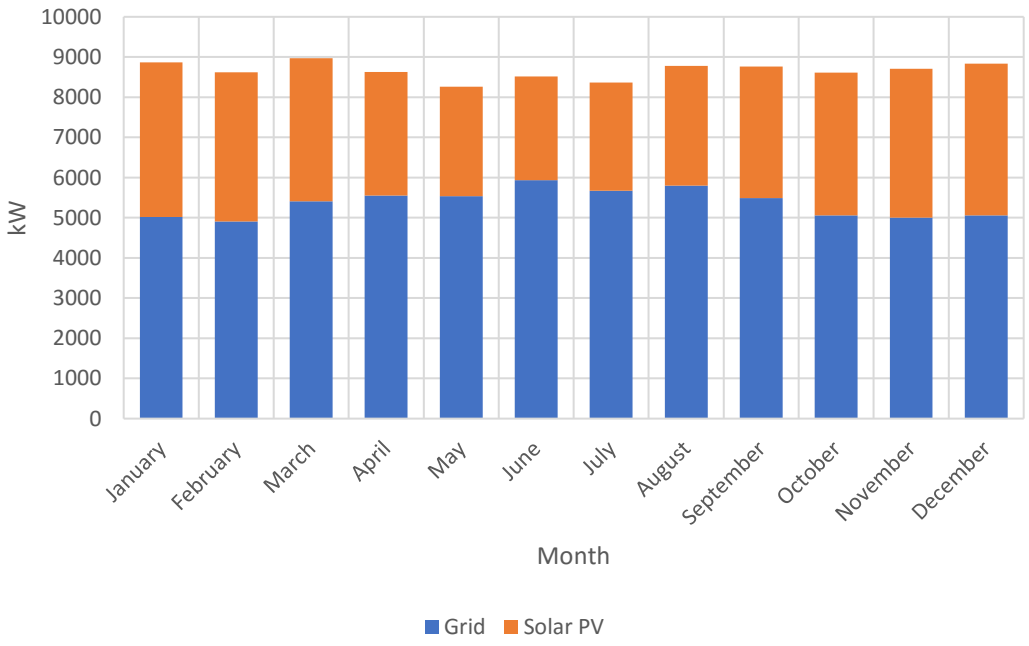

Figure 4.18 Grid-solar results for site A

The gird-solar system energy results for site A is tabulated in figure 4.18. Site A is approximately 75 km from the site. The GHI is less than 2030kWh/m^2. This represents average solar resources. The renewable fraction is only 37.6%.

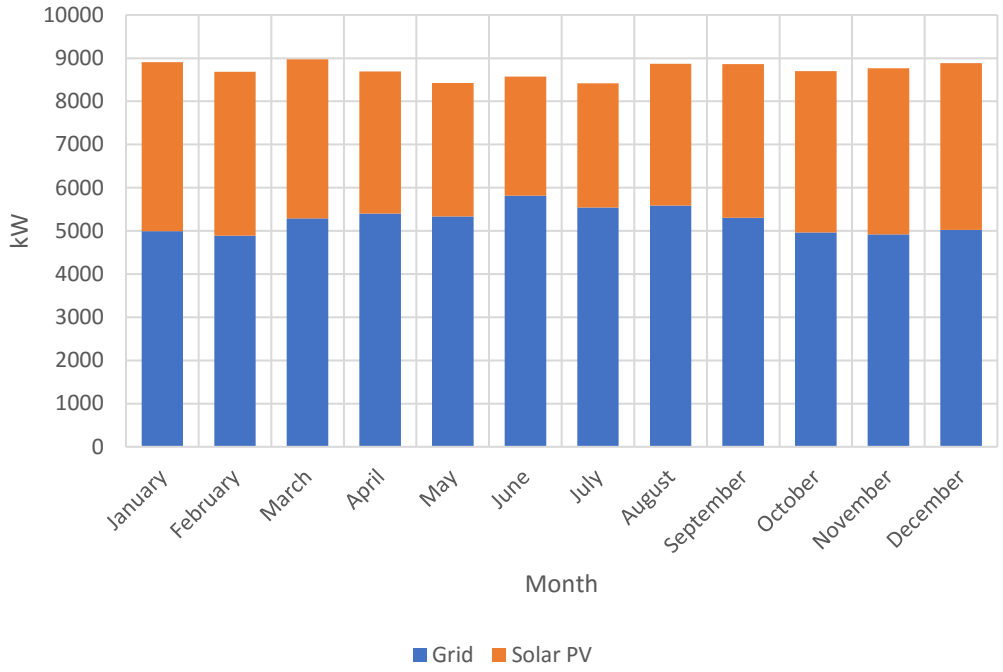

Figure 4.19 Grid-solar results for site B

The grid-solar system energy results for site B is tabulated in figure 4.19. The GHI for site B is approximately 2220 kWh/m^2. The renewable fraction is 40%.

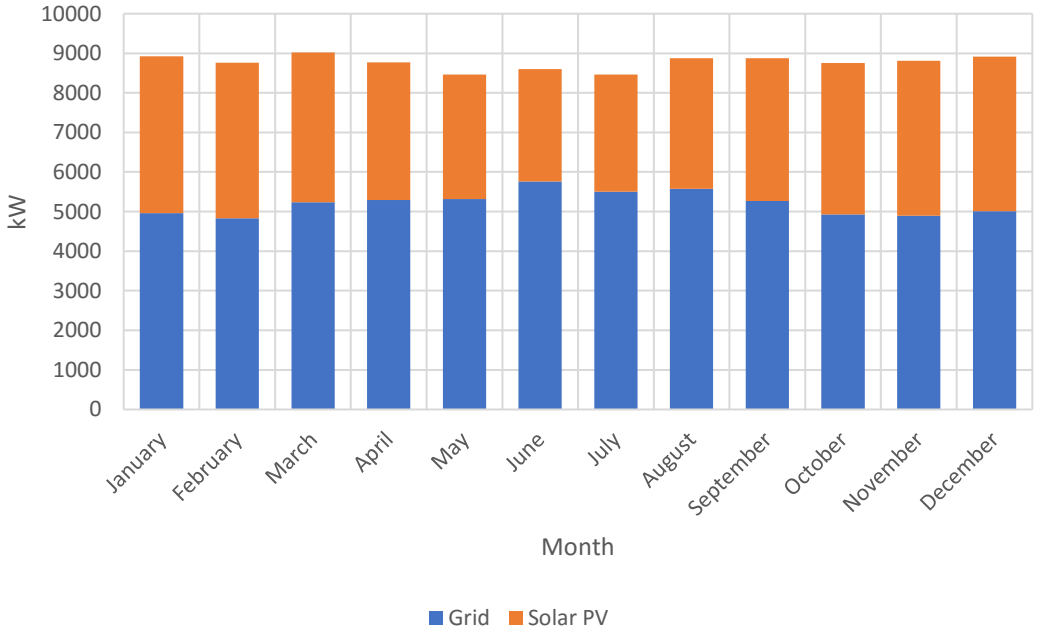

Figure 4.20 Grid-solar results for site C

The grid-solar system energy results for site 3 is tabulated in figure 4.20. The GHI for site C is approximately 2350 kWh/m^2. According to the GHI map of South Africa, site C represents the best solar resources. The results obtained for site C, confirms the latter. The renewable fraction is 60%.

4.2.4.3 Hydro Energy Results

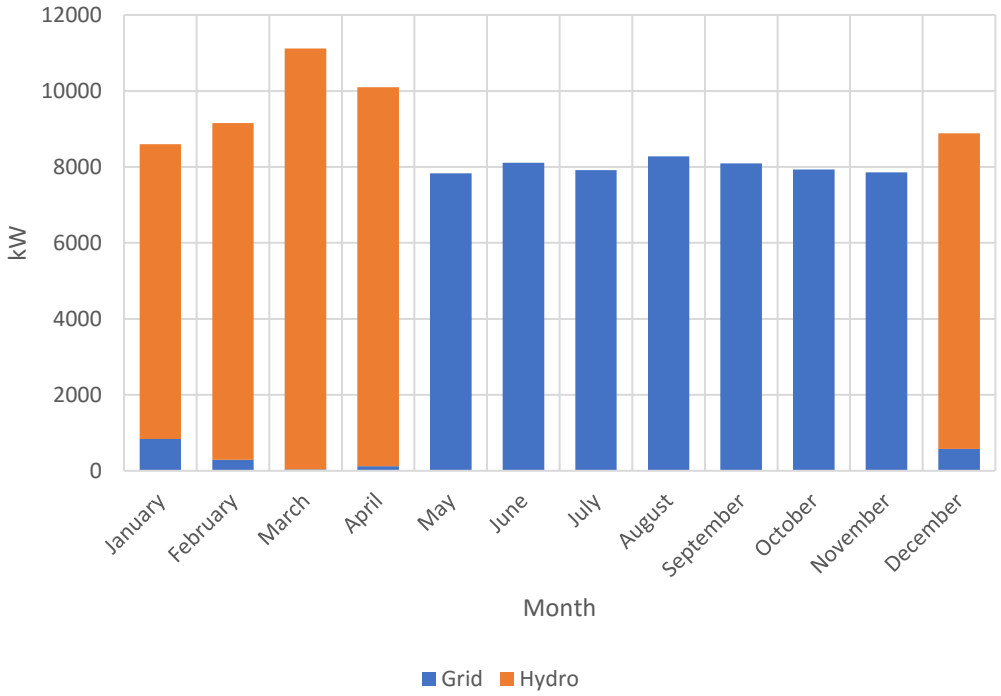

Figure 4.21 Hydro-grid energy results

The grid-hydro system energy results are tabulated in figure 4.21. The renewable fraction is 55%.

The aim of the analysis was to determine the economic viability of suitably sized renewable energy systems. The optimization results obtained from HOMER for the three sites are given table 4.13. It represents the system architecture that matches the load. Considering the complexity of a hybrid system, which would involve multiple contracts with various IPP's, a single IPP was selected per site. Considering the intermittent nature of solar and wind resources, grid and RE system was proposed.

The results show that wind energy offers the best renewable energy fraction and offers the highest energy produced per year. Site A, offers the best energy yield due to good wind resources along the coast. The average daily production is 9 hours per day. The site is located relatively close to the load. Solar energy has the potential to offer equally high renewable fraction but is dependent on solar resources. In the Northern Cape,

where irradiance levels are higher compared to the coastal areas, energy yield is higher. Site 3 offers the best renewable fraction at 60% but is located 625 km from the site.

Hydropower offers reasonable energy production but is dependent on the system design and stream flow. During summer months when the stream flow is greater than the design flow, almost all energy could be supplied by hydropower.

Table 4.13: Optimized systems architecture for Steel Processing Plant

Site	System	Energy (MWh/year)	RE fraction (%)	Max RE Output (kW)
Site A	Grid + Wind	86.13	60.4	16 400
	Grid + Solar	75.78	37.6	15 798
Site B	Grid + Wind	81.46	51.1	16 400
	Grid + Solar	76.48	39.8	15 791
Site C	Grid + Wind	82.88	54.8	16 400
	Grid + Solar	76.83	59.5	15 768
	Grid + Hydro	80.74	54.7	12 668

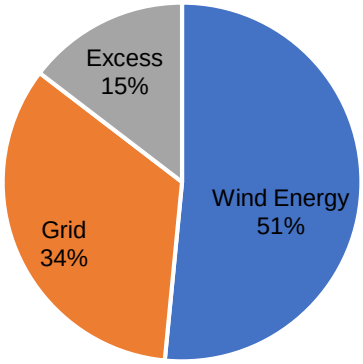

Figure 4.22: Breakdown of electricity used for optimal system

The average consumption per annum of the plant is 71 MWh. The optimal systems for this load are a grid-wind system, which produces 86MWh per annum.

The cash flow summary which consist of LCOE, NPC and operating cost was generated by HOMER is tabulated in table 4.14. From the cost analysis is can be seen that wind energy presents the best financial case for all scenarios. For site A, the LCOE is 0.065 $/kWh compared to the existing blended average electricity cost of 0.062

$/kWh paid to the supply authority. The NPC and operating cost of the system is the lowest of all the wind sites at $69.4 m and $2.881 m respectively. The solar site closest to the load has the lowest LCOE, NPC and operating cost. The system consisting of hydropower energy and grid has the highest LCOE, NPC. The cost of small hydropower systems is not competitive at present. The penetration depends on available water resources and high investment capital.

Table 4.14: Cost analysis for Steel Processing Plant

Site	System	LCOE ($/kWh)	NPC ($m)	Operating Cost ($m)
Site A	Grid + Wind	0.065	69.4	2.881
	Grid + Solar	0.077	73.1	3.367
	Grid + Solar + Battery	0.098	92.4	3.714
Site B	Grid + Wind	0.072	73.2	3.185
	Grid + Solar	0.086	82.7	4.135
	Grid + Battery	0.107	102.0	4.483
Site C	Grid + Wind	0.074	74.4	3.277
	Grid + Solar	0.086	82.4	4.112
	+ Battery	0.106	101.7	4.461
	Grid + Hydro	0.090	90.7	3.423

4.3 Case Study 2 - Mineral Smelter

4.3.1 Wind System – Technical Results

Simulations were conducted in DIgSILENT PowerFactory. The results for each technology based on load flow analysis per site location is given below.

4.3.1.1 Impact of voltage profile

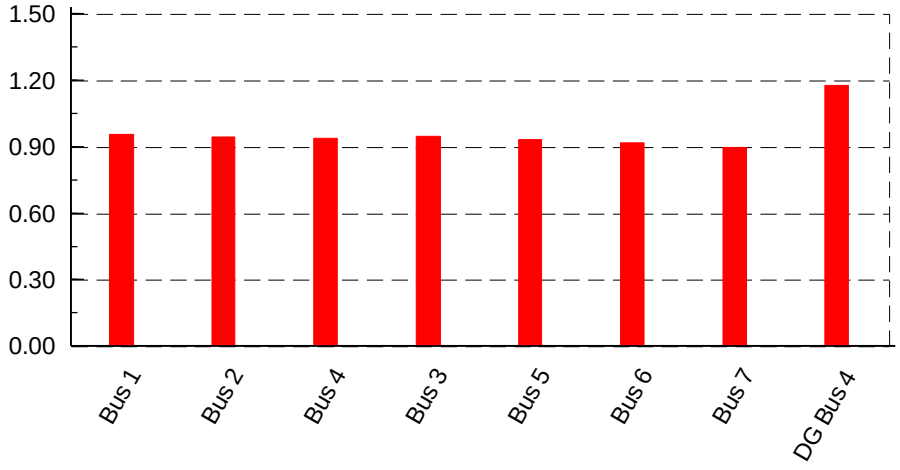

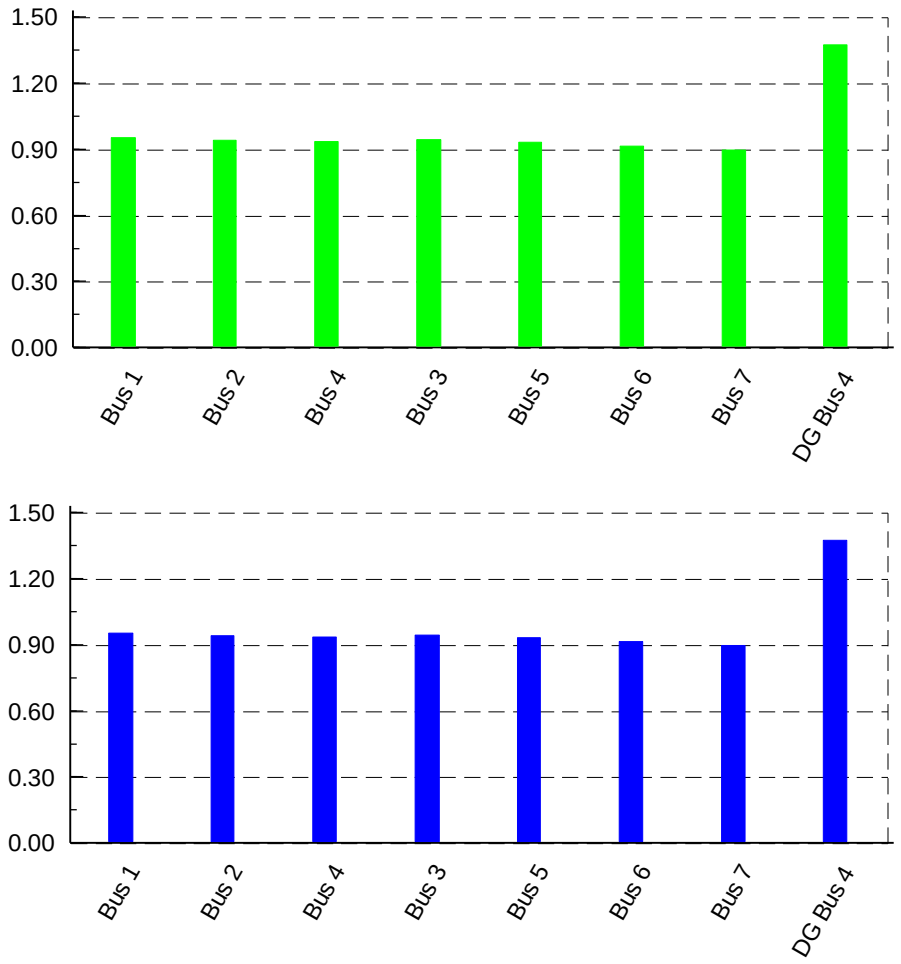

Figure 4.23: Voltage profile (pu) at selected buses for site A (top), B (middle) & C (bottom)

3.6.3.2 Impact on fault level

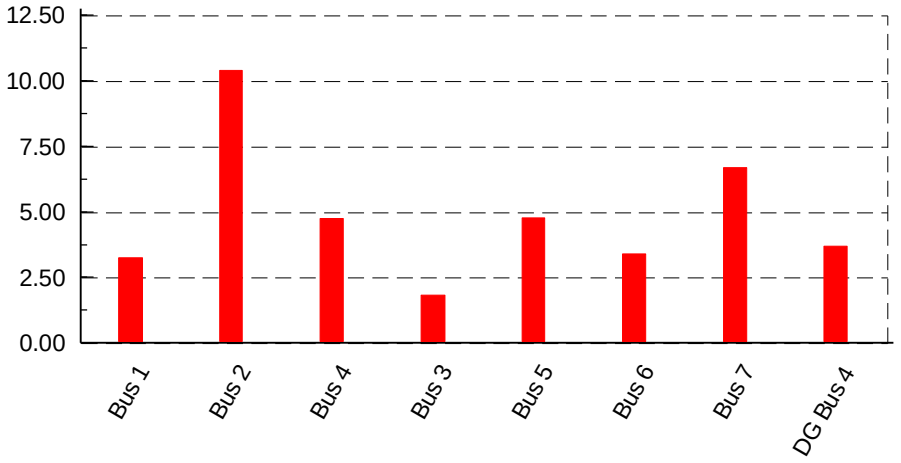

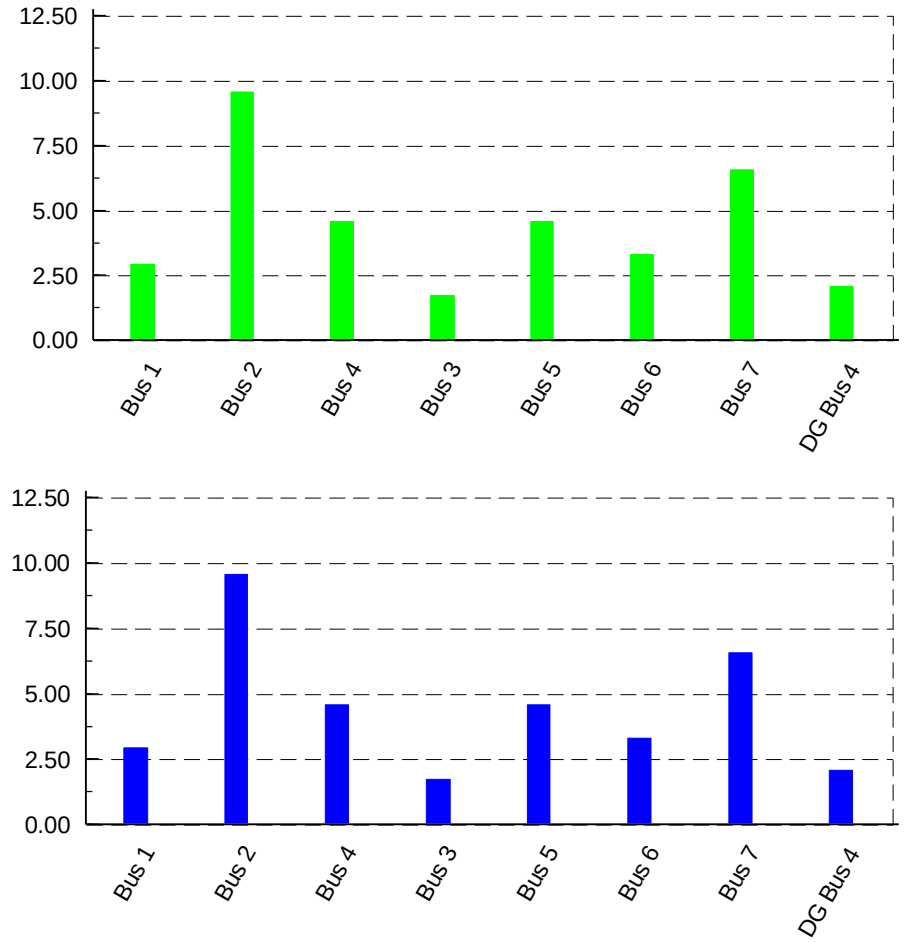

Figure 4.24: Fault level (kA) at selected buses for site A (top), B (middle) & C (bottom)

3.6.3.3 Impact on thermal loading

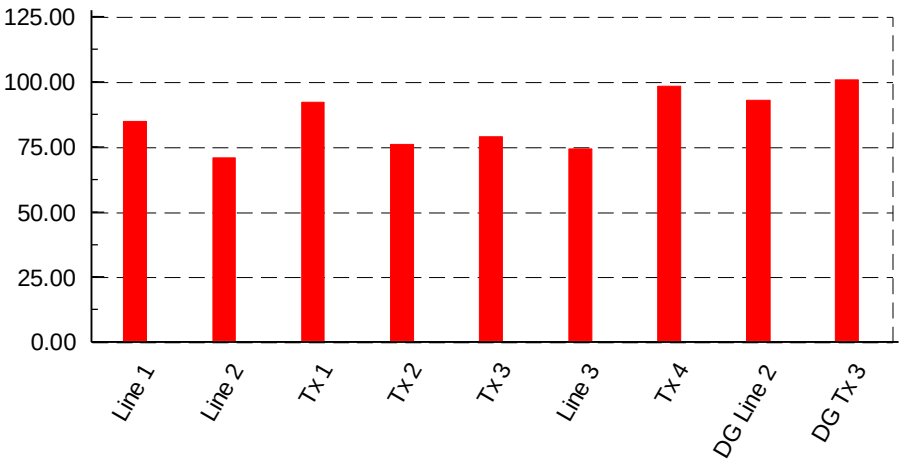

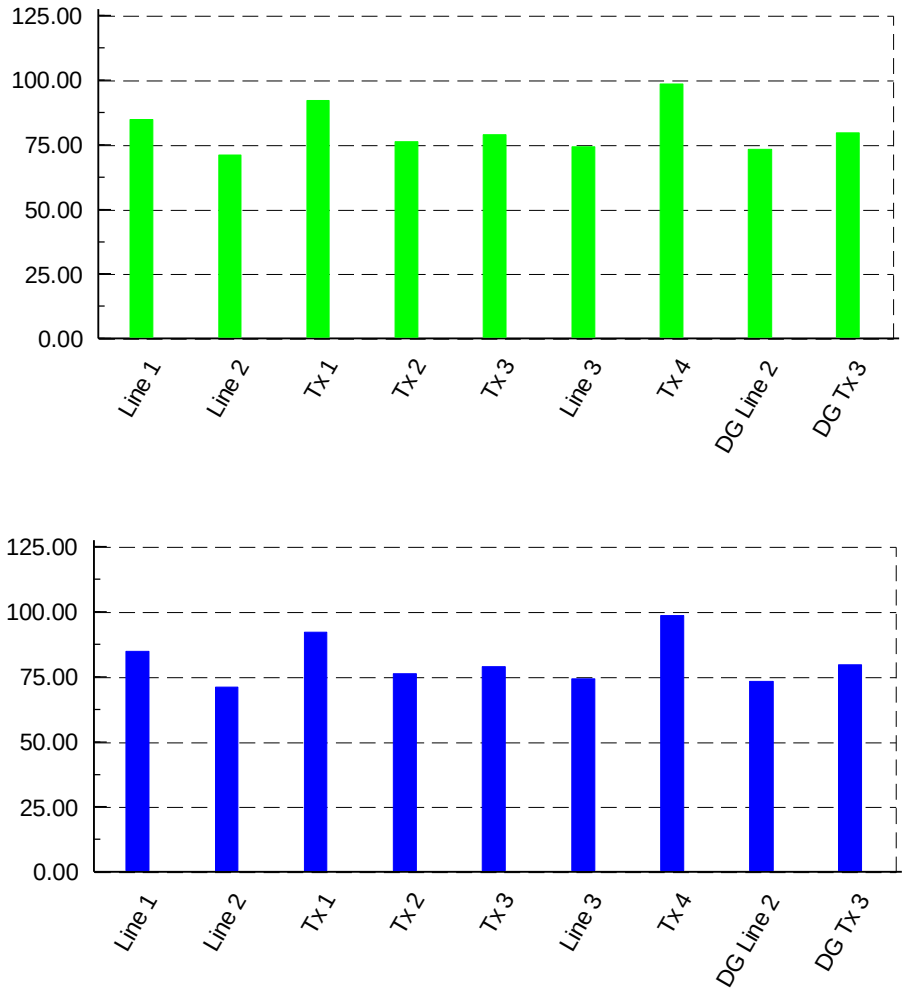

Figure 4.25: Thermal loading (%) of equipment at site A (top), B (middle) & C (bottom)

3.6.3.4 Impact on power loss

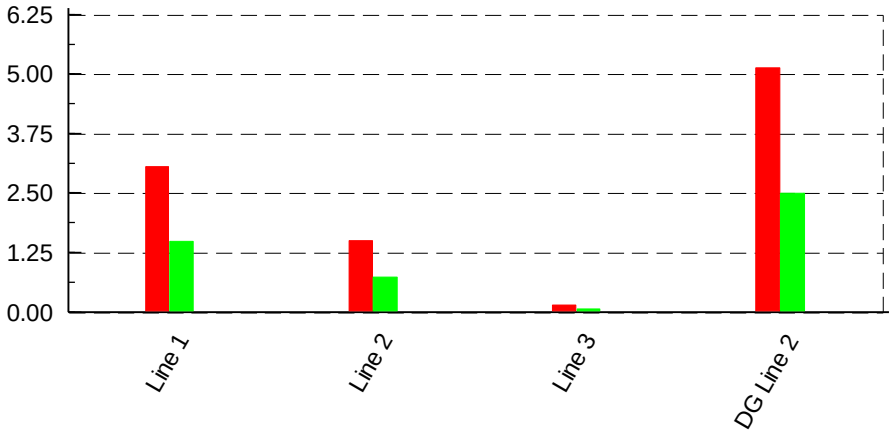

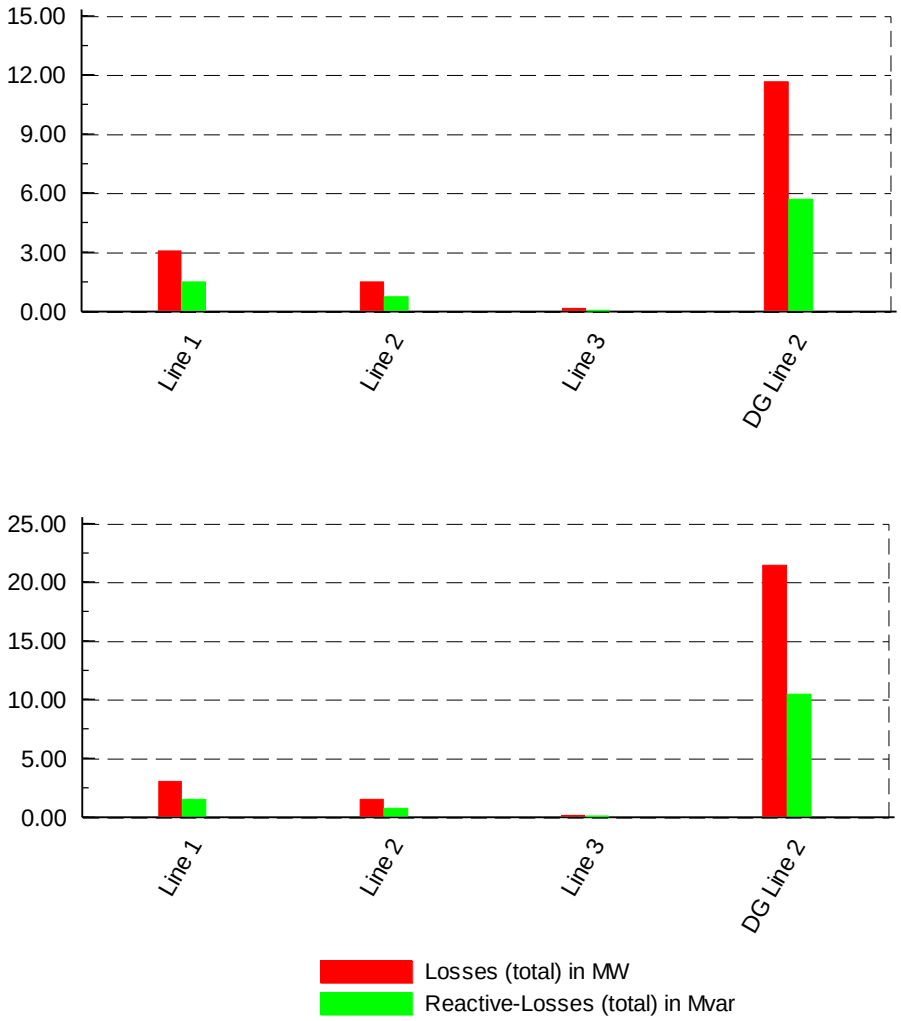

Figure 4.26: Transmission loss at site A (top), B (middle) & C (bottom)

3.6.4 Solar Power Technical Results

3.6.4.1 Impact on voltage profile

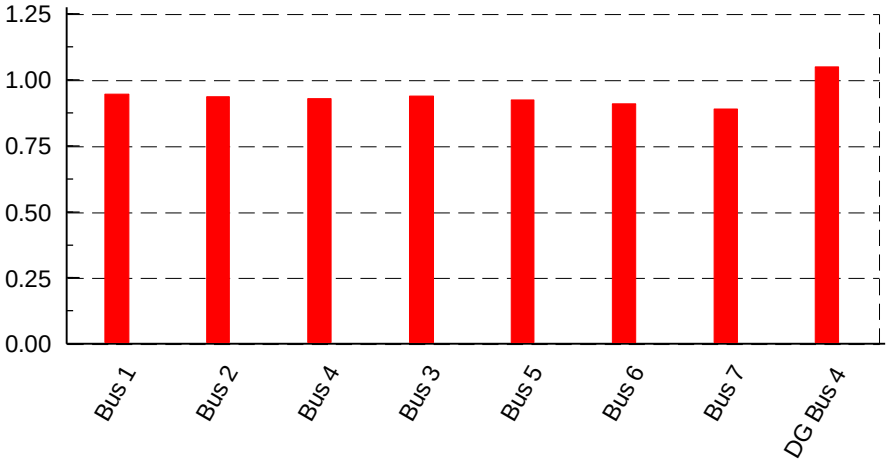

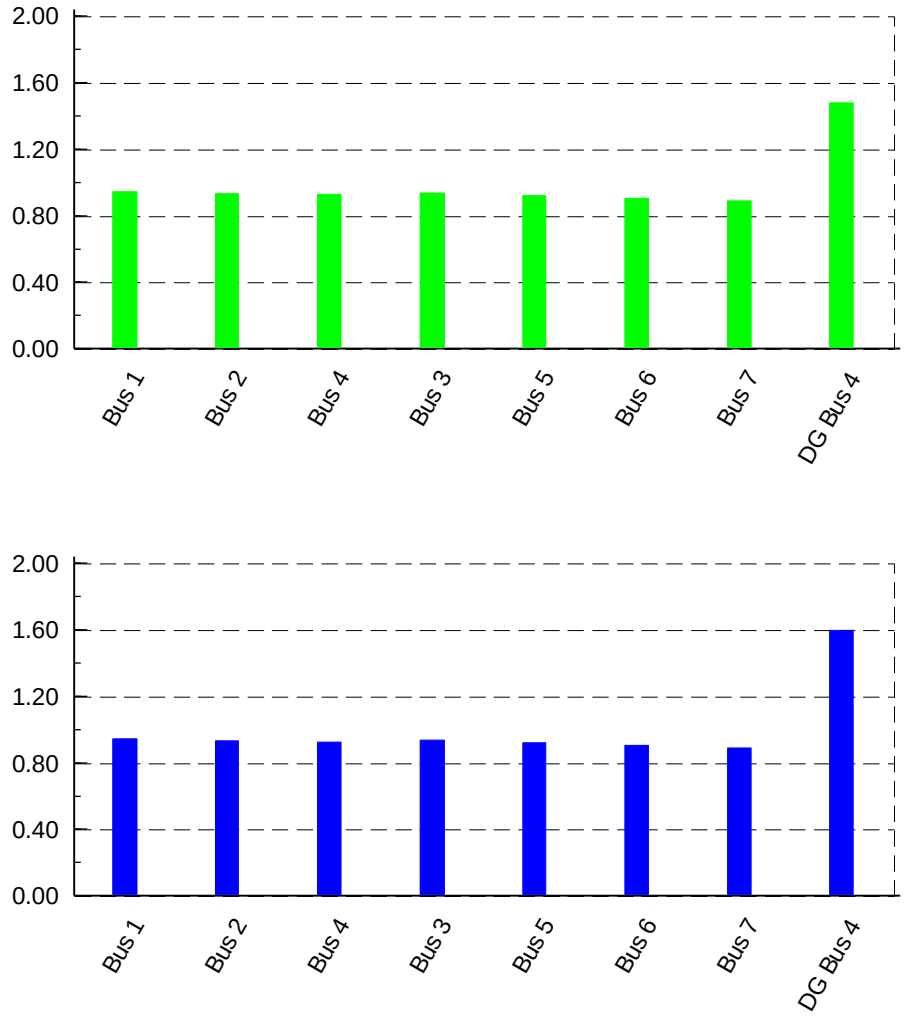

Figure 4.27: Voltage profile (pu) at selected buses at site A (top), B (middle) & C (bottom)

3.6.4.2 Impact on fault level

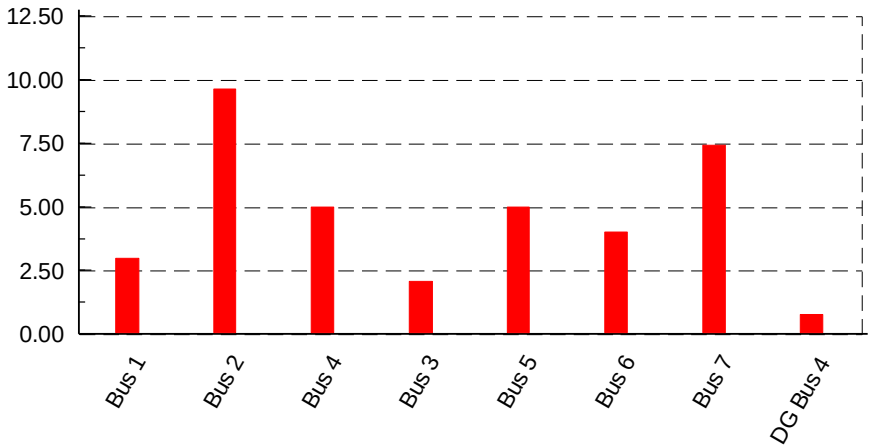

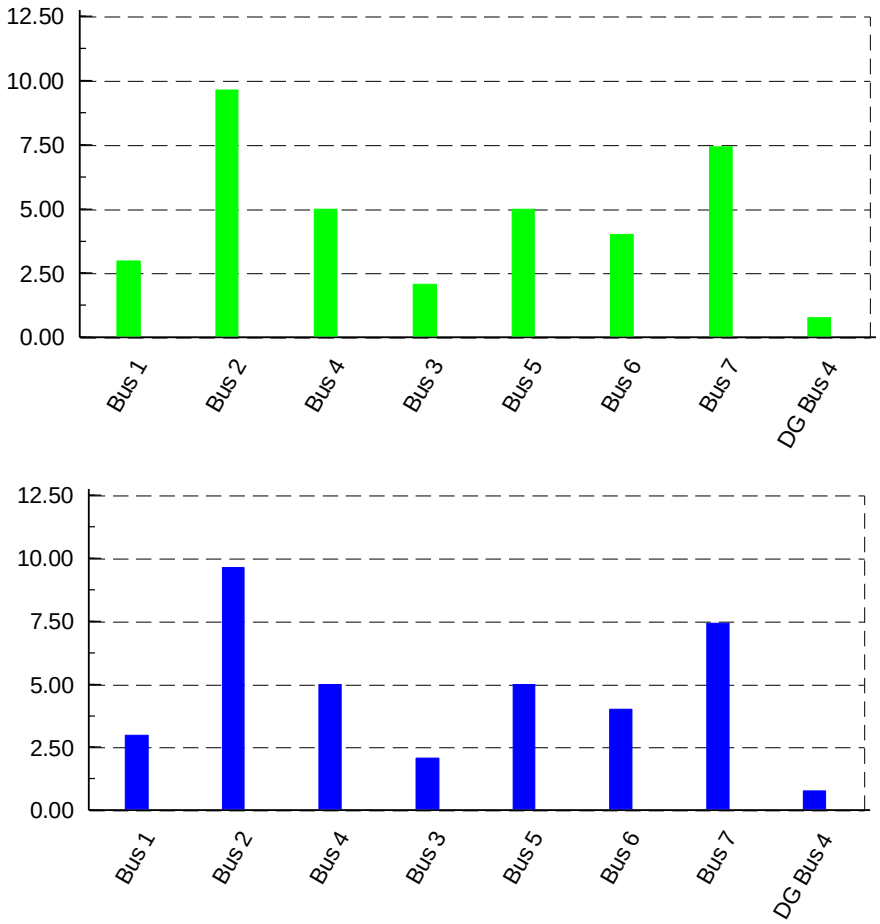

Figure 4.28: Fault level (kA) at selected buses at site A (top), B (middle) & C (bottom

3.6.4.3 Impact on thermal loading

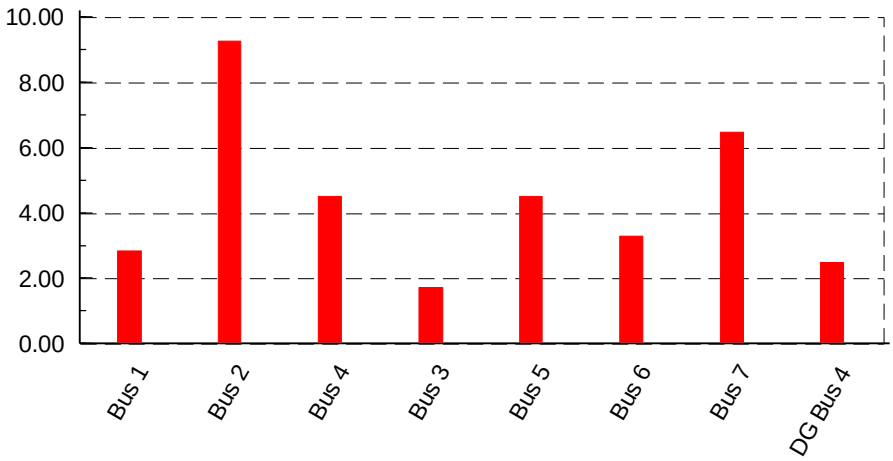

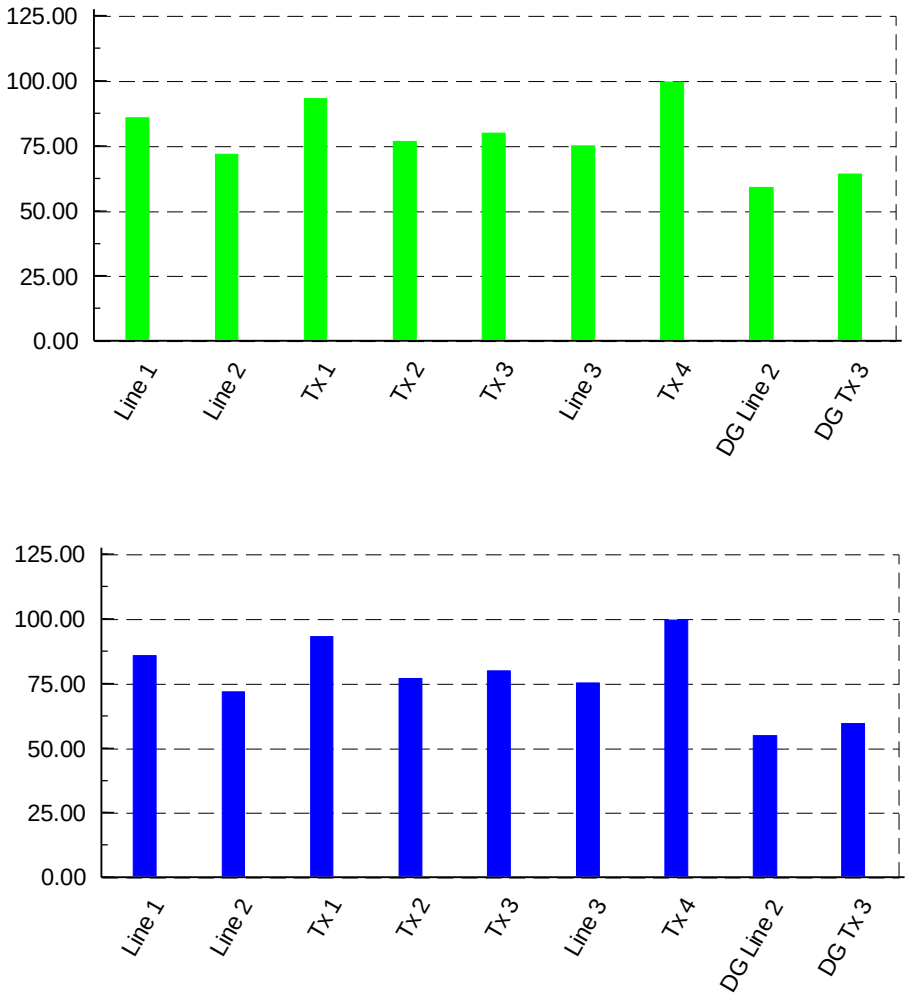

Figure 4.29: Thermal loading (%) of equipment at site A (top), B (middle) & C (bottom)

3.6.4.4 Impact on power loss

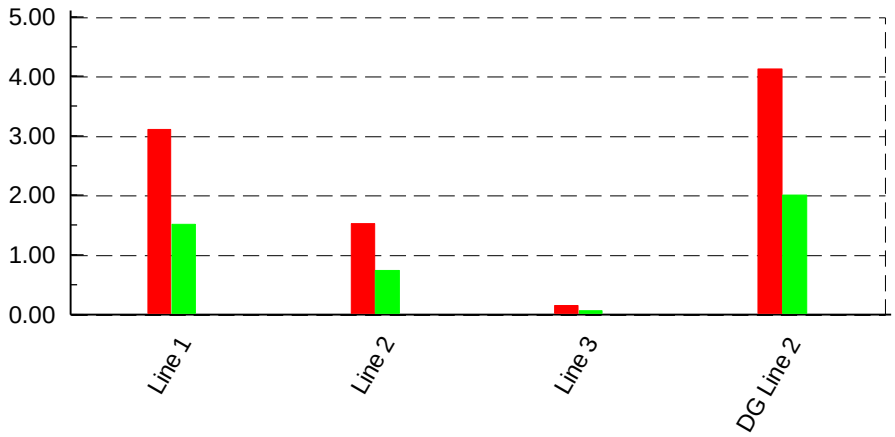

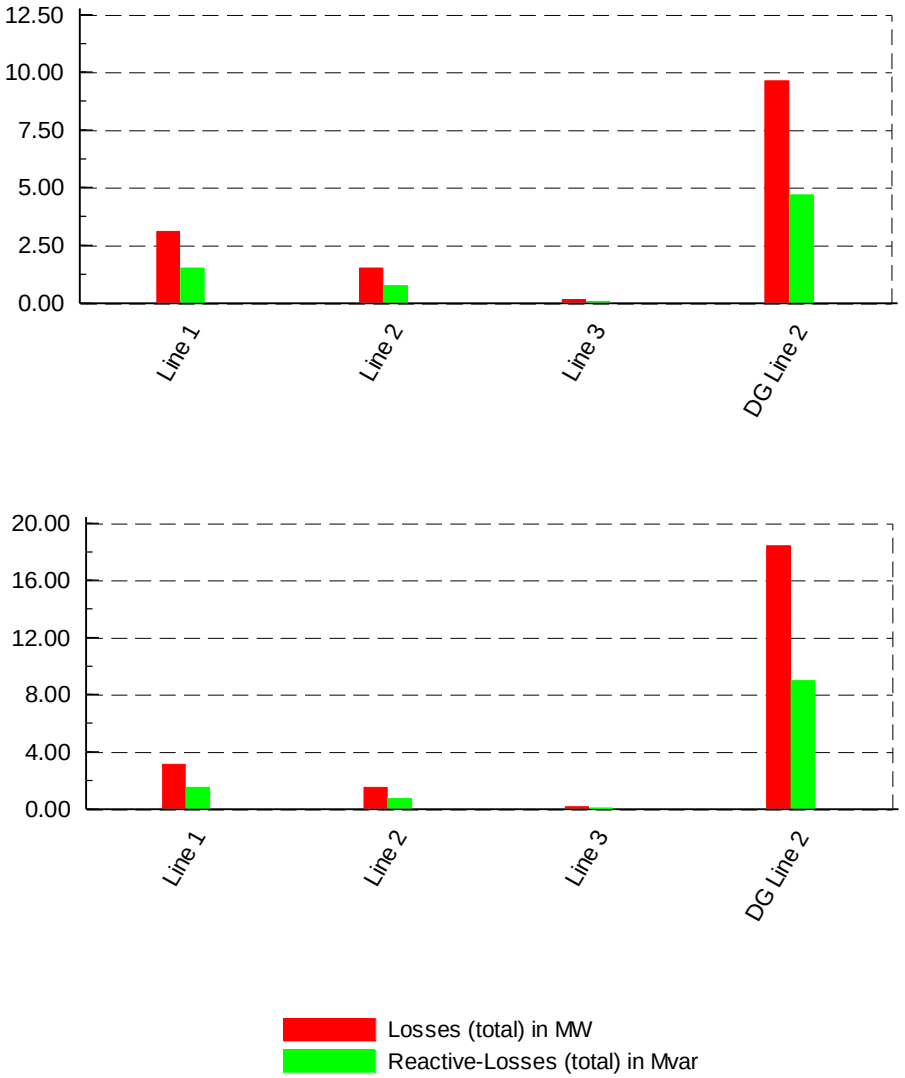

Figure 4.30: Transmission loss at site A (top), B (middle) & C (bottom)

A detailed technical analysis of the results for the second case study is provided in table 4.15 – 4.18. For the second case study, the effect on bus 2 is of particular interest as the mineral smelter is connected to this bus. The results for the voltage profile analysis show that injecting 76 MW of wind energy improves the voltage profile, but still violates the lower limit of 0.95pu. The voltage profile for site A at DG 4 is within prescribes limits, but at site B and C, the voltage has exceeded the limit of 1.095 at the POC.

Table 4.15: Analysis of voltage profile for Wind Systems

Bus No.	Base Case	Site A	Variation (%)	Site B	Variation (%)	Site C	Variation (%)
2	0.934	0.942	0.85	0.942	0.85	0.941	0.74
MTS	0.992	1.000	0.80	0.999	0.70	0.998	0.60
DG 4	-	1.070	-	1.175	8.94	1.372	22.01

Table 4.16: Analysis of fault contribution for Wind Systems

Bus No.	Base Case	Site A	Variation (%)	Site B	Variation (%)	Site C	Variation (%)
2	8.959	10.378	13.67	10.004	10.45	9.550	6.19
MTS	3.659	4.796	23.71	4.510	18.87	4.143	11.68
DG 4	-	3.692	-	2.701	26.84	2.076	43.77

The contribution to the fault at site A is the greatest at 14% and 23% at bus 2 and the MTS bus, respectively. The fault decreases as the distance from the load increases. Site A, being closest to the load has the greatest impact on the fault level. The thermal loading on equipment is marginal and within safe operating limits. The line losses increase significantly as the distance between the load and DG increases. The losses at site C increased by 76% compared to site A.

Table 4.17: Thermal loading of selected equipment

Line No.	Base Case	Site A	Variation (%)	Site B	Variation (%)	Site C	Variation (%)
1	85.40	84.70	0.82	84.70	0.82	84.80	0.70
2	71.50	70.80	0.98	70.90	0.84	70.90	0.84
DG 4	-	92.80	-	84.90	8.53	73.20	21.12

Table 4.18: Line losses (MW)

Line No.	Base Case	Site A	Variation (%)	Site B	Variation (%)	Site C	Variation (%)
1	3.106	3.052	1.74	3.056	1.61	3.062	1.42
2	1.522	1.494	1.84	1.496	1.71	1.499	1.51
DG 4	-	5.127	-	11.665	56.05	21.425	76.07

The overall results for the wind system show that the profile remains virtually unchanged. The maximum fault contribution at the POC has increased by 28%. Protection relays will have to be readjusted based on new calculated fault levels. The thermal loading of the lines remains virtually unchanged for all sites. All lines and network equipment remain within safe limits.

4.3.2 Solar System – Technical Results

A detailed technical analysis of the results for the solar system is provided in table 4.19 – 4.22. The effect on bus 2 where the steel processing plant is connected and the DG

4, which represents the POC, will be discussed. The results for the voltage profile analysis show that injecting solar energy at all the sites, independent of distance has no effect on the voltage profile when compared to the base case. The voltage at bus 2 has violated the minimum levels. The voltage profile at DG 4 for all sites has exceeded the upper limit of 1.095pu. The fault contribution is greatest at site A, but the contribution at all sites is marginal. The thermal loading of equipment from all sites is within safe operating limits. The line loss at site C is the greatest at 32 MW.

Table 4.19: Analysis of voltage profile for Solar Systems

Bus No.	Base Case	Site A	Variation (%)	Site B	Variation (%)	Site C	Variation (%)
2	0.934	0.934	0.0	0.932	0.21	0.932	0.0
MTS	0.992	0.992	0.0	0.990	0.20	0.990	0.0
DG 4	-	1.104	-	1.478	25.30	1.594	30.74

Table 4.20: Analysis of fault contribution for Solar Systems

Bus No.	Base Case	Site A	Variation (%)	Site B	Variation (%)	Site C	Variation (%)
2	8.959	9.250	3.16	9.194	2.56	9.163	2.23
MTS	3.659	3.809	3.94	3.813	4.04	3.800	3.71
DG 4	-	1.705	-	0.501	70.2	0.417	75.54

Table 4.21: Thermal loading of selected equipment

Line No.	Base Case	Site A	Variation (%)	Site B	Variation (%)	Site C	Variation (%)
1	85.40	85.40	0.0	85.60	0.23	85.60	0.23
2	71.50	71.50	0.0	71.60	0.14	71.70	0.28
DG 2	-	79.00	-	59.10	25.19	54.80	30.63

Table 4.22: Line losses (MW)

Line No.	Base Case	Site A	Variation (%)	Site B	Variation (%)	Site C	Variation (%)
1	3.106	3.106	0.0	3.119	0.42	3.122	0
2	1.522	1.522	0.0	1.529	0.46	1.530	0
DG 2	-	7.968	-	27.311	70.82	31.943	70.06

4.3.3 Economic results
3.6.6.1 Wind Energy

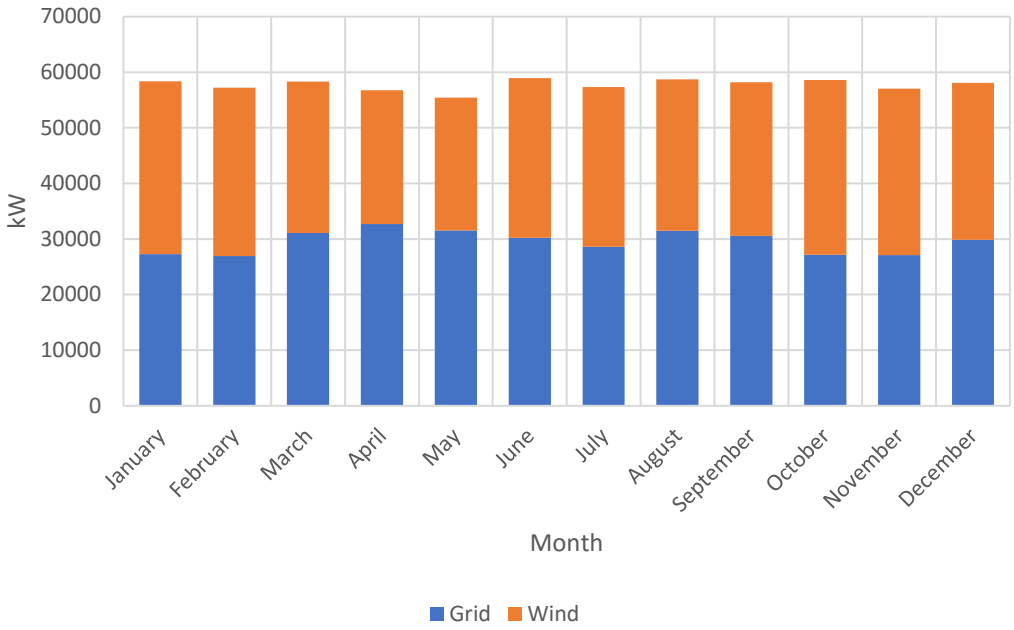

Figure 4.31: Grid-wind generation results for site A

The optimization results for the grid-wind system at site A is tabulated in figure 4.31. The renewable fraction for site 1 is 48%.

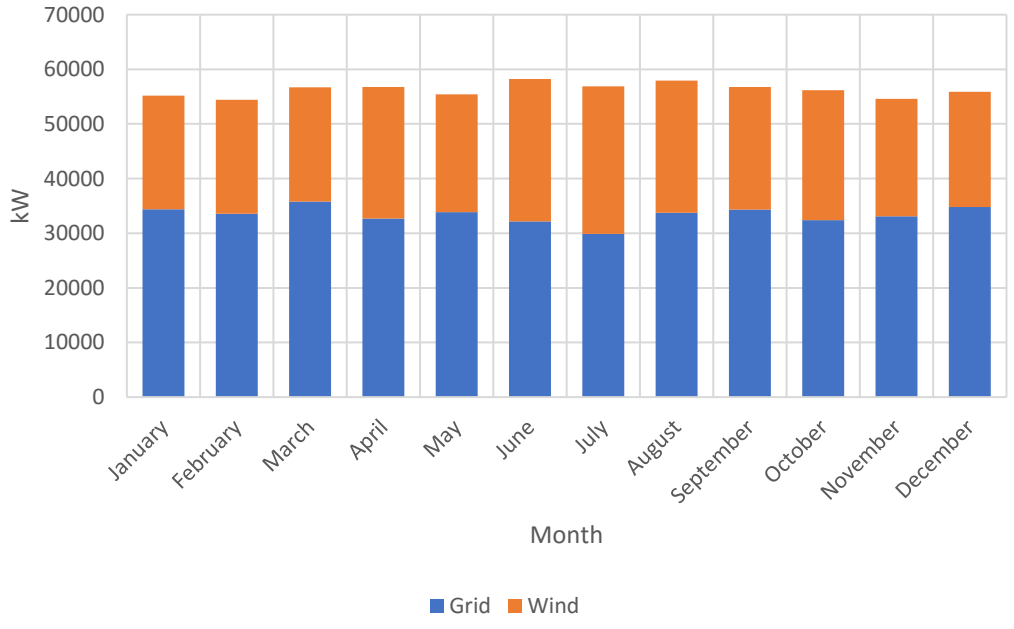

Figure 4.32: Grid-wind generation results for site B

The optimization results for the grid-wind system at site B is tabulated in figure 4.32. The renewable fraction for site B is 40%.

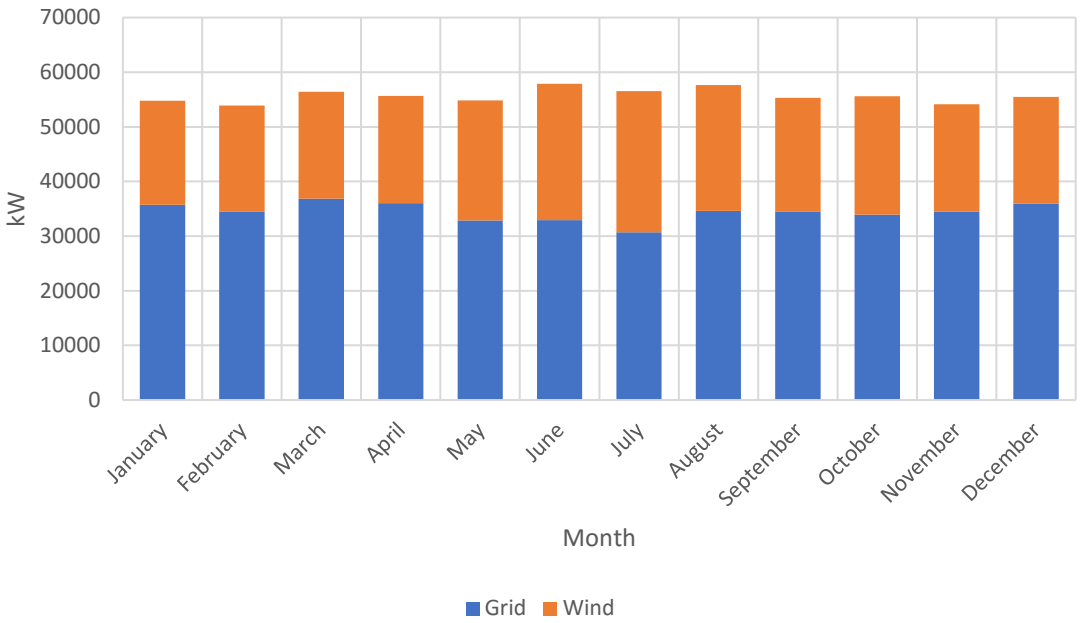

Figure 4.33: Grid-wind generation results site C

The optimization results for the grid-wind system at site C is tabulated in figure 4.33. The renewable fraction for site C is the lowest at only 38%.

3.6.6.2 Solar Energy

HOMER ran various simulations for the same load with solar PV resources.

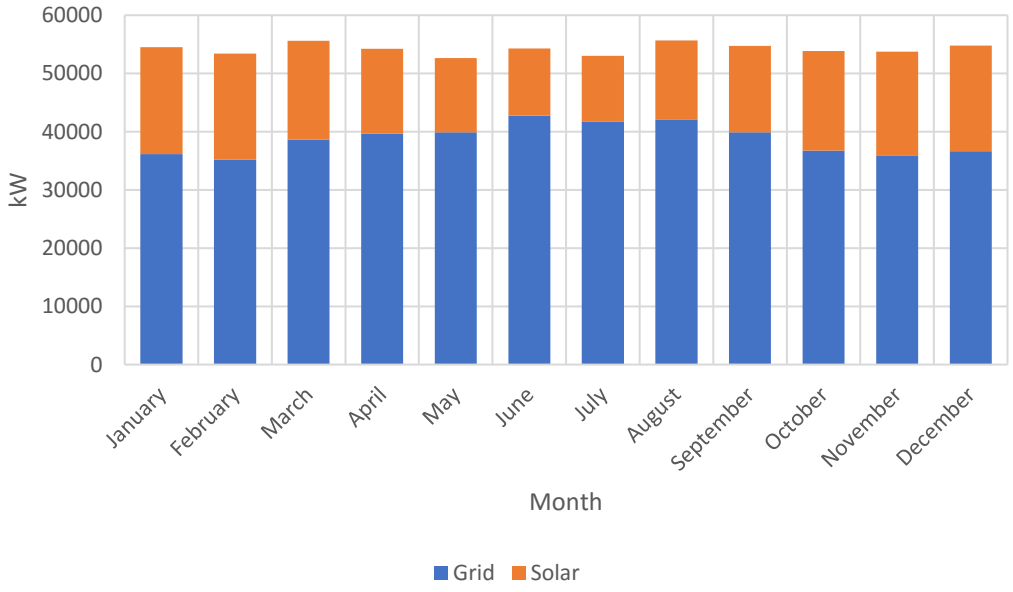

Figure 4.34: Grid-solar generation results site A

The optimization results obtained from HOMER for the grid-solar system at site A is tabulated in figure 4.34. The renewable fraction for site A is the lowest at only 28%.

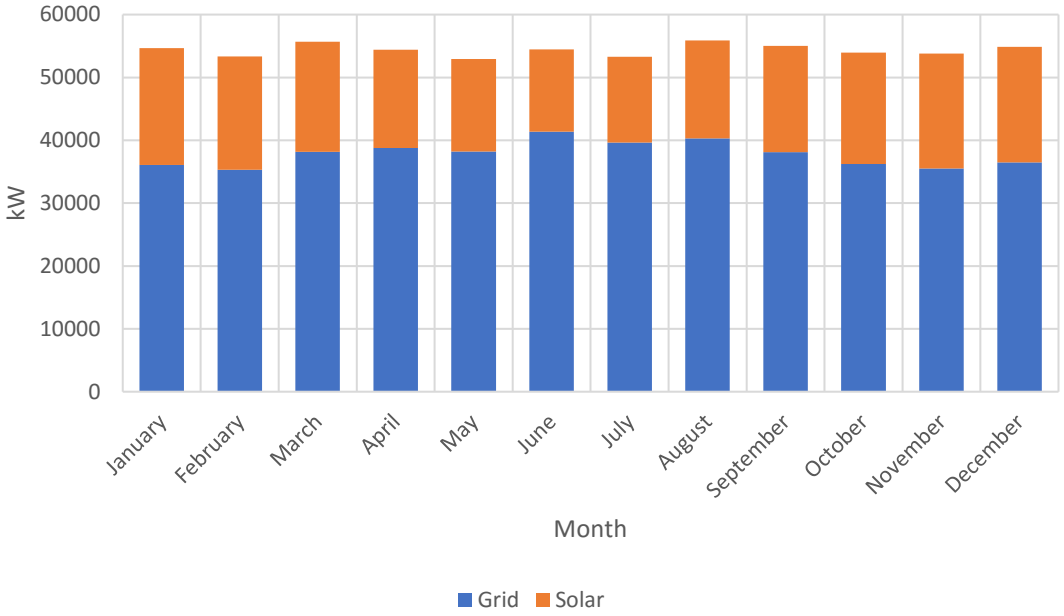

Figure 4.35: Grid-solar generation results site B

The optimization results for the grid-solar system at site B is tabulated in figure 4.35. The renewable fraction for site B is 30%.

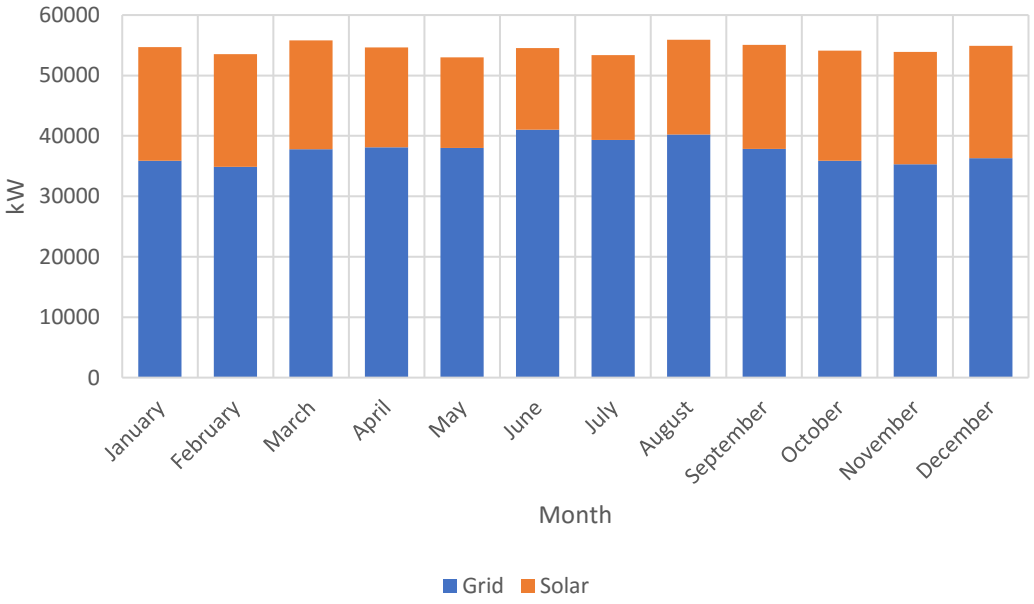

Figure 4.36: Grid-solar generation results site C

The optimization results for the grid-solar system for the last site is tabulated in figure 4.36. The renewable fraction is 31%.

Three systems were modelled in HOMER based on the load. The RE systems were sized to match the load. The optimization results that represents the system architecture was obtained from HOMER for the three sites and are tabulated in table

4.23. As for the first case study, due to the complexity of a hybrid system which would involve multiple contracts with various IPP's, a single IPP was selected per site. Considering the intermittent nature of solar and wind resources, grid and RE system was proposed.

The results show that wind energy offers the best renewable energy fraction and offers the highest energy produced per year. It is interesting to note that the RE fraction has decreases for wind and solar energy. Site A again offers the best energy yield due to good wind resources along the coast. The average daily production is 9 hours per day. The combined wind and grid system produced 503 MWh of renewable energy per year. The remaining wind sites produces less energy per year due to the decreased wind resources.

Table 4.23: Optimized systems architecture for Mineral Smelter

Site	System	Energy (MWh/year)	RE fraction (%)	RE Output (kW)
Site A	Grid + Wind	503	48.3	78 431
	Grid + Solar	474	28.2	75 003
Site B	Grid + Wind	491	40.5	78 431
	Grid + Solar	476	30.3	75 009
Site C	Grid + Wind	488	38.1	78 431
	Grid + Solar	477	31.0	74 896

Solar energy produced closest to the load at site A has the least RE fraction. As mentioned before, this is a consequence of the lack of solar resources along the coast of South Africa. In the Northern Cape, where irradiance levels are higher compared to the coastal areas, energy yield is higher. This is evident from the data generated at site C that this site offers the best renewable fraction at only 31%. The site is however located 625 km from the load which has additional wheeling cost implications. The system at site 3 produces 477 MWh of energy per year. The optimally sized grid-wind system produces 503 MWh. The breakdown of energy used compared to energy produced is given below. The possibility exists for excess energy to be sold to the utility.

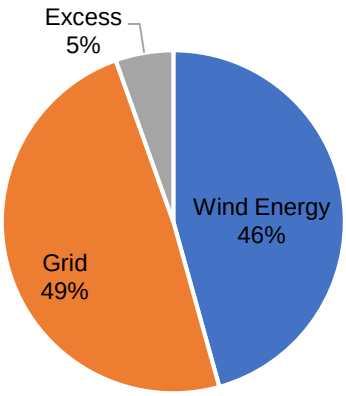

Figure 4.37: Breakdown of electricity used for optimal system

From the cost analysis is can be seen that for site A, wind energy has reached grid parity. The cost of electricity for the system is 0.063 $/kWh compared to the existing blended average electricity cost of 0.062 $/kWh paid to the supply authority. Based on the results released by The Department of Energy of South Africa for the latest REIPPP contract awards in 2018, the cost of energy generated from wind for 140 MW was as little as 0.0448 $/kWh (Department of Energy, 2018). This is a major leap forward for renewable energy and the justification about the potential for RE and wheeling of energy. The NPC and operating cost of the system is the lowest of all the wind sites at $69.4m and $2.881m respectively. The solar site closest to the load has the lowest LCOE, NPC and operating cost.

Table 4.24: Cost analysis for Mineral Smelter

Site	System	LCOE ($/kWh)	NPC ($m)	Operating Cost ($m)
Site A	Grid + Wind	0.063	398	19.5
	Grid + Solar	0.068	403	24.1
	Grid + Solar + Battery	0.748	442	24.8
Site B	Grid + Wind	0.069	423	21.4
	Grid + Solar	0.066	396	23.6
	Grid + Solar + Battery	0.073	435	24.3
Site C	Grid + Wind	0.070	430	22.0
	Grid + Solar	0.066	394	23.4
	Grid + Solar + Battery	0.073	433	24.1

4.4 Cost Projections

4.4.1 Case Study 1 – Steel Plant

The current blended current cost of electricity for industrial applications is 0.062 $/kWh. In 2017, the utility applied to NERSA for 19.90% increase in tariff for the new financial year. NERSA approved 5.23% in 2017 (NERSA, 2017). The current cost and projected cost for wind and solar energy for a 16 MW system is illustrated in figure 4.38. The cost projection from coal-based energy is based on an annual increase of 5.23%. The cost projection from wind and solar energy is based on a conservative price decrease of 2.5% per annum. From the results in can be seen that the cross-over point would be as early as 2019.

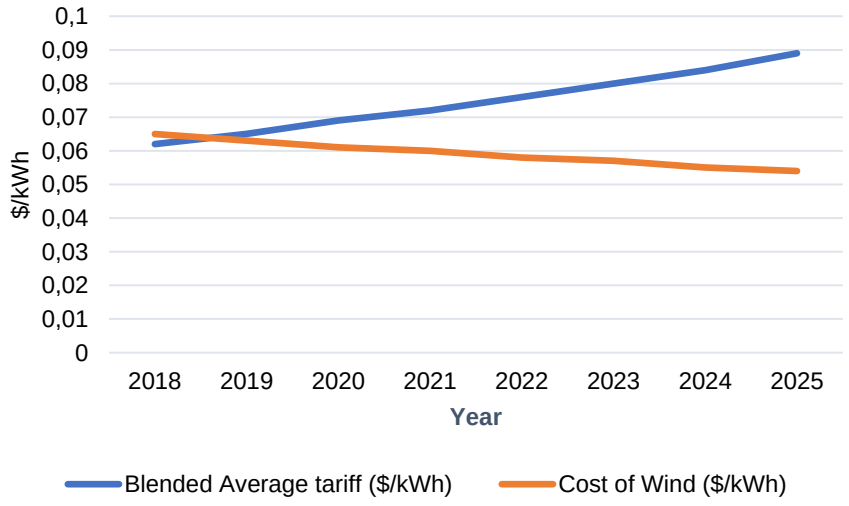

Figure 4.38: LCOE cost comparison of wind and grid

Based on similar conservative cost projection of 2.5% per annum, solar energy grid parity would be reached by 2021. Based on more aggressive cost reduction, grid parity could be reached with 18 months.

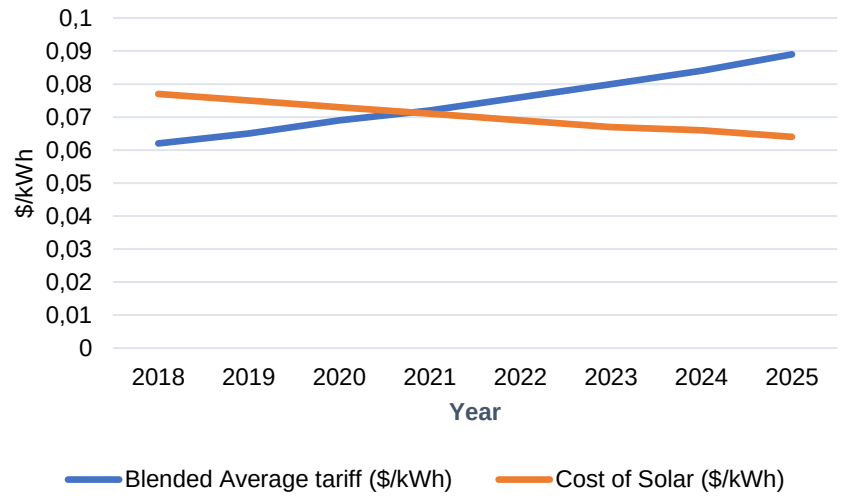

Figure 4.39: LCOE cost comparison of solar and grid

4.4.2 Case Study 2 – Mineral Smelter

Based on LCOE results obtained from HOMER for the second case study, future cost of wind and solar was calculated. As before, the current blended average cost applied to industry from fossil fuel was compared to projected wind and solar for the proposed 76 MW systems. The cost projection from coal-based energy is based on an annual increase of 5.23%. The cost projection from wind and solar energy is based on a conservative price decrease of 2.5% per annum. From the results in can be seen that the grid parity was reached in 2018. Based on the announcement of preferred bidders for the latest REIPPP released by the Department of Energy (DOE) in March, 2018, the lowest cost of wind energy produced was 0.045 $/kWh (DOE, 2018). This was based on 140 MW wind project.

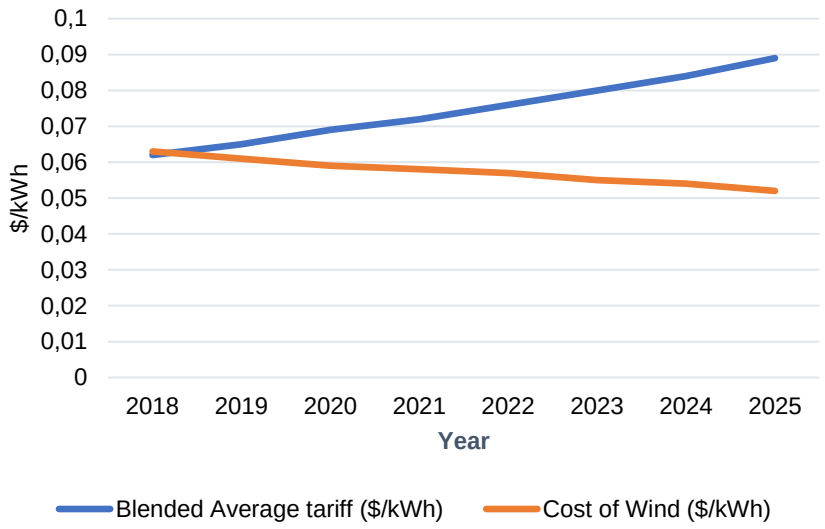

Figure 4.40: LCOE cost comparison of wind and grid

Based on similar conservative cost projection of 2.5% per annum, solar energy grid parity would be reached by 2019. Based on DOE information, the cost of solar energy for 76 MW projects in 2018 has already reached grid parity. If a more aggressive approach is considered as per The Renewables Energy Agency, PV will decline by another 57% by 2025.

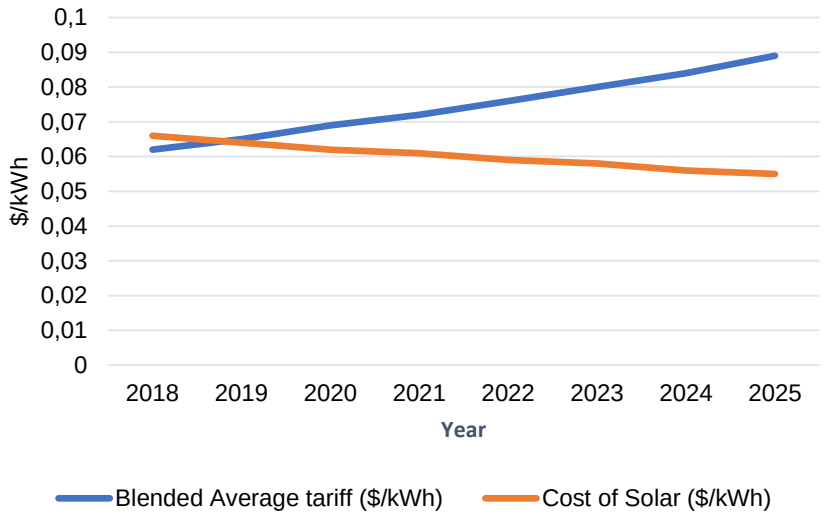

Figure 4.41: LCOE cost comparison of solar and grid

4.5 Chapter Summary

In this chapter, the results of the case studies were analysed and discussed. From the results it can be concluded that DG technology and size does not alter the voltage profile of bus where DG is connected, neither does it have any effect on the bus at the POC. The results show that in all cases the impact is less than 1% of the base case. Asynchronous and synchronous generators have an impact on fault level at POC and at the bus where DG is connected. It is evident from the results that the size of DG and the proximity to the load has inversely proportional. A variance of up to 28% of the fault level compared to the base case was experience for asynchronous generators at site A. Inverter-based DG has a marginal impact on voltage profile and fault level. Results from both case studies, confirmed that thermal ratings of equipment are within design limitations. Losses are mainly experienced on lines between DG and POC.

The economic results show that grid-wind energy is the most viable option. This solution presents the best LCOE, renewable energy fraction and NPC. Results show that on an average day, the average wind production is 9 hours, whereas the average solar production is limited to 4.5 hours. Cost projection based on current tariffs show that for larger systems such 76 MW, wind has already reached grid parity. Projections indicate that for large solar systems such as 76 MW, grid parity could be reached by 2019. Hydropower is not a feasible option at present, based on LCOE.

Large scale solar PV projects are reaching very competitive levels globally with recent bids from Mexico, Dubai, Chile and Abu Dhabi received at 0.039 $kWh, 0.0336$ kWh, 0.0328 $/kWh and $0.0272 $/kWh respectively received.

CHAPTER FIVE
CONCLUSION AND RECOMMENDATIONS

5.1 Conclusion

Eskom's recent supply problems, escalating electricity prices and drive by consumers to reduce carbon footprint, has highlighted the need to explore alternative energy supply. Third party transportation of energy, commonly known as wheeling of energy, is one method of addressing the energy needs of consumers. In deregulated markets, wheeling has been successfully implemented, but in South Africa, where Eskom has monopolized electricity generation, the concept has seen pockets of success.

This study into the viability of energy wheeling, in a South African context, has been undertaken from an industrial consumer's perspective. The study showed that the viability of wheeling is dependent on two key aspects. Firstly, DG technology has to be financially viable when compared to conventional energy supply. Secondly, connecting DG to the network alters network parameters, which has to be thoroughly investigated and mitigated.

It is against this backdrop that technical and economic analysis have been conducted on an existing distribution network, feeding two main industrial loads. The conventional distribution system which was used as the base case, was compared to a system supplied by a suitably sized DG technology. The analysis was conducted with the aid of two software simulation packages namely, DIgSILENT PowerFactory and HOMER.

DIgSILENT PowerFactory was used to determine the impact of DG technology and size on network parameters such as the voltage profile, fault level contribution, power loss on transmission lines and thermal loading of equipment. The impact of DG location on network parameters was analysed as well. Various DG technologies were profiled, but wind, solar and hydro power were selected based on renewable energy potential and cost as illustrated in Chapter 2. HOMER was used to conduct a cost analysis of wind, solar and hydropower.

The results of the study show that:

- Wind and solar energy offer the best potential based on available renewable resources. The coastal areas, particularly the west and east coast of South Africa, presents the best wind potential. It was found that the average wind speed at these areas is above 8 m/s at 100 m above sea level. This is

considered above average wind resources. The best solar potential is located in the Northern Cape where the Global Horizontal Irradiance (GHI) level is above 2200 kWh/m^2.

- Wind energy presents the most financially viable option for both case studies in terms of levelized cost of electricity (LCOE) and net present cost (NPC). The LCOE for 16 MW and 70 MW wind energy at the site with the best wind potential was 0.065 $/kWh and 0.063 $/kWh respectively. The blended average cost of fossil-based electricity is 0.062 $/kWh.

- In markets where the electricity structure, i.e. generation, transmission and distribution have been deregulated, wheeling has been very successful. In South Africa, Eskom's monopoly on the generation and transmission of electricity is limiting the growth of IPP's. The cost of wheeling energy is perceived to be expensive, but this charge is a standard network tariff charge, charged by supply authorities to recover infrastructure costs.

- For both case studies, the impact on the voltage profile at various buses is negligible. As the distance from the DG and the substation increases, the voltage profile at the POC, in almost all the cases, violated the upper limit of 1.095pu. Voltage control measures should be implemented where minimum and maximum voltages levels are exceeded. It was found that asynchronous and synchronous generators have a greater fault contribution than inverter-based DG. The fault contribution increased base on DG size but decreases as the distance increases between the load and the DG. Power loss on short lines is negligible, but there is a significant loss on the line between the load and DG based as the distance between the DG and the load increases. Overall, thermal loading of lines increased marginally, but decreased based on distances between the DG and the load.

Eskom's new coal fired power stations are producing electricity at 0.0824 $/kWh whereas the lowest tariffs for the latest bid window for REIPPP is 0.0448 $/kWh. Wheeling of energy for large scale wind projects, greater than 70 MW, has reached grid parity. Based on the technical and economic results, wheeling of wind energy is a realistic opportunity for industry where load demands exceed 70 MW.

Within the next 2 years, smaller projects, typically less than 70 MW, will become economically viable as the cross-over point between Eskom's blended tariffs and the

cost of renewable energy is reached. According to price projection, large scale solar energy will become viable by 2019. In order for wheeling to be as successful as in some developed countries, our own electricity market has to be deregulation. Deregulation could hold the key to the successful implementation of energy wheeling. This could open up the local electricity market for greater competition as proven by international experience. Internationally, wheeling has been very successful and has resulted in greater efficiencies and price reduction as a result of competition.

5.2 Recommendations

This study focused on specific industry sectors and provides a general overview of the potential that exist for third party transportation of energy. The technical scope to evaluate the viability of wheeling is limited but could be broadened to include a full analysis of network parameters. A detailed analysis of the actual financial impact on a specific business could be evaluated.

REFERENCES

Babu, C.A. & Ashok, S. 2010. Optimal Captive Power Wheeling for Industrial Load Management. *International Energy Journal*, 11:1-8

Baggini, A. 2008. *Handbook of Power Quality*. Chichester, West Sussex: John Wiley & Sons.

Banerjee, S.G., Romo, Z., McMahon, G., Toledano, P., Robinson, P., Arroyo, I. 2015. *The Power of the Mine. A Transformative Opportunity for Sub-Saharan Africa*. Washington DC: International Bank for Reconstruction and Development / The World Bank

Banks, D. & Schäffler, J. 2006. *The potential contribution of renewable energy in South Africa*. Johannesburg: Sustainable Energy & Climate Change Project

Bio2Watt. 2015. *Bronkhorstspruit Biogas Plant*.
https://www.bio2watt.com/bio2watt%E2%80%99s-bronkhorstspruit-biogas-plant-(pty)-ltd.html
[accessed 12 June 2017]

CAISO. 2017. *Wheeling Access Charges*.
https://www.caiso.com/Documents/WheelingCharges.pdf
[accessed 13 June 2017]

Darling Wind Farm. 2010. *What is a Wind Farm?*
http://www.darlingwindfarm.com/index.html
[accessed 14 June 2017]

Department of Energy. 2015. *Integrated Energy Plan*. Pretoria: Dept of Energy.

Department of Minerals & Energy. 1998. *White Paper on the Energy Policy of the Republic of South Africa*. Pretoria: Dept of Minerals and Energy.

Department of Science and Technology. 2014. *The State of Green Technologies in South Africa.* Pretoria: Academy of Science of South Africa.

Department of Trade and Industry. 2014. *Industry Supply Analysis: Ferrous Metals Downstream Sector.* Pretoria: Dept of Trade and Industry.

Doble, M & Kumar, M. 2007. *Green Chemistry & Engineering*. Massachusetts: Academic Press.

Dulua, L. I., Abrudean, M., Bica, D. 2013. Effects of distributed generation on electric power systems. *7th International Conference Interdisciplinarity in Engineering*, Targu Mures, 10-11 October 2013. Romania: Procedia Technology: 681 – 686

Eskom. 2017. *Tariffs and Charges.*
http://www.eskom.co.za/CustomerCare/TariffsAndCharges/Pages/Tariffs_And_Charges.asp
[accessed 22 April 2017]

Eskom. 2016. *List of fact sheets*.
http://www.eskom.co.za/IR2016/Documents/Eskom_fact_sheets_2016.pdf
[accessed 22 April 2017]

Eskom. 2011. W*heeling / offset of energy*.
http://www.eskom.co.za/CustomerCare/TariffsAndCharges/Documents/Wheeling30March2011.pdf
[accessed 10 April 2017]

Eskom. 2010. *Energy efficiency series; Towards an energy efficient mining sector.* http://www.eskom.co.za/sites/idm/Documents/121040ESKD_Mining_Brochure_paths.pdf [accessed 10 April 2017]

EIUG. 2017. *Organisation profile.* http://eiug.org.za/ [accessed 16 April 2017]

Firinc, Ă. S. D., Mircea, I., Hiyasat, A., & Mircea, P. M. 2015. Simulation of the systems with renewable energy sources using HOMER software. *Journal of Sustainable Energy*, 6(2):60-64

First Solar. 2017. *Utlity Scale PV Plants*. http://www.firstsolar.com/en/PV-Plants/Utility-Scale [accessed 20 April 2017]

Fraas, L.M., Partain, L.D. 2010. *Solar Cells and Their Application*, 2nd ed. New Jersey: John Wiley & Sons.

Funabashi, T. 2016. *Integration of Distributed Energy Resources in Power Systems: Implementation, Operation & Control*. Loondon: Academic Press.

Gabriel, C. A. 2016. What is challenging renewable energy entrepreneurs in developing countries? *Renewable and Sustainable Energy Reviews*, 64:362–371, August 15

Gaonkar, D. N. 2007. Steady State Voltage Rise and Its Control in Distribution System with Distributed Generation. *International Energy Journal*, 8:225-234.

González-longatt, F. M. 2007. Impact of Distributed Generation over Power Losses on Distribution System. *9th International Conference. Electrical Power Quality & Utilization*. Barcelona, 9-11. October 2007.

Goetzberger, A & Hoffman, V. 2005. *Photovoltaic Energy Generation*. New York: Springer

GreenCape. 2017. *Utility-scale renewable energy Market Intelligence Report*. https://www.greencape.co.za/assets/Uploads/GreenCape-Renewable-Energy-MIR-2017-electronic-FINAL-v1.pdf [accessed 18 April 2017]

Heier, S. 2014. *Grid Integration of Wind Energy: Onshore and Offshore conversion Systems*. Chichester, West Sussex: John Wiley & Sons

Heeter, J., Vora, R., Mathur, S., Renewable, N., & Madrigal, P. 2016. *Wheeling and Banking Strategies for Optimal Renewable Energy Deployment: International Experiences*. National Renewable Energy Laboratory. https://www.nrel.gov/docs/fy16osti/65660.pdf [accessed 24 April 2017]

ICLEI. 2015. *Nelson Mandela Bay Municipality, South Africa embedded energy generation experience in a South African metropolitan municipality*. http://www.cityenergy.org.za/uploads/resource_318.pdf [accessed 25 May 2017]

IRENA. 2017a. *Electricity Storage and Renewables: Costs and Markets to 2030.* International Renewable Energy Agency, Abu Dhabi.

IRENA. 2017b. *Power Generation Costs in 2017*. International Renewable Energy Agency, Abu Dhabi.

IRENA. 2017c. *Renewable Energy Prospects for India*. International Renewable Energy Agency, Abu Dhabi.

IRENA. 2016. *Solar PV in Africa: Costs and Markets.* International Renewable Energy Agency, Abu Dhabi.

IRENA. 2015. *Renewable Power Generation Cost in 2014.* International Renewable Energy Agency, Abu Dhabi.

IRENA. 2013. Concentrating Solar Power: Technology Brief. International Renewable Energy Agency, Abu Dhabi.

Jenkins, N., Ekakanayake, J.B., Strabac, G. 2010. *Distributed Generation*. London: The Institution of Engineering and Technology,

Kalogirou, S.A. 2014. *Solar Energy Engineering: Process and Systems*, 2nd ed. London: Acedemic Press.

Keller, J., & Kroposki, B. 2010. *Understanding Fault Characteristics of Inverter-Based Distributed Energy Resources.* National Renewable Energy Laboratory.

Khartchenko, N. 2014. Advanced Energy Systems, 2nd ed. New York: CRC Press.

Klunne, W. 2016. *World Small Hydropower Development Report 2016: South Africa*. United Nations Industrial Development Organization. https://www.unido.org/sites/default/files/201611/WSHPDR_Executive_Summary_2016_0.pdf (accessed 24 April 2017]

KPMG. 2014. T*he Energy Report Philippines: Growth and Opportunities in the Philippine Electric Power Sector*, 2013-2014 ed. https://home.kpmg.com/content/dam/kpmg/ph/pdf/InvestmentGuide/2013PHInvestmentGuideInvestmentGuideTheEnergyReportPhilippines.pdf [accessed 02 May 2017]

Kutz, M (ed). 2007. *Environmentally Conscious Energy Production*. New York: John Wiley & Sons.

Luthra, S., Kumar, S., Garg, D., & Haleem, A. 2015. Barriers to renewable/sunstainable energy technologies, adoption: Indian perspective. *Renewable and Sustainable Energy Reviews*, 41:762-776, September.

Luque, A. & Hegedus, S. (2011). *Handbook of Photovoltaic Science & Engineering*, 2nd ed. Chichester, West Sussex: John Wiley & Sons (UK)

Marquard, A., Bekker, B., Eberhard, A., & Gaunt, T. 2007. *South Africa's Electrification Programme*: An overview and assessment. Cape Town: Graduate Schoool of Business, University of Cape Town.

Martin, R. 2016. MIT Technology Review. *First Solar's Cells Break Efficiency Record.* https://www.technologyreview.com/s/600922/first-solars-cells-break-efficiency-record [accessed 25 April 2017]

Masaud, T., & Mistry, R. D. 2016. Fault Current Contribution of Renewable Distributed Generation : An Overview and Key Issues. *2016 IEEE Conference on Technologies for Sustainability*, Arizona, 9-11 October 2016.

Masters, C.L., 2002. *Voltage rise:* The big issue when connecting embedded generation to long 11kV overhead lines. *Power Engineering Journa*l, 16(1):5 – 12, February 02

Media Update. 2015. *South Africa is becoming a leader in renewable energy*. https://www.mediaupdate.co.za
[accessed 12 April 2017]

NASA. 2017. *Surface meteorology and Solar Energy*. https://ecosweb.larc.nasa.gov
[accessed 12 October 2017]

NERSA. 2014. *Grid Connected Code for Renewable Power Plants Connected to the Electricity Transmission Systems or the Distribution System in South Africa* - version 2.8, July 2014. Pretoria: National Energy Regulator of South Africa.

NERSA. 2013. *NERSA Consultation Paper :Eskom MYPD 3 Price increases and its influence on the sustainability of the Steel Industry in SA: ArcelorMittal South Africa*. http://www.nersa.org.za/Admin/Document/Editor/file/Consultations/Electricity/Presentations/arcelorMittal.pdf
[accessed 03 May 2017]

NERSA. 2011. *Regulatory Rules on Network Charges for Third-Party Transportation of Energy. Nersa Consultation Paper,* May 2011*.* Pretoria: National Energy Regulator of South Africa.

Napp, T. A., Gambhir, A., Hills, T. P., Florin, N., & Fennell, P. S. 2014. A review of the technologies , economics and policy instruments for decarbonising energy-intensive manufacturing industries. *Renewable and Sustainable Energy Reviews*, *30*:616–640

Newbery, D., & Eberhard, A. (2008). *South African Network Infrastructure Review: Electricity*. Pretoria: National Treasury and the Department of Public Enterprises of South Africa.

Olson, A., Allen, D., Sawyer, F. 2017. *Review of Capital Costs for Generation Technologies*. https://www.wecc.biz/Administrative/%20E3%20WECC%20Capital%20Costs%20v1.pdf
[accessed 22 April 2017]

Pegels, A. 2010. Renewable energy in South Africa: Potentials, barriers and options for support. *Energy Policy*, 38(9):4945–4954, May 10.

Pail, B. & Vadhera, S. 2016. Renewable Energy Systems for Generating Electric Power : A Review. *1st IEEE International Conference on Power Electronics. Intelligent Control and Energy Systems*, Delhi, 4-6 July 2016.

Power X. 2017. *A brief history*. http://www.powerx.energy/powerx-about-us
[accessed 27 June 2017]

Rajasthan Energy. 2017. *Charges payable for the Open Access on Transmission and Distribution System in Rajasthan: 2017-18*. http://energy.rajasthan.gov.in/content/dam/raj/energy/corporate-one-lines-viewer/pdf/OPENACCESS/Transmissionandothercharges.pdf
[accessed 26 June 2017]

REN21. 2017. *Renewables Global Futures Report: Great Debates towards 100% Renewable Energy.* Paris: REN21 Secretariat.

Rivkin, A. & Silk, L. 2013. *Wind Power Operations, Maintenance, Diagnosis, and Repair: The Art and Science of Wind Power*. Burlington, Massachusetts: Jones & Bartlett Publishers.
Sager, M. 2014. *Renewable Energy Vision 2030 – South Africa*. Cape Town: World Wide Fund for Nature, South Africa.

SALGA. 2014. *Municipal Wheeling Agreement for Green Power Development: Nelson Mandela Bay Metropolitan Municipality.*
http://www.cityenergy.org.za/uploads/resource_341.pdf
[accessed 28 June 2017]

SEA. 2017. *The Sustainable energy solutions for South African local government: A practical guide.* Cape Town: Sustainable Energy Africa

SMUD. 2017. *Distribution Wheeling Service Rate Schedule DWS*.
https://www.smud.org/media/documents/electric-rates
[accessed 10 May 2017]

Solargis. 2017. *Maps and GIS data*.
http://solargis.com
[accessed 14 April 2017]

Sood, Y. R., Padhy, N. P., & Gupta, H. O. 2004. Assessment for feasibility and pricing of wheeling transactions under deregulated environment of power industry. *International Journal of Electrical Power and Energy System, 26*(3):163–171.

Sood, Y. R., Padhy, N. P., & Gupta, H. O. 2002. Wheeling of power under deregulated environment of power system - A bibliographical survey. *IEEE Transactions on Power Systems*, (17(3):870-878.

Srivastava, R., & Giri, V. K. 2016. Optimization of Hybrid Renewable Resources using HOMER. *International Journal of Renewable Energy Research*, 6(1):157-163

Statistics South Africa. 2017. *Mining: A brief history*.
http://www.statssa.gov.za/
[accessed 23 April 2017]

Sunpower. 2016. *Solar Technology Efficiency*: *More Breakthroughs are Coming*
https://us.sunpower.com/blog/2016/06/26/sunpower-solar-module-verified-241-percent-efficient/https://us.sunpower.com
[accessed 16 April 2017]

World Bank. 2017. *South Africa: Country Overview*.
https://www.worldbank.org/en/country/southafrica/overview
[accessed May 2017]

World Energy Council. 2016. *World Energy Trilemma Index | 2016, Benchmarking the sustainability of National Energy Systems.* London: World Energy Council, Company Limited in partnership with OLIVER WYMAN.

World Energy Council. 2016. *World Energy Resources | 2016*. London: World Energy Council, Company Limited

The Guardian. 2008. *Gold mines shut as South Africa forced to ration power supply.*
https://www.theguardian.com/world/2008/jan/26/southafrica.international
[accessed 24 April 2017]

Viawan, F. A. 2008. Voltage Control and Voltage Stability of Power Distribution Systems in the Presence of Distributed Generation. Unpublished PhD dissertation, Chalmers University of Technology, Gothenburg, Sweden.

Walling, R. A. R., Saint, R., Member, S., Dugan, R. C., Burke, J., Kojovic, L. A., & Member, S. 2008. Summary of Distributed Resources Impact on Power Delivery Systems. *IEEE Transction on Power Delivery*, 23:1636-1644

WASA. 2017. *Best wind source areas in South Africa*.
http://www.wasaproject.info
[accessed 16 April 2017]

Wiser, R. & Bollinger, M. 2016. *2015 Wind Technologies Market Report.* Oak Ridge, Tennessee: U.S. Department of Energy

Yelland, C. 2011. Eskom-BHP Billiton and the secret electricity pricing deals. http://www.ee.co.za/article
[accessed 25 April 2017]

Zabava, T., Tristiu, I., Mandis, A., Bulac, C. 2015. Short Circuit Currents Calculation in Distribution Electrical Networks in the presence of Distribution Generation. University Politehnica of Bucharest, *Scientific Bulletin*, 77:443-454.

Zhang, H.L., Baeyens, J., Degreve, J., Caceres, G. 2013. Concentrated solar power plants : Review and design methodology. *Renewable and Sustainable Energy Reviews*, 22:466–481

APPENDICES

APPENDIX A: Wind Turbine Data

Wind Turbine Electrical parameters

Parameter	Data
Rated current	2000 kW
Cut-in wind speed	4 m/s
Cut-out wind speed	25 m/s
Type	4pole doubly fed generators, slip rings
Frequency	50 Hz
Wind Class	IEC IIA

APPENDIX B: PV Solar Components

PV parameters

PV panel electrical parameters

Parameter	Data
Nominal Power	327 W
Power Tolerance	+/- 5%
Panel efficiency	20.3%
Rated Voltage	72.9 V
Rated Current	5.97 A
Maximum System Voltage	1000 V
Power Temperature Coefficient	-0.35%/^{0}C

Inverter parameters

Inverter Electrical parameters

Parameter	Data
Vdc	570-950 V
Vdc min	545 V
Vdc max	1100 V
Idc max	6400 A
Nominal AC power @ pf = 1	2200 kVA
Nominal AC power @ pf = 0.8	1760 kVA
Efficiency	98.6%

APPENDIX C: Hydro Turbine Data

Hydro Turbine Data

Parameter	Data
Voltage	690 V
Nett Head	15.34
Capacity	4010 W
PF	0.95

APPENDIX D: Overhead conductors

Aluminium Conductor Steel Reinforced Electrical properties

Conductor name	Electrical properties		
	Resistance (Ω/km)	Reactance (Ω/km)	Current Rating (A)
Fox	0.786	0.3829	190
Panther	0.136	0.489	290
Chickadee	0.143	0.370	647
Kingbird	0.089	0.331	773